

DYNAMICS OF QUANTUM CORRELATIONS IN CLEAN AND DISORDERED MANY-PARTICLE SYSTEMS

By
UTKARSH MISHRA
PHYS08201004005

Harish-Chandra Research Institute, Allahabad

A thesis submitted to the
Board of Studies in Physical Sciences
In partial fulfillment of requirements
for the Degree of
DOCTOR OF PHILOSOPHY
of
HOMI BHABHA NATIONAL INSTITUTE



November, 2016

Homi Bhabha National Institute¹

Recommendations of the Viva Voce Committee

As members of the Viva Voce Committee, we certify that we have read the dissertation prepared by Utkarsh Mishra entitled "Dynamics of Quantum Correlations in Clean and Disordered Many-Particle System" and recommend that it may be accepted as fulfilling the thesis requirement for the award of Degree of Doctor of Philosophy.

| | |
|-------------------------------------|------------------|
| Chairman – Professor Dileep Jatkari | Date: 15/11/2016 |
| Guide / Convener – Prof. Ujjwal Sen | Date: 15/11/2016 |
| Co-guide - - | Date: |
| Examiner – Professor Anil Shaji | Date: 15/11/16 |
| Member 1- Professor Sumathi Rao | Date: 15/11/2016 |
| Member 2- Prof. Aditi Sen De | Date: 15.11.2016 |

Final approval and acceptance of this thesis is contingent upon the candidate's submission of the final copies of the thesis to HBNI.

I/We hereby certify that I/we have read this thesis prepared under my/our direction and recommend that it may be accepted as fulfilling the thesis requirement.

Date: 15/11/2016

Place: Allahabad


Ujjwal Sen

¹ This page is to be included only for final submission after successful completion of viva voce.

1948

1948

1948

1948

1948

1948

1948

1948

1948

1948

1948

1948

1948

1948

1948

1948

STATEMENT BY AUTHOR

This dissertation has been submitted in partial fulfillment of requirements for an advanced degree at Homi Bhabha National Institute (HBNI) and is deposited in the Library to be made available to borrowers under rules of the HBNI.

Brief quotations from this dissertation are allowable without special permission, provided that accurate acknowledgement of source is made. Requests for permission for extended quotation from or reproduction of this manuscript in whole or in part may be granted by the Competent Authority of HBNI when in his or her judgment the proposed use of the material is in the interests of scholarship. In all other instances, however, permission must be obtained from the author.


Utkarsh Mishra

DECLARATION

I, hereby declare that the investigation presented in the thesis has been carried out by me. The work is original and has not been submitted earlier as a whole or in part for a degree / diploma at this or any other Institution / University.

Utkarsh Mishra
Utkarsh Mishra

List of Publications arising from the thesis

Journal

1. Quantum superposition in composite systems of microscopic and macroscopic parts resistant to particle loss and local decoherence, Utkarsh Mishra, Aditi Sen (De), and Ujjwal Sen, *Phys. Rev. A*, **2013**, 87, 052117.
2. Tuning interaction strength leads to ergodic-nonergodic transition of quantum correlations in anisotropic Heisenberg spin model, Utkarsh Mishra, R. Prabhu, Aditi Sen (De), and Ujjwal Sen, *Phys. Rev. A*, **2013**, 87, 052318.
3. Local decoherence-resistant quantum states of large systems, Utkarsh Mishra, Aditi Sen (De), and Ujjwal Sen, *Phys. Lett. A*, **2015**, 379, 261-271.
4. Survival of time-evolved quantum correlations depends on whether quenching is across critical point in XY spin chain, Utkarsh Mishra, Debraj Rakshit, and R. Prabhu, *Phys. Rev. A*, **2016**, 93, 042322.
5. Constructive Interference between disordered couplings enhances multipartite entanglement in quantum Heisenberg spin glass models, point in XY spin chain, Utkarsh Mishra, Debraj Rakshit, and R. Prabhu, Aditi Sen (De), and Ujjwal Sen, *New J. Phys.*, **2016**, 18, 083044.

Utkarsh Mishra

Utkarsh Mishra

Further Publications not used substantially in the thesis

Journal

1. Enhancing robustness of multipartite quantum correlations using weak measurement, Uttam Singh, Utkarsh Mishra, Himadri Shekhar Dhar, *Ann. Phys.*, **2014**, *350*, 50-68.
2. Benford's law gives better scale exponents in phase transitions of quantum XY models, Ameya Deepak Rane, Utkarsh Mishra, Anindya Biswas, Aditi Sen (De), and Ujjwal Sen, *Phys. Rev. E*, **2014**, *90*, 022144.

Preprint

1. Time dynamics of multiparty quantum correlations indicates energy transfer route in light-harvesting complexes, Titas Chanda, Utkarsh Mishra, Aditi Sen (De), and Ujjwal Sen, arXiv:1412:6519 [quant-ph].


Utkarsh Mishra

ACKNOWLEDGEMENTS

First and foremost, I would like to take this opportunity to express my sincere gratitude towards my advisor Prof. Ujjwal Sen for his continuous support during my Ph.D. His guidance and immense knowledge helped me in the course of my research and in writing of this thesis. I am sincerely grateful to my advisor for sharing his illuminating views on a number of problems related to this thesis.

Besides my advisor, I would like to thank Prof. Aditi Sen De and Prof. A. K. Pati, for their continuous encouragement. I am thankful to the members of my thesis advisory committee for their support to continue my research without any obstructions. I express my deep gratitude to the faculty members who have been instructors of the courses that I had credited at HRI. The courses were extremely helpful for me.

It has been a great experience to work with Dr. Prabhu Ramappa (Prabhu da) as a collaborator. He has always been available for my doubts even beyond working hours. Apart from project problems, he has shared details of several papers that fill the gap of understanding the key concepts of the problems. I heartily thank him for all his support and encouragement.

I will never forget all the beautiful moments which I shared with my friends at HRI. I would like to acknowledge all of them for their support. I would like to express my gratitude towards the whole QIC group for their support at various occasions during my Ph.D. time. I am immensely thankful to the administration of HRI, for their help and support. I am thankful for the HPC clusters at HRI, on which all the numerical calculations relevant to this thesis were done.

A special thanks to my family members for their constant support and patience.

Contents

| | |
|---|-------------|
| SYNOPSIS | vii |
| LIST OF FIGURES | xiii |
| LIST OF TABLES | xxv |
| 1 Introduction | 1 |
| 2 Quantum channels | 11 |
| 2.1 Introduction | 11 |
| 2.2 Operator-sum representation of quantum channels | 12 |
| 2.2.1 Bit flip channel | 14 |
| 2.2.2 Bit-phase flip channel | 14 |
| 2.2.3 Phase damping channel | 15 |
| 2.2.4 Amplitude damping channel | 16 |
| 2.2.5 Depolarizing channel | 17 |
| 2.3 Chapter summary | 18 |
| 3 Quantum correlations | 19 |
| 3.1 Bipartite entanglement | 19 |

| | | |
|----------|--|-----------|
| 3.1.1 | Concurrence | 22 |
| 3.1.2 | Logarithmic negativity | 23 |
| 3.2 | Bipartite quantum correlations | 24 |
| 3.2.1 | Quantum discord | 24 |
| 3.2.2 | Quantum work-deficit | 26 |
| 3.3 | Multipartite entanglement | 27 |
| 3.3.1 | Generalized geometric measure | 28 |
| 3.4 | Chapter summary | 29 |
| 4 | Macroscopic quantum superpositions | 31 |
| 4.1 | Introduction | 31 |
| 4.2 | Schrödinger cat state | 32 |
| 4.3 | Characterization of macroscopic quantum superposition | 34 |
| 4.4 | Chapter summary | 36 |
| 5 | A family of robust macroscopic quantum superposition states | 39 |
| 5.1 | Introduction | 39 |
| 5.2 | The $H_{C_N}^m$ state as macroscopic quantum states | 41 |
| 5.3 | Effect of local decoherence on the H-cat state | 42 |
| 5.3.1 | Effect of particle loss on the quantum correlations of the H-cat | 42 |
| 5.3.2 | Effect of depolarizing channel on the quantum correlations of the H-cat | 45 |
| 5.3.3 | Effect of both particle loss and local decoherence on the H-cat | 45 |
| 5.4 | Noise effects on entanglement of other micro:macro states | 49 |
| 5.5 | Effect of decoherence on the $H_{C_N}^m$ state | 51 |
| 5.5.1 | Effect of local phase damping channel on the $H_{C_N}^m$ state . . . | 51 |
| 5.5.2 | Effect of local amplitude damping channel on the $H_{C_N}^m$ | 54 |
| 5.5.3 | Effect of local depolarizing channel on the $H_{C_N}^m$ state | 56 |

| | | |
|----------|---|-----------|
| 5.5.4 | A comparison of the local decohering channels | 57 |
| 5.6 | Effect of decoherence on the GHZ state | 57 |
| 5.6.1 | Effect of local phase damping channel on the GHZ state | 58 |
| 5.6.2 | Effect of local amplitude damping channel on the GHZ state | 59 |
| 5.6.3 | Effect of local depolarizing channel on the GHZ state | 60 |
| 5.7 | Effect of local bit and bit-phase flip channels on the GHZ and the $H_{C_N}^m$ states and their comparison | 62 |
| 5.8 | Effect of local decoherence in other macroscopic quantum states | 65 |
| 5.8.1 | G state | 65 |
| 5.8.2 | $H_{C_N}^{N-1}$ state | 68 |
| 5.9 | Chapter summary | 71 |
| 6 | Behavior of quantum correlations under time evolution of spin models: Ergodicity | 73 |
| 6.1 | Introduction | 73 |
| 6.2 | The model | 75 |
| 6.3 | Statistical mechanical properties | 77 |
| 6.3.1 | Time-evolution | 77 |
| 6.3.2 | Ergodicity and ergodicity Score | 78 |
| 6.4 | Single- and two-site density matrices of time-dependent Heisenberg Model | 79 |
| 6.5 | Ergodicity of physical quantities in quantum XY model | 80 |
| 6.6 | Quantum Heisenberg XYZ spin chain with magnetic field | 81 |
| 6.6.1 | Quantum correlations in equilibrium and evolved states | 81 |
| 6.6.2 | Statistical mechanical properties of quantum correlation mea- sures | 83 |
| 6.7 | Quantum Heisenberg XYZ spin ladder with magnetic field | 85 |
| 6.8 | 2D Quantum Heisenberg XYZ model with magnetic field | 87 |

| | | |
|----------|---|------------|
| 6.9 | Behavior of quantum correlations under sudden quenching in coupling constant in XY spin chain | 88 |
| 6.10 | Instantaneous quenching in the interaction strength | 90 |
| 6.11 | Dynamics of quantum correlations under quenching | 91 |
| 6.12 | Effect of thermal fluctuations | 95 |
| 6.13 | Chapter summary | 97 |
| 7 | Constructive interference between disordered couplings | 101 |
| 7.1 | Introduction | 101 |
| 7.2 | The ordered and disordered quantum Heisenberg models | 102 |
| 7.2.1 | Quenched averaging | 102 |
| 7.2.2 | The Heisenberg quantum spin glasses | 103 |
| 7.3 | Enhancement score for the quenched disordered systems | 104 |
| 7.3.1 | Enhancement score and physical quantities | 104 |
| 7.3.2 | Enhancement score for the Heisenberg quantum spin glasses | 106 |
| 7.4 | Constructive interference between planar and azimuthal couplings in GGM | 109 |
| 7.4.1 | Constructive interference in systems realizable with current technology | 111 |
| 7.4.2 | Approximate GGM and sustenance of Venus regions in larger systems | 113 |
| 7.5 | Chapter summary | 115 |
| 8 | Summary and conclusion | 117 |
| | Appendix | 121 |
| A | LOCC | 121 |
| B | Entropy of entanglement | 122 |

| | | |
|----------|--|------------|
| C | The Jordan-Wigner transformation for the infinite quantum XY spin chain | 123 |
| D | Magnetization in the quantum XY model | 126 |
| E | Nearest-neighbour correlators in the quantum XY model | 127 |
| | References | 129 |

Synopsis

Quantum correlations of shared systems form the backbone for a large majority of information protocols that are either not possible classically or are possible with a reduced efficiency. It has recently been realized that quantum correlations can be a tool in dealing with quantum many-body systems. In the proposed thesis, we investigate the properties of quantum correlations in paradigmatic clean and disordered quantum many-body systems.

We highlight here the main results obtained in the proposed thesis.

- We identify a macroscopic quantum superposition state (Schrödinger cat state) that is resistant to particle loss and all types of decoherence. The resilience to particle loss and noise is better than that in the existing cat states in the literature. These results are published in Refs. [1,3].
- We uncover an ergodic-nonergodic transition of quantum correlations that leads to the identification of a transition in the anisotropic Heisenberg quantum spin model. These results are published in Refs. [2,5].
- We find that quenched disordered couplings in a quantum Heisenberg spin glass model can constructively interfere to enhance genuine multipartite entanglement in the ground state. This result is in Ref. [4].

The content of the proposed thesis is divided into two parts. In the first part of the thesis, we describe our results on “macroscopic quantum superposition states” and effects of local decoherence on the quantum correlation properties of these states. In the second part of the thesis, we explore the connection between quantum information theory and many-body physics in two related contexts. First, we study the dynamics of bipartite quantum correlations and investigate their fundamental statistical mechanical properties in the quantum XYZ Hamiltonian, under quenched dynamics of an external magnetic field, on one-dimensional (1D), quasi 1D (ladder), and 2D lattices. Next, we investigate properties of the multisite quantum and classical correlations in the ground state of an XYZ model with randomly distributed independent quenched Gaussian nearest-neighbor interactions.

Understanding the effects of local quantum decoherence on “macroscopic quantum superposition states” have their importance not only in realizing quantum devices, e.g., quantum computers, but also in addressing fundamental questions, such as the quantum measurement problem and the quantum-to-classical transition. A

“macroscopic quantum superposition state” was first introduced by E. Schrödinger in his seminal 1935 paper through the concept of the Schrödinger cat, which is an entangled state between a microscopic system and a macroscopic one. The microscopic system can be an atom, which can decay spontaneously, with the undecayed state, $|\text{up}\rangle$, and the decayed state, $|\text{down}\rangle$, making up a two-dimensional complex Hilbert space (qubit). The macroscopic system was also conceived as a qubit made up of the alive and dead states of a cat, respectively denoted as $|\text{alive}\rangle$ and $|\text{dead}\rangle$. The quantum state of the combined micro-macro system was considered to be $\frac{1}{\sqrt{2}} (|\text{up}\rangle|\text{alive}\rangle + |\text{down}\rangle|\text{dead}\rangle)$.

Demonstration of micro-macro quantum states in various physical systems, like superconductors, nanoscale magnets, laser cooled trapped ions, photons in a microwave cavity, and C_{60} molecules have been proposed. Moreover, quantumness of such physical states plays an important role in several quantum communication and computational tasks. The advantages of the quantum communication and computation protocols over their classical counterparts vitally depend on the amount of quantum coherence present in the system. For realization of communication networks and computational devices that have a quantum advantage and that are scalable, it is important to identify systems which can retain their quantum coherence even with an increase in the number of particles under decoherence.

We identify a class of macroscopic quantum states which are robust against a large spectrum of physically reasonable local noise models – they are effectively decoherence-free for certain local noisy channels, and weathers decoherence better than other known macroscopic superposition states for the remaining channels.

The robustness of entanglement and other quantum correlations of the entire state is considered in the microscopic to macroscopic partition. The macroscopic part contains, in general, a relatively larger number of particles than the microscopic part. For specificity, we consider quantum states which has an unit amount of entanglement in the micro to macro bipartition.

In case of the Schrödinger cat state, being realized by using the Greenberger-Horne-Zeilinger (GHZ) state, the two macroscopic sectors, modeling the “alive” and “dead” states of the “cat”, are distinguished by their magnetizations. In the case of the cat state that we consider, which we refer to as the H-cat state, the “alive” and “dead” parts are macroscopically distinct in terms of their violations of Bell inequalities. We compute the critical visibilities for the states of the macroscopic sector beyond which they violate local realism.

In order to capture the quantum correlation properties, characterizing the ro-

bustness of the macroscopic superposition state against environmental noise, we calculate logarithmic negativity, an entanglement quantifier, and quantum discord, an information-theoretic quantum correlation measure, of the H-cat states, including the Greenberger-Horne-Zeilinger state. Employing these measures, we observed that the proposed macroscopic superposition state is more robust against loss of a finite fraction of its particles and simultaneously against local decoherence mechanisms, than in other cat states. For example, for 10 particles in the macroscopic part, the H-cat state can preserve entanglement up to 44% of local depolarizing noise, while the GHZ state remains entangled until 28% of the same noise. Quantum discord, with qualitatively similar behavior, becomes $< 5 \times 10^{-4}$ for $p \approx 0.44$ in case of the GHZ state while the same happens for the H-cat state for $p \approx 0.85$, where p represents the properties of local depolarizing noise. We believe that these findings will help us to identify a potential candidate for quantum memory devices.

In the second part of the thesis, we discuss the behavior of quantum correlations in many-body systems described by XYZ (Heisenberg) Hamiltonians, both in “clean” and “disordered” cases. The discussion is in two separate but related contexts. In the first, we consider a clean system, which is quenched to zero at the initial instant. The ensuing dynamics is then investigated and we find that the system supports an ergodic-nonergodic transition. We study the ergodic behavior of quantum correlations, belonging to the entanglement-separability paradigm and the information-theoretic one, by analyzing their properties, in the equilibrium as well as the time-evolved state of the quantum anisotropic XYZ model, in 1D, quasi 1D, and 2D lattices. The logarithmic negativity and the concurrence are considered as measures belonging to the former paradigm while quantum discord and quantum work-deficit are considered as those of the latter one. We find that although the entanglement measures are ergodic irrespective of the system parameters, the information-theoretic measures exhibit a rich picture with respect to their statistical-mechanical properties. Specifically, we find that the zz-interaction strength has a crossover value, for a given xy anisotropy and a given information-theoretic quantum correlation measure, that indicates a transition from nonergodic to ergodic behavior for that measure. The qualitative features of the measures in the entanglement-separability paradigm and the information-theoretic one are the same in the one-dimensional, ladder, and two-dimensional square lattices. However, in the square lattice, the information-theoretic measures are more sensitive to the change of the zz-interaction strength than in other dimensions. Such a dimension-dependent change of ergodic behavior is absent for the entanglement measures.

In the second “context” of the second part, we consider quenched disordered quantum spin-models and investigate their quenched averaged quantum correlations. There are two different disorder interactions that are considered, and we refer to them as “planar” and “azimuthal” disorders. We analyse the effects of these disorders on the ground state, for bipartite and multipartite, classical and quantum, correlations. More precisely, we examine the behavior of (single-site) magnetization, two-site classical as well as quantum correlations, and multipartite entanglement, measured by the generalized geometric measure, for the ground states of the corresponding Hamiltonian. The relevant results are presented for various system sizes, ranging from five to twenty quantum spin-1/2 particles. While the small systems were dealt by exact numerical diagonalization, we adopt the density matrix renormalization group techniques to investigate comparatively larger spin systems. We find that in the presence of impurities in the couplings, there exists different parameter regions for different observables which show enhancement due to disorder – also known as the order from disorder phenomenon. The physical quantities like magnetization, classical correlators, bipartite and multipartite entanglement always find a range of parameters in which they increase with the introduction of disorder. Perhaps more radically, our studies uncover the novel phenomenon of constructive interference of disordered couplings, where we observe that the parameters of the system can be tuned in such a way that disorder-induced order appears due to simultaneous presence of randomness in two different couplings, while it is absent when disorder is present individually in either of the couplings. Interestingly, the constructive interference, which is caused due to the interplay between competing random coupling strengths in different directions, appears only in the multipartite entanglement, and is absent in bipartite as well as single-site physical quantities considered, exhibiting the significance of multiparty observables in cooperative physical phenomena. We believe that the results obtained in the proposed thesis will be important for both fundamental and practical aspects of the emerging field of quantum information technology.

REFERENCES

1. *Quantum superposition in composite systems of microscopic and macroscopic parts resistant to particle loss and local decoherence*,
Utkarsh Mishra, Aditi Sen(De), and Ujjwal Sen, Phys. Rev. A **87**, 052117 (2013).
2. *Tuning interaction strength leads to an ergodic-nonergodic transition of quantum correlations in the anisotropic Heisenberg model*,
Utkarsh Mishra, R. Prabhu, Aditi Sen(De), and Ujjwal Sen, Phys. Rev. A **87**, 052318 (2013).
3. *Local decoherence-resistant quantum states of large systems*,
Utkarsh Mishra, Aditi Sen(de), and Ujjwal Sen, Phys. Lett. A **379**, 261 (2015).
4. *Constructive interference between disordered couplings enhances multiparty entanglement in quantum Heisenberg spin glass models*,
Utkarsh Mishra, Debraj Rakshit, R. Prabhu, Aditi Sen (De), and Ujjwal Sen, New J. Phys.**18**, 083044 (2016).
5. *Survival of time-evolved quantum correlations depends on whether quenching is across critical point in XY spin chain*,
Utkarsh Mishra, Debraj Rakshit, and R. Prabhu, Phys. Rev. A **93**, 042322 (2016).

List of Figures

| | | |
|-----|---|----|
| 2.1 | Schematic diagram showing the process of evolution of a quantum system, S , represented by a density matrix ρ_S , defined on the Hilbert space \mathcal{H}_S . An initial quantum state of the principal system is combined with an environment such that the system and environment are in a product state. The combined system is evolved using a global unitary operator acting on the Hilbert space, $\mathcal{H}_S \otimes \mathcal{H}_E$, with \mathcal{H}_E being the Hilbert space corresponding to the environment. At the end of the evolution, the environment degrees of freedom are traced out and the resulting expression is a representation of the system's evolution alone. | 13 |
| 3.1 | Concurrence (C), quantum-discord (QD) and logarithmic negativity (LN) of the Werner state (Eq. 3.8) against the parameter λ | 25 |
| 4.1 | Schematic representation of Schrödinger's cat paradox experiment. | 33 |
| 5.1 | Entanglement after particle loss in H-cat state. The horizontal axis represents the number of particles lost (l) from the macroscopic part of the H-cat state while the vertical one represents the entanglement between the micro and the macro parts of the H-cat state after particle loss. The entanglement with respect to l is plotted for different initial number of particles, N . The vertical axis is measured in ebits, while the horizontal one is in particles. | 43 |
| 5.2 | Quantum discord after particle loss in H-cat state. Other notations are the same as in Fig. 5.1. | 44 |

| | | |
|-----|--|----|
| 5.3 | Entanglement of GHZ and H-cat states against local decoherence. While the continuous lines are for the GHZ states, the discontinuous ones are for the H-cat. The horizontal axis represents the dimensionless (decohering noise) parameter p , and the vertical axis is the entanglement in the micro : macro bipartition (in ebits). | 46 |
| 5.4 | Quantum discord of GHZ and H-cat states against local decoherence. We plot the quantum discord (in ebits) on the vertical axis against the depolarizing parameter p (dimensionless) on the horizontal axis. The dashed line is for the GHZ state, while the continuous one is for the H-cat. The system is of 8 particles, so that $N = 7$. The states are led into local depolarizing channels at all the parties. The quantum discord of the output state is calculated in the micro : macro partition, where the measurement is carried out in the micro part. | 47 |
| 5.5 | Effect of local decoherence and particle loss on H-cat state. Entanglement (measured in ebits) in the micro : macro bipartition is plotted on the vertical axis against a base of the dimensionless depolarizing parameter p , and the number of lost particles (l). The H-cat state under consideration is of 11 qubits, so that $N = 10$ | 48 |
| 5.6 | Effect of local decoherence and up to 10% particle loss on a H-cat state of $10^3 + 1$ qubits. All other considerations except the values of N and l are the same as in Fig. 5.5. The inset shows the details near $p = 0$ | 49 |

| | | |
|------|--|----|
| 5.7 | Entanglement and quantum discord of the local phase damped $H_{C_N}^m$ state. We plot the logarithmic negativity (in ebits) and quantum discord (in bits) on the vertical axes versus the decoherence parameter p (dimensionless) on the horizontal axes, for the $H_{C_N}^m$ state, after each of the qubits are affected by phase damping noise. The plots are displayed for $m = 1, 2$, and 3 . Note that for $m = 1$, the $H_{C_N}^m$ state is the same as the H_C state. All plots are for $N = 6$ and for $k = 1$. Here, and in the rest of the paper, we mostly plot the curves for the different quantities for a modest number of particles in the large sector (which, in the current case implies that we are dealing with a $2^7 \times 2^7$ matrix). This is despite the fact that in many cases, we can consider bigger system sizes and even have analytical results for arbitrary N . We however feel that the curves for the relatively modest system sizes will give the reader a feeling of the situation in a potential experimental realization of the phenomena considered. . . . | 52 |
| 5.8 | Independence of quantum discord of the local phase damped $H_{C_N}^1$ state on the number of particles in the macroscopic sector. Quantum discord (in bits) for the $H_{C_N}^1$ state (i.e., the H_C state) for different values of N after the state is local phase damped, is plotted on the vertical axis, against the decoherence parameter p (dimensionless) on the horizontal axis. Here, the microscopic part of the state consists of a single particle (i.e., $k = 1$). This shows that the quantum discord, like entanglement, is independent, up to numerical accuracy, of size of the macroscopic sector. A similar feature holds for higher values of k . The inset shows the same figure blown up near $p = 0$ | 54 |
| 5.9 | Independence of quantum discord of the local amplitude damped $H_{C_N}^m$ state on the number of particles in the macroscopic sector. All other considerations are the same as in Fig. 5.8, except that we do not have the inset here. | 55 |
| 5.10 | Logarithmic negativity and quantum discord against the noise parameter of amplitude damping channel, for the local amplitude damped $H_{C_N}^m$ state. All other considerations are the same as in Fig. 5.7. . . . | 56 |
| 5.11 | Logarithmic negativity and quantum discord for the local depolarized $H_{C_N}^m$ state against the noise parameter of the depolarizing channel. All other considerations are the same as in Fig. 5.7. | 57 |

- 5.12 How much quantum correlation is retained against which noise? Logarithmic negativity and quantum discord for different noisy channels in the micro : macro bipartition for the $H_{C_N}^1$ state for $k = 1$. Here we have taken $N = 6$. The vertical axes are in ebits for logarithmic negativity and in bits for quantum discord. The dimensionless parameter p on the horizontal axes corresponds to the noise parameter in the LPDC, the LADC, or the LDPC. 58
- 5.13 Comparison of the entanglements of the local amplitude damped $H_{C_N}^m$ and GHZ_{N+k} states. We plot here the difference, \mathcal{D} , between the logarithmic negativities (logarithmic negativity of the noisy $H_{C_N}^m$ state minus that of the noisy GHZ_{N+k} state) of the local amplitude damped $H_{C_N}^m$ and GHZ_{N+k} states for $k = 1$ and $m = 1, 10, 20, 30$, on the vertical axes, against the amplitude damping parameter, p , on the horizontal axes, for different number of qubits, N , in the macroscopic part. The logarithmic negativities are measures in ebits, while N is measured in qubits. p is a dimensionless parameter. The curves are plotted in the respective cases only up to a certain value of N , that depends on m . For higher N , the curves are always positive with respect to the vertical axis. The highest value of N , for a given m , that is plotted in a given panel, is however not necessarily the highest value of N , for which $\mathcal{D} \geq 0$ for all p . The $\mathcal{D} = 0$ line is marked on all the panels for ease of reference. 61
- 5.14 The panels are the same as in Fig. 5.11, except that there is an additional curve in each panel corresponding to the GHZ state for $k = 1$, $N = 6$. See Table I for numerical values. 62
- 5.15 $H_{C_N}^1$ (left panel) and GHZ (right panel) after being affected by local depolarizing channels for different number of particles in the macroscopic sectors. The vertical axes represent logarithmic negativity (in ebits) in the micro : macro bipartition, the horizontal axes correspond to the depolarizing parameter, p (dimensionless). We choose $N = 6$. As is clear from the panel on the right, increase of k for a fixed N leads to increase in logarithmic negativity for the GHZ state. The insets reveal the situations where the entanglements vanish. The axes of the insets represent the same quantities as of the corresponding parent figures. 63

| | | |
|------|--|----|
| 5.16 | The panels are the same as in Fig. 5.12, except that all the curves correspond now to the noise-affected GHZ states instead of the $H_{C_N}^1$ states. Comparing the panels here with those of Fig. 5.12, we see that the noise-affected GHZ states behave very differently from the corresponding noise-affected $H_{C_N}^1$ states. This is especially true for the entanglements of the local phase damped states and for the quantum discords of the states after being affected by any type of noise. . . . | 63 |
| 5.17 | Effect of local bit flip error on the $H_{C_N}^m$ state for $N = 6, 8, 10$, $m = 1$, and $k = 1$ with respect to its logarithmic negativity and quantum discord in the $\mu : M$ bipartition. Other considerations are the same as in Fig. 5.7. | 64 |
| 5.18 | Entanglement of the noisy G state depends on the number of particles in the macroscopic sector. The logarithmic negativity (in ebits) of the noisy G state is plotted on the vertical axes against the decohering parameter p (dimensionless) on the horizontal axes, for different values of N . The left panel is for the local phase damping channels while the right one is for the local amplitude damping channels. | 68 |
| 5.19 | The panels here are the same as in Fig. 5.12, except that the curves here pertain to the noisy G states. For numerical values, see Table I. | 69 |
| 5.20 | The plot here is the same as the left panel in Fig. 5.14, except that the curve for the GHZ state is replaced by that for the G state. The inset shows a magnified view of the curves in an intermediate zone. The numerical values of p at which the entanglements vanish, for the different states, are given in Table I. | 70 |
| 5.21 | The panels in this figure are the same as in Fig. 5.18, except that here they are for the $H_{C_N}^{N-1}$ state. | 71 |
| 5.22 | The panels in this figure are the same as in Fig. 5.12, except that here they pertain to the $H_{C_N}^{N-1}$ state, for $N = 6$ | 71 |

- 6.1 Behavior of quantum correlations in the equilibrium state. We plot quantum correlation measures of nearest-neighbor reduced states of the canonical equilibrium states, for a system of 12 quantum spin- $\frac{1}{2}$ particles arranged as a ring and described by the Hamiltonian H with respect to $J\beta$, and the relative strength of the zz -interaction, δ , for different values of γ . The left plots are for logarithmic negativity and the right ones are for quantum discord. The left plots are for $\gamma = 0.2$ while the right one are for $\gamma = 0.8$. Quantum discord is measured in bits. All other axes in the figures correspond to dimensionless parameters. 82
- 6.2 Quantum correlations of the time-evolved states. The system under consideration is the same as in Fig. 6.1, but for 8 spins. The evolution is assumed to begin in the equilibrium state at $t = 0$ and at an exemplary value of the temperature given by $J\alpha = 20$. Logarithmic negativity (top plots) and quantum discord (bottom plots) of the nearest-neighbor reduced states of the time-evolved states, are plotted against the initial magnetic field, a , and $\frac{Jt}{\hbar}$, for different values of δ . Here we choose $\gamma = 0.8$. The left plots are for $\delta = 0.2$ and the right ones are for $\delta = 0.8$. All axes correspond to dimensionless quantities except those for quantum discord, which is measured in bits. 83
- 6.3 Ergodicity score for quantum discord. The ergodicity score for quantum discord of the anisotropic Heisenberg XYZ chain (with a magnetic field) of 8 spins, arranged in a ring, is plotted against δ and the applied initial magnetic field a , for a fixed $\gamma = 0.8$. The initial state of the time-evolution is the $t = 0$ canonical equilibrium state at a temperature given by $J\alpha = 20$. The ergodicity score is measured in bits. All other physical parameters used in the figure are dimensionless. 84

- 6.4 Comparing ergodicity scores for quantum discord and quantum work-deficit. The ergodicity score for quantum discord (left) and quantum work-deficit (right) of the nearest-neighbor reduced state of the time-evolved states of the anisotropic Heisenberg XYZ chain (with a magnetic field) of 12 spins, arranged in a ring, is plotted against δ , for different values of γ and a for fixed initial magnetic field $a = 0.6$. Here we choose $J\alpha = 20$ for the $t = 0$ canonical equilibrium state from which the evolution starts off. The depicted curves are for $\gamma = 0.4$ (red circles), $\gamma = 0.6$ (pink triangles), and $\gamma = 0.8$ (green squares). The ergodicity score for quantum discord is measured in bits, while that for quantum work-deficit is measured in qubits. All other quantities used in the figure are dimensionless. 85
- 6.5 Behavior of quantum correlations in the equilibrium state. We plot quantum correlation measures of nearest-neighbor reduced states of the canonical equilibrium states, for a system of 8 quantum spin- $\frac{1}{2}$ particles arranged as a ladder and described by the Hamiltonian H with respect to $J\beta$, and the relative strength of the zz -interaction, δ , for different values of γ . The top plots are for logarithmic negativity and the bottom ones are for quantum discord. The left plots are for $\gamma = 0.2$ while the right one are for $\gamma = 0.8$. Quantum discord is measured in bits. All other axes in the figures correspond to dimensionless parameters. 86
- 6.6 Ergodicity curves in the Heisenberg XYZ ladder. The ergodicity scores of quantum discord (left) and quantum work-deficit (right) of a nearest-neighbor reduced state, along a rail, of the time-evolved state, in the ladder, of 8 spins is plotted with respect to the relative strength of the zz -interactions. The transition points, where the system moves from nonergodic to ergodic behavior of the information-theoretic measures are qualitatively similar to those in one-dimension, for a fixed γ . The depicted plots are for $\gamma = 0.4$ (red circles), $\gamma = 0.6$ (pink triangles) and $\gamma = 0.8$ (green squares). For the evolved state, $a = 0.6$, $J\alpha = 20$. The units are the same as in Fig. 6.4. 87

- 6.7 Ergodicity scores in the 2D Heisenberg XYZ model. The ergodicity scores of quantum discord (left) and quantum work-deficit (right) in the nearest-neighbor reduced state of the time-evolved state, with respect to the strength of the zz -interaction for the anisotropic Heisenberg XYZ model on a 2D square lattice, consisting of 12 spins in a torus. The plots are for $\gamma = 0.6$ (pink triangles) and $\gamma = 0.8$ (green squares). For the time-evolved state, $a = 0.6$, $J\alpha = 20$. The units are the same as in Fig. 6.4. 88
- 6.8 The quenching scheme employed in section 6.9. In case A , the final coupling constant is fixed in the disordered phase, i.e., $\tilde{J}_2 < 1$. In case B , the final coupling constant is fixed in the region of ordered phase, i.e., $\tilde{J}_2 > 1$. In both the cases, the initial coupling constant \tilde{J}_1 is varied from the values ranging from the disorder to the ordered phase. Such situations cover both the scenarios i.e., when \tilde{J}_1 and \tilde{J}_2 are in same phase or \tilde{J}_1 and \tilde{J}_2 are different phases. All quantities are dimensionless. 89
- 6.9 Dynamics of nearest neighbor concurrence (left) and quantum discord (right) in the evolved state of quantum XY model against time, t , and quenched coupling \tilde{J}_1 . The final coupling is fixed at $\tilde{J}_2 = 0.5$. We choose $\gamma = 0.5$. The base axes represent dimensionless quantities, while the vertical axis in the top (right) panel is in ebits (bits). 91
- 6.10 Variation of the nearest neighbour concurrence (left panel) and quantum discord (right panel) of the evolved state in XY model with respect to quenched coupling constant \tilde{J}_1 and t , where $\tilde{J}_2 = 2.0$ and $\gamma = 0.5$. The dimensions are the same as in Fig. 6.9. 93
- 6.11 (a) Plot of the difference in entanglement between the final and the initial two-site states, δC , in the quantum XY spin chain against \tilde{J}_1 and \tilde{J}_2 . The negative values (the blue regime) in the difference indicates that the initial bipartite entanglement is more as compared to the final bipartite entanglement in the $J_1 - J_2$ plane, while the positive value (the red regime) reveals that bipartite entanglement is enhanced during dynamics compared to the initial state. Here $\gamma = 0.5$ and $h = 1.0$. (b) The plot of the difference in quantum discord between the final and the initial two-site states, δD . The dimensions are same as in Fig. 6.9. 94

- 6.12 Long-time behavior of the nearest neighbor concurrence in the quantum XY model with sudden quenching in the couplings. The coupling strengths J_1 and J_2 are varied from 0 to 3. The anisotropy parameter of the Hamiltonian is fixed at $\gamma = 0.5$. The different plots are for different values of β of the initial quantum state. (a) $\beta \rightarrow \infty$, (b) $\beta = 3.0$. (c) $\beta = 2.0$, and (d) $\beta = 0.8$. All the quantities are dimensionless, except concurrence, which is in ebits. 96
- 6.13 Long-time behavior of quantum discord of nearest-neighbour spins in the infinite quantum XY chain with sudden quenching in the couplings. Other details are same as in Fig. 6.12, except that quantum discord is measured in bits. 97
- 7.1 Order from disorder in the planar spin glass. The enhancement scores ($\Delta_\lambda^{\mathcal{Q}}$) for different physical quantities are plotted in the different panels. In all cases, the disordered Hamiltonian is $H_{\langle J \rangle}$, while the ordered one is H . For the plots, we consider a system of 6 spins. And, we choose $\gamma = 0.7$ and $h = 0.8$. The planar spin glass Hamiltonian consists of 6 i.i.d Gaussian random variables, J_{ij} , which are each of mean $\langle J \rangle$ and standard deviation unity. The quantities that are plotted here are the enhancement scores for (a) magnetization ($\Delta_\lambda^{M_z}$), (b) the zz -classical correlator ($\Delta_\lambda^{T_{zz}}$) (c) bipartite quantum correlation as quantified by concurrence (Δ_λ^C), and (d) genuine multipartite quantum correlation measure quantified by GGM ($\Delta_\lambda^{\mathcal{E}}$). In these panels, the quantities along ordinates are $\langle \lambda \rangle$, while the abscissae represent the μ . Quenched average of the observable is performed over 5×10^3 random realizations. The regions represented in red are the ones for which $\Delta^{\mathcal{Q}}$ is positive indicating that the corresponding physical quantity \mathcal{Q} attains a higher value with the introduction of disorder in these regions. The areas represented in blue are the ones for which $\Delta^{\mathcal{Q}}$ is negative and they point to parameter regions where the \mathcal{Q} is higher in the corresponding clean system. In the white regions, \mathcal{Q} remains unaltered by the introduction of disorder in the system. All the parameters plotted here are dimensionless. 105

- 7.2 Order from disorder in azimuthal spin glass. The plots in the different panels are for (a) $\Delta_{\mu}^{M_z}$, (b) $\Delta_{\mu}^{T_{zz}}$, (c) Δ_{μ}^C , and (d) $\Delta_{\mu}^{\mathcal{E}}$. The disordered Hamiltonian for the enhancement scores is $H_{\langle\delta\rangle}$, whose 6 i.i.d. Gaussian random variables, δ_{ij} , have mean $\langle\delta\rangle$ and unit standard deviation. In each of these panels, the ordinate is λ and the abscissa is $\langle\mu\rangle$. All other considerations are the same as in Fig. 7.1. 107
- 7.3 Order from disorder when both planar and azimuthal couplings are quenched disordered. The plots in the different panels are for (a) $\Delta_{\lambda,\mu}^{M_z}$, (b) $\Delta_{\lambda,\mu}^{T_{zz}}$, (c) $\Delta_{\lambda,\mu}^C$, and (d) $\Delta_{\lambda,\mu}^{\mathcal{E}}$. The disordered Hamiltonian in this case is $H_{\langle J, \delta \rangle}$. The J_{ij} (δ_{ij}) are i.i.d. Gaussian random variables with mean $\langle J \rangle$ ($\langle \delta \rangle$) and unit standard deviation. In the panels, the ordinates represent $\langle \lambda \rangle$ while the abscissae represent $\langle \mu \rangle$. All other considerations are as in Fig. 7.1. 109
- 7.4 Constructive interference. The panels exhibit plots with the enhancement score of GGM, denoted as $\Delta^{\mathcal{E}}$, as the ordinate, and the system parameter, α , as the abscissa for Heisenberg spin glasses with (a) $N = 5$, (b) $N = 6$, (c) $N = 7$, and (d) $N = 8$, where N is the number of quantum spin-1/2 particles in the system. In all these plots, red circles connected with dashed lines represent the cases when disorder is present in both the couplings (planar as well as azimuthal), and for these cases, α represents $\langle \lambda \rangle$ and $\Delta^{\mathcal{E}}$ represents $\Delta_{\lambda,\mu}^{\mathcal{E}}$. We choose $\langle \delta \rangle = -0.9$. The blue squares connected with dotted lines are for the cases when disorder is present only in the planar coupling. In these cases, α represents $\langle \lambda \rangle$, $\Delta^{\mathcal{E}}$ represents $\Delta_{\lambda}^{\mathcal{E}}$, and δ is fixed at -0.9 . The green triangles connected with dash-dotted lines represent the cases when disorder is present only in the azimuthal coupling. In these cases, α represents λ , $\Delta^{\mathcal{E}}$ represents $\Delta_{\mu}^{\mathcal{E}}$, and $\langle \delta \rangle = -0.9$. The black solid lines, parallel to the horizontal axes are drawn to separate the positive and negative regions of the enhancement score of GGM. For all the plots, we have chosen $\gamma = 0.7$ and $h = 0.8$. All quantities plotted here are dimensionless. 110
- 7.5 The enhancement scores for (a) magnetization, M_z , (b) T_{zz} -correlator, and (c) concurrence, C , against α for systems with $N = 6$. All other descriptions are the same as given in Fig. 7.4. 112

- 7.6 DMRG data of the enhancement score $\Delta^{\mathcal{E}^{(2)}}$ as a function of α for (a) $N = 8$, (b) $N = 12$, (c) $N = 16$, and (d) $N = 20$. All other descriptions are the same as in Fig. 7.4. The insets show blow-ups of the regions with constructive interference. 113
- 7.7 The DMRG data of the enhancement scores for (a) magnetization, M_z (b) classical correlator, T_{zz} , and (c) concurrence for systems with $N = 20$. All other considerations are the same as given in Fig. 7.4. The magnetizations used here in panel (a) are for the site $N/2$ 114

List of Tables

5.1 Comparison of “critical values” of decoherence at which the entanglement vanishes for different states under different noisy channels. The critical point has been taken at the value of decoherence parameter where logarithmic negativity becomes less or equal to 10^{-4} . The values are exhibited as percentages of the noise level that the corresponding state can sustain before becoming separable. The states considered to construct this Table consists of one qubit in its minuscule sector and six qubits in its large sector. The first column shows the type of local noise acting on the state. The second, third, fourth, fifth, sixth, seventh, and eighth columns exhibit the critical values for the $H_{C_N}^1$, $H_{C_N}^2$, $H_{C_N}^3$, GHZ, G , $H_{C_N}^{N-1}$, and $H_{C_N}^N$ states respectively. The G state appears in Eq. (5.31). Note that the critical values for the GHZ and $H_{C_N}^N$ states are the same for the LPDC and LDPC, while they differ for the LADC. 65

Introduction

Quantum mechanics has been a subject of interest for many research communities including physicists, philosophers, chemists, biologists, mathematicians and computer scientists. For a long time, the fundamental concepts of quantum mechanics seemed mysterious and for example questions were raised on the completeness of the theory [1]. Despite all these, the theory has emerged as a successful one for explaining many phenomena, especially in the microscopic world, and its predictions matches with experiments very precisely. Quantum information theory [2] is a subject which deals with situations where laws of quantum mechanics are used in storing, processing, and communicating *information*. This technique of information manipulation has been fruitful in enhancing efficiencies of certain communication and computation protocols, reducing the required physical resources for communication, and inventing information processing tasks that were impossible in the classical domain. Numerous quantum information processing protocols [3–6] and computational algorithms [7–10] have been developed and several have been experimentally implemented in the laboratories across the world [11–19]. A key resource in these protocols is identified as quantum correlations [20, 21], such as entanglement [1]. Entanglement [1, 20, 22] is a distinctive correlation, that has no classical counterpart. A widely used definition of entanglement is in terms of local (quantum) operations and classical communication (LOCC)¹. Entanglement is a property present exclusively in entangled quantum states, the latter being those that cannot be prepared using LOCC [23, 24]. Entanglement has been used as a resource in various quantum information and computation tasks [25], which are either impossible using classical resources or possible with reduced efficiencies. Some of the fundamental quantum protocols that exploit

¹See Appendix A for a definition of LOCC.

entanglement are quantum dense coding [3], quantum teleportation, quantum error-correction [5], entanglement-based quantum cryptography [6], and one-way quantum computation [10]. Several non-classical phenomena have however been discovered in which entanglement is absent or potentially irrelevant [26–45]. To understand and quantify the resource necessary for exhibiting such non-classicality, an information-theoretic approach to quantum correlations have been proposed [21, 46–51]. Similar to entanglement, information-theoretic quantum correlations also have no classical analogy, in general. Along with being proposed as a resource, quantum correlations also find applications in many-body systems [52–68], for example in studying the critical phenomena, and more recently, in looking for the possibility of coherence in biological systems [69–74].

One of the challenges of realizing quantum information processing tasks is the control of composite quantum systems evolving in the presence of environmental noise [2]. For example, for certain quantum communication protocols, a quantum correlated state acts as a channel between two or more parties to perform the protocol, and the performance of the protocol depends on the amount of quantum correlation present in the state. For instance, in quantum teleportation [4], perfect teleportation is possible only if two parties share a maximally entangled state. However, quantum correlations can be very fragile against environmental effects [2], and may vanish due to the onslaught of temperature, magnetic field, or other external noise. This is one of the main obstacles for practical implementation of quantum computing and information processing tasks. Therefore, it is very important to maintain the initial quantum correlation in a shared state in order to achieve quantum advantage in communication and computation protocols. Hence, to understand the usefulness of a quantum correlated state, consideration of external environment is very important in a given protocol. The action of the environment is defined by the type of error introduced in the state while performing the protocol. For example, if a quantum bit (qubit) is acted upon by an environment that flips the bits that define the qubit, it can mathematically be represented by the action of the Pauli operator, σ^z , on the qubit. A general quantum theory that models and characterizes such environmental effects in quantum information theory is studied under the *quantum operations* formalism [75–81]. We discuss the general formalism of quantum operations in chapter 2. In particular, we consider the Kraus decomposition for completely positive and trace preserving channels. We then discuss several model environments in terms of quantum channels.

Quantum correlations in a multipartite quantum state can be categorized into

two broad paradigms: the entanglement-separability and the information-theoretic. The idea of characterizing quantum correlations in the entanglement-separability paradigm is based on the assumption that the product or separable states have no quantum correlations. Examples of measures for two-party quantum states that are based on the entanglement-separability paradigm are entanglement of formation (E_F) [24, 82], entanglement cost (E_C) [23, 83], distillable entanglement (E_D) [23, 24], concurrence (C) [82], and logarithmic negativity (E_N) [84–89]. The other approach is to define quantum correlation within an information-theoretic paradigm. Examples of bipartite quantum correlations that belong to this paradigm are quantum discord [47] and quantum work-deficit [48]. In chapter 3, we discuss about the bipartite quantum correlations of both the paradigms. We also briefly consider multipartite quantum entanglement and its quantification.

One of the requirements for scalability of quantum information processing and computation protocols is the generation of quantum correlated states of a large number of particles. Moreover, entanglement of certain multipartite states have their importance in understanding the fundamental concepts of quantum mechanics. A Quantum state that is important from a fundamental perspective, as well as from the perspective of applications, is the Schrödinger cat state [22], that has, for example, been used to understand the validity of quantum correlations at macroscopic scale. It is an entangled state between a “microscopic” and “macroscopic” system. The microscopic system can be an atom, which can decay spontaneously, with the undecayed state, $|\text{up}\rangle$, and the decayed state, $|\text{down}\rangle$, making up a two-dimensional complex Hilbert space (qubit). The macroscopic system was also conceived as a qubit made up of the “alive” and “dead” states of a cat, respectively denoted as $|\text{alive}\rangle$ and $|\text{dead}\rangle$. As we have not seen a cat being simultaneously in states of dead and alive, this thought experiment has triggered a debate on the validity of the fundamental principles of quantum mechanics at the macroscopic scale. Several interpretations have been given in order to settle this “paradox”. One argument, albeit a contested one, that provides a reason for the difficulty in the observation of the alive and dead cat states simultaneously, is the *decoherence* mechanism [90]. This is related to the fundamental question: does there exist any limit on the system size beyond which the quantum effects are not observable?

The question of existence of the quantum superposition principle at the macroscopic scale has been investigated extensively in the past (see [91], for a review, and references therein). The basic idea is to investigate the quantuness of a superposition state composed of macroscopic objects that are distinguishable at the macroscopic

scale, like the $|\text{alive}\rangle$ and the $|\text{dead}\rangle$ states of the cat in the Schrödinger’s thought experiment. To investigate this from the point of view of experimental scenarios, the macroscopic objects, e.g., the cat, can be replaced by states of multiparty systems. In that case, a cat-like state is written as $|\Psi\rangle \propto |A_N\rangle + |B_N\rangle$, where $|A_N\rangle$ and $|B_N\rangle$ are states of systems made of several particles, and are distinguishable in some sense, like the alive and the dead cats. This idea of replacing macroscopic degrees of freedom with quantum states of multiparty systems in order to capture the essence of the Schrödinger cat state in a real experiment has, e.g., been discussed in Leggett [92], Mermin [93], and of course, Schrödinger [22]. The current experimental limit of a Schrödinger cat state that has been prepared, e.g., in the ion trap, is a 14-qubit state [94]. We describe the Schrödinger cat thought experiment and a few proposed methods to detect macroscopicity in chapter 4.

The classic example of a Schrödinger cat state is the Greenberger-Horne-Zeilinger (GHZ) state [95,96] (for experimental demonstrations, see e.g., [94,97–99]). Demonstration of Schrödinger like cat states in various physical systems, like superconductors [100–104], nanoscale magnets [105–107], laser cooled trapped ions [108], photons in a microwave cavity [109], and C_{60} molecules [110] have been proposed. Macroscopic quantum superposition in superconducting quantum interference devices (SQUID) [111] has already been experimentally achieved (see also [112–114]). There is therefore a need to characterize macroscopic quantum superposition states also for understanding of these recent experimental developments [92,115–125].

An interesting decoherence model that one can consider while studying macroscopic superpositions is the loss of particles from the state. For example, if one prepares a quantum state with polarization degrees of three or four photons, and pass it to an absorptive optical cavity, a most natural environment effect would be loss of photons. Therefore, apart from the dissipative and dephasing effects it is important also to consider the effect of particle loss from the macroscopic sector of the state. However, as is well-known, the GHZ state loses *all* quantum coherence if even a single qubit is lost. For the study of noise effects on the GHZ state, see e.g., [126–134] (See [135–141] for further work in this direction). Therefore, it is interesting to construct quantum superposition states of large particles that are robust to both kinds of decoherence: particle loss as well as particle number preserving quantum decoherence mechanisms. In chapter 5 of the thesis, we will investigate robustness properties of several quantum states, akin to the Schrödinger cat, and will identify states that better withstand decoherence as compared to the GHZ state. In particular, we identify a class of macroscopic quantum states, the $H_{C_N}^m$ states, whose

macroscopic sector is built by using W states [142–145], or more generally, Dicke states [146] with m excitations, and by an orthogonal product state. We introduce the explicit form of this class of states in chapter 5. In this chapter, we also study the effect of local decoherence on the quantum correlation properties of the $H_{C_N}^m$ states.

In chapters 6 and 7 of the thesis, we study the behavior of quantum correlations in large quantum systems. Investigation of quantum correlations in many-body systems have gained considerable interest in the past years and is important for the efficient use of such systems for quantum information technologies. The wide interest in such activities is also due to the fact that several concepts developed in quantum information science turn out to be useful tools to detect co-operative phenomena [54,65,147], like quantum phase transitions [148,149], and can help to develop approximate methods to obtain the ground states of non-integrable systems [150–152]. We consider quantum spin systems and explore the connection between quantum information theory and many-body physics in two related contexts. First, we study the dynamics of bipartite quantum correlations and investigate their fundamental statistical mechanical properties in the quantum XY and XYZ Hamiltonian, under quenched dynamics of an external magnetic field, on one-dimensional (1D), quasi 1D (ladder), and 2D lattices. Next, we investigate properties of the multisite quantum and classical correlations in the ground state of an XYZ model with randomly distributed independent quenched Gaussian nearest-neighbor couplings.

Investigation of many-body systems in the non-equilibrium regime from a quantum information perspective [10, 54, 153–165] have gained interest in recent years. In this respect, dynamical evolution of a closed many-body quantum system under sudden quench have been studied extensively [166–172]. Note that, experimentally realizable physical systems, e.g., ultracold atoms in an optical lattice [173], can be prepared in a controlled way, making them effectively isolated from the environment [17]. This, in turn, has generated a lot of interest in recent times in the nonequilibrium dynamics of otherwise closed quantum systems due to external disturbance, both experimentally [174–177] and theoretically [153, 178–184].

Quenching, which involves sudden change in certain parameters of the system, has attracted interest, in particular, due to their feasibility in experiments using, for example, cold atomic gases [185–187] (for a review, see [153]). Spin magnetic systems subjected to sudden quenching have been shown to exhibit non-intuitive behavior, e.g., revival and collapse phenomena of the nearest-neighbor entanglement in the quantum XY model [61,184]. Sudden quenching in XY model has been performed to

investigate the long time behavior of entanglement in the system [188](cf. [189, 190]). It was observed that the entanglement of the time evolved state in the XY model does not approach to its equilibrium value. This observation was argued to characterize the ergodicity of entanglement and was related with the validity of a statistical mechanical description for entanglement [188]. A statistical mechanical description of a physical quantity is valid only when the time-average of the quantity matches with its ensemble average, and in that case, the physical quantity is termed as ergodic. Ergodicity of physical quantities in spin models has been of interest to researchers for a long time [188–200]. In particular, the question of ergodicity of physical quantities like magnetization, classical correlations, entanglement, quantum discord, and quantum work-deficit in quantum XY spin chains have been investigated [188, 189, 191, 192, 201, 202].

In chapter 6, we consider the validity of the statistical mechanical description of quantum correlation measures of anisotropic Heisenberg models in one-dimension, ladder, and two-dimension [203]. Specifically, we find that the entanglement measures remain ergodic, irrespective of the initial strength of the applied magnetic field in the z -direction and the interaction strengths, whereas for intermediate values of the initial magnetic field, the information-theoretic measures like quantum discord and quantum work-deficit show a transition from nonergodic to ergodic behavior, with the tuning of the strength of the two-body interaction in the z -direction. The results hold irrespective of the relative strengths (“anisotropy”) of the xx - and yy -interactions. However, the transition point depends on the xy -anisotropy (i.e., the parameter that controls the relative strength of the xx - and yy -interactions) and the strength of the magnetic field.

In Sec. 6.9 of chapter 6, we also investigate the dynamics of bipartite quantum correlations of the evolved state, starting from the zero-temperature state of the XY spin chain of infinite size, after a sudden change in the nearest-neighbor coupling strength from some initial value to a final value [204]. In the evolution process, the final Hamiltonian is termed as the driving Hamiltonian. We characterize the quantum correlations for both finite time and large time limits in this model. In particular, for varied choices of initial states we study the dependence of the dynamical behavior of quantum correlations, viz. entanglement and quantum discord, on the driving Hamiltonian. Our results show that survival of any finite amount quantum correlation present in a initial state followed by a quench distinctly depends on the driving Hamiltonian and on whether quenching is across the critical point in the XY spin chain.

Disordered many-body systems form one of the centrestages of research in many body sciences and lead to a plethora of interesting phenomena and applications. Studying the effect of disorder in many-body systems is important and can hardly be overestimated [205–214]. Realization of most physical systems inherently results in impurities or defects, which may suppress the physical properties of the systems [215–219]. Moreover, disordered systems, both classical and quantum, display counterintuitive phenomena like disorder-induced order or order from disorder in several physical quantities like magnetization, classical correlators, and entanglement [214, 220–226]. At the same time, disordered systems sustain rich phases like spin glass [227–230] and Bose glass [231, 232], and phenomena like Anderson localization [233] and high T_c -superconductivity [234–236]. Recent experimental developments, especially in ultra-cold gases, give rise to the possibility of introducing disorder in a controlled way [237–243] and hence paves the way for novel recipes of observation of these properties in the laboratory.

A paradigmatic disordered system consists of an one-dimensional array of quantum spin-1/2 particles, governed by the Heisenberg spin glass Hamiltonian with natural or engineered quenched disordered couplings in an external magnetic field. These systems allow the order from disorder phenomenon – disorder-induced enhancement – for bipartite and multipartite observables.

Many of the quantum information protocols implemented in quantum many-body systems assumed that the system is clean, i.e., there is no intrinsic or engineered disorder present in the system. However, in reality it is difficult to avoid these inherent impurities while performing experiments. It may seem plausible that the presence of disorder would deteriorate the effectiveness of the observed data as compared to the case when disorder is not present. Therefore, great care is normally given to remove the impurities and make the sample as clean as possible. This, on the other hand, raises an interesting question: are materials with inherent impurities always of less importance as compared to the case when the sample is clean. Study of magnetization on disordered many-body systems, during the 1980s, shows that it may not always be the case. For example, magnetization can increase in certain disordered models as compared to the case when the same model is considered without disorder. This and similar other phenomena has been one of the main reason for the interests in the study of disordered systems.

In chapter 7, we concentrate on the behavior of different observables for the ground state of one-dimensional quenched disordered quantum Heisenberg (or XYZ) models or quantum Heisenberg spin glass models [244]. Specifically, we consider

three paradigmatic classes of disordered Heisenberg spin glass Hamiltonians: the quenched disorder is in (a) the “planar” couplings, or (b) the “azimuthal” couplings, or in (c) both the planar and azimuthal couplings. Although entanglement, especially multiparty entanglement, is known to be fragile, we find that both bipartite and multipartite entanglement can be enhanced by the introduction of all the disorder combinations mentioned. More important, and rather engrossing, is the uncovering of parameter ranges where the individual insertions of planar and azimuthal quenched disorder couplings do not result in disorder-induced enhancement of a multiparty entanglement measure, while the same appears in the simultaneous presence of the disorders. We term the phenomenon as “constructive interference of the disordered couplings” and the coupling parameter ranges as the “Venus regions”. Importantly, such constructive interference is not observed in single- as well as two-site physical quantities like magnetization, classical correlators, and bipartite entanglement. Moreover, changing the Hamiltonian, for example, to the XY model also wipes out the phenomenon. To our knowledge, this is the first time that such constructive interference of quenched disorders, which is qualitatively different from the order from disorder phenomena, known since the 1980s, is observed. Multiparty entanglement is known to be an essential ingredient in several quantum information protocols. The results obtained have therefore the potential for important applications in actual realization of such protocols.

The counterintuitive nature of constructive interference for a physical quantity leads us to believe that it can have implications in fundamental and applicational regimes. Moreover, multiparty quantum information processing tasks typically have origins in the bipartite domain in the sense that information processing tasks that have already been considered in the bipartite domain are usually generalized to the multipartite case. These generalizations are very important. However, instances where the converse occurs are few and far between, and indicates important diversions from the usual track (see e.g. [5, 10, 143, 245–252]). The fact that constructive interference is observed only for multipartite entanglement in the presence of impurities is also in the spirit of these latter instances.

Chapters 4 and 5 are, in the main, based on the publications

1. *Quantum superposition in composite systems of microscopic and macroscopic parts resistant to particle loss and local decoherence*,
Utkarsh Mishra, Aditi Sen(De), and Ujjwal Sen, Phys. Rev. A **87**, 052117 (2013).

2. *Local decoherence free macroscopic quantum states*, **Utkarsh Mishra**, Aditi Sen(De), and Ujjwal Sen, Phys. Lett. A **379**, 261 (2015).

Chapter 6 is mainly based on the publications

1. *Tuning interaction strength leads to an ergodic-nonergodic transition of quantum correlations in the anisotropic Heisenberg model*, **Utkarsh Mishra**, R. Prabhu, Aditi Sen(De), and Ujjwal Sen, Phys. Rev. A **87**, 052318 (2013). and preprint
2. *Survival of time-evolved quantum correlations depends on whether quenching is across critical point in XY spin chain*, **Utkarsh Mishra**, Debraj Rakshit, and R. Prabhu, Phys. Rev. A **93**, 042322 (2016).

Chapter 7 is mainly based on the preprint

1. *Constructive interference between disordered couplings enhances multiparty entanglement in quantum Heisenberg spin glass models*, **Utkarsh Mishra**, Debraj Rakshit, R. Prabhu, Aditi Sen De, Ujjwal Sen, New J. Phys. **18** , 083044 (2016).

Quantum channels

2.1 Introduction

The change in state of a quantum system is modeled by the evolution operation allowed by quantum mechanics where a quantum system in an initial state evolves to some final state. A general quantum evolution of a quantum system is described by adding an ancillary to the system and then evolve the system plus ancillary with a global unitary operator and then trace out the ancillary part. In this chapter, we will focus on the unitary evolution of a closed composite quantum state of a system (S) interacting with an environment (ancillary, denoted by E) and discuss the representation of the general evolution of the system, S , alone. A schematic diagram of the scenario is shown in Fig. 2.1.

In most quantum information theoretic protocols, it is desirable to transfer a certain amount of information from one observer to another using shared quantum states. For example, in quantum dense coding [3] a sender wishes to send classical information to a receiver using a shared quantum state. The important quantity to investigate here is the rate of transfer of classical bit per quantum bit. If there is no external noise, then this rate is 2 classical bits per qubit at most. However, the information content is hampered by the external noise which introduces errors in the message sent to a distant place. For example, the rate in case of dense coding is no longer 2 bit/qubit, due to the presence of noise [25, 253]. Therefore, it is very important to understand the process by which error is introduced in manipulating quantum states.

2.2 Operator-sum representation of quantum channels

In this section, we will discuss the operator-sum representation of quantum evolution of a system. For the description, we will consider the Schrödinger picture. A parallel formalism can be discussed by using the Heisenberg picture. In the Schrödinger picture, the operators are time independent and the state evolves with time. Let us consider a composite Hilbert space \mathcal{H}_{SE} of two Hilbert spaces \mathcal{H}_S and \mathcal{H}_E , such that $\mathcal{H}_{SE} = \mathcal{H}_S \otimes \mathcal{H}_E$, with dimensions d_S and d_E respectively. Typically, $d_E \gg d_S$, although this is not a necessary condition. Let us consider that a quantum state $\rho_{SE}(t=0)$ at the initial time $t=0$, defined on \mathcal{H}_{SE} , evolves to another quantum state $\rho_{SE}(t)$ at some time t . This picture of quantum operations provide the effect of noise created by the environment (E) on the system (S) via the global unitary operation, the initial environment state, and the operation of tracing out the environment. The evolution of the initial system-environment state is governed by a unitary operator ($U_{SE}(t)$) that acts *globally* on $\rho_{SE}(t=0)$, and is given as

$$\rho_{SE}(t) = U_{SE}(t)\rho_{SE}(t=0)U_{SE}^\dagger. \quad (2.1)$$

Here, though the dynamics of the system (S) alone might be open but the full system-environment dynamics is closed. The density matrix of the system (S), denoted by $\rho_S(t)$, at any time t , can be obtained by tracing out the environment (E) part from the whole state $\rho_{SE}(t)$. If tr_E denotes the tracing over the environment E then

$$\rho_S(t) = \text{tr}_E(U_{SE}\rho_{SE}(t=0)U_{SE}^\dagger). \quad (2.2)$$

where $\{|a\rangle_E, a = 1, \dots, d_E\}$, is an orthogonal basis of the environment (E).

We will consider the case when the initial density matrix, $\rho_{SE}(t=0)$, is a product of density matrices of the system S and the environment E . If $\rho_S(t=0)$ denotes the density matrix of the system S , and $\rho_E(t=0)$ denotes the density matrix of the environment E at the initial time $t=0$, then Eq. (2.2) can be expressed as

$$\rho_S(t) = \sum_a \langle a|_E U_{SE} \left(\rho_S(t=0) \otimes \rho_E(t=0) \right) U_{SE}^\dagger |a\rangle_E. \quad (2.3)$$

Assume now that the environment is in some pure state at the initial time, i.e., $\rho_E(t=0) = |e\rangle_E \langle e|$. This assumption has been referred to as the “church of the larger Hilbert space”, and is attributed to J. Smolin. Using this, Eq. (2.3) can be

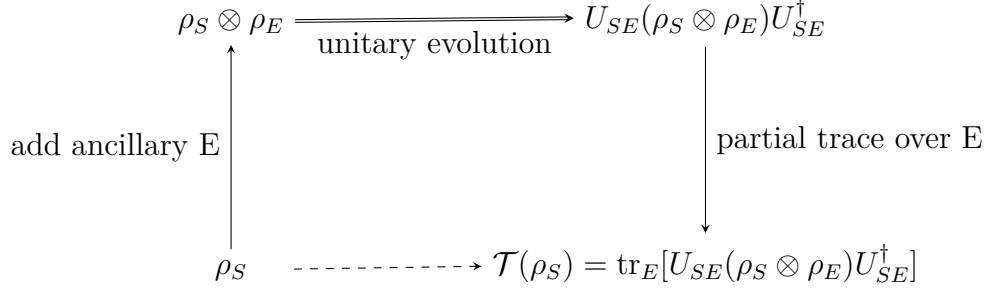


Figure 2.1: Schematic diagram showing the process of evolution of a quantum system, S , represented by a density matrix ρ_S , defined on the Hilbert space \mathcal{H}_S . An initial quantum state of the principal system is combined with an environment such that the system and environment are in a product state. The combined system is evolved using a global unitary operator acting on the Hilbert space, $\mathcal{H}_S \otimes \mathcal{H}_E$, with \mathcal{H}_E being the Hilbert space corresponding to the environment. At the end of the evolution, the environment degrees of freedom are traced out and the resulting expression is a representation of the system’s evolution alone.

written as

$$\rho_S(t) = \sum_a K_a \rho_S(t=0) K_a^\dagger, \quad (2.4)$$

where the “Kraus operator”, $K_a \equiv {}_E \langle a | U_{SE} | e \rangle_E$, is an operator on the Hilbert space of the system S and Eq. (2.4) is known as the operator-sum representation [75–78]. We therefore, have the quantum operation, \mathcal{T} , taking $\rho_S(t=0)$ to $\rho_S(t)$,

$$\rho_S(t) = \mathcal{T}(\rho_S(t=0)), \quad (2.5)$$

where $\rho_S(t)$ is given by Eq. (2.4). See Fig. 2.1 for a schematic representation.

The transformation map \mathcal{T} is termed as a *superoperator* and is a linear map that transforms a density matrix to another density matrix. It is to be noted that the operator-sum representation is not unique and one can obtain other representations that are equivalent up to change of bases.

Note that we have

$$\sum_a K_a^\dagger K_a = \mathbb{I}. \quad (2.6)$$

Importantly, an operator, \mathcal{T} , given by Eq. (2.5), for arbitrary operators $\{K_a\}$ on \mathcal{H}_S such that Eq. (2.6) holds, can always be implemented by adding an environment state, performing a global unitary, and tracing out the environment.

We enumerate below some examples of such quantum channels operations on the qubit space.

2.2.1 Bit flip channel

The bit flip channel corresponds to the bit flip error. In bit flip error, if the initial qubit is in the state $|0\rangle$ then under the action of bit flip channel, it get flipped to $|1\rangle$ with probability p while remaining intact with probability $(1 - p)$. Similarly, for the case if the initial state is in $|1\rangle$ orientation. The action of bit flip channel on the basis states $\{|0\rangle_S, |1\rangle_S\}$ of the system S , is given as

$$\begin{aligned}
|0\rangle\langle 0|_S &\rightarrow (1 - p)|0\rangle\langle 0|_S + p|1\rangle\langle 1|_S \\
|0\rangle\langle 1|_S &\rightarrow (1 - p)|0\rangle\langle 1|_S + p|1\rangle\langle 0|_S \\
|1\rangle\langle 0|_S &\rightarrow (1 - p)|1\rangle\langle 0|_S + p|0\rangle\langle 1|_S \\
|1\rangle\langle 1|_S &\rightarrow (1 - p)|1\rangle\langle 1|_S + p|0\rangle\langle 0|_S.
\end{aligned} \tag{2.7}$$

In matrix representation, the bit flip transformation on a single-qubit state ρ is given as

$$\rho' = \mathcal{T}(\rho) = \begin{pmatrix} (1 - p)\rho_{00} + p\rho_{11} & (1 - p)\rho_{01} + p\rho_{10} \\ (1 - p)\rho_{10} + p\rho_{01} & (1 - p)\rho_{11} + p\rho_{00} \end{pmatrix}. \tag{2.8}$$

Here $|0\rangle_S$ and $|1\rangle_S$ are the eigenstates of the Pauli operator, σ^z , with eigenvalues $+1$ and -1 respectively.

2.2.2 Bit-phase flip channel

The action of bit-phase flip channel on the basis states $\{|0\rangle_S, |1\rangle_S\}$ of a qubit system is given as

$$\begin{aligned}
|0\rangle\langle 0|_S &\rightarrow (1 - p)|0\rangle\langle 0|_S + p|1\rangle\langle 1|_S \\
|0\rangle\langle 1|_S &\rightarrow (1 - p)|0\rangle\langle 1|_S - p|1\rangle\langle 0|_S \\
|1\rangle\langle 0|_S &\rightarrow (1 - p)|1\rangle\langle 0|_S - p|0\rangle\langle 1|_S \\
|1\rangle\langle 1|_S &\rightarrow (1 - p)|1\rangle\langle 1|_S + p|0\rangle\langle 0|_S.
\end{aligned} \tag{2.9}$$

A quantum bit, initially in the state ρ , affected by both bit and phase flip errors, then transforms into

$$\rho' = \begin{pmatrix} (1-p)\rho_{00} + p\rho_{11} & (1-p)\rho_{01} - p\rho_{10} \\ (1-p)\rho_{10} - p\rho_{01} & (1-p)\rho_{11} + p\rho_{00} \end{pmatrix}. \quad (2.10)$$

Here the initial state remains intact with probability $(1-p)$ and bit-phase flip error occurs with probability p .

2.2.3 Phase damping channel

Phase damping happens when e.g., a photon travels through a wave guide, and scatters randomly. The unitary representation of a phase damping channel is given as

$$\begin{aligned} |0\rangle_S|0\rangle_E &\rightarrow \sqrt{1-p}|0\rangle_S|0\rangle_E + \sqrt{p}|0\rangle_S|1\rangle_E \\ |1\rangle_S|0\rangle_E &\rightarrow \sqrt{1-p}|1\rangle_S|0\rangle_E + \sqrt{p}|1\rangle_S|2\rangle_E \end{aligned} \quad (2.11)$$

The initial state of the environment changes whether the system, S , is in $|0\rangle_S$ or $|1\rangle_S$ state. By using the formula $K_a = {}_E\langle a|U|0\rangle_E$, the Kraus operators for the phase damping channels are given by

$$K_0 = \sqrt{1-p}\mathbb{I}, K_1 = \sqrt{p} \begin{pmatrix} 1 & 0 \\ 0 & 0 \end{pmatrix}, K_2 = \sqrt{p} \begin{pmatrix} 0 & 0 \\ 0 & 1 \end{pmatrix}, \quad (2.12)$$

where \mathbb{I} is an identity matrix in the qubit Hilbert space. The Kraus operators satisfy the normalization condition given in Eq. (2.6). By substituting these operators in Eq. (2.4), the evolution of an initial single qubit state ρ under phase damping is given as

$$\rho \rightarrow \rho' = (1-p)\rho + K_1\rho K_1 + K_2\rho K_2. \quad (2.13)$$

Hence under this noise model, the final state becomes

$$\rho' = \begin{pmatrix} \rho_{00} & (1-p)\rho_{01} \\ (1-p)\rho_{10} & \rho_{11} \end{pmatrix}, \quad (2.14)$$

where $\rho_{ij}(i, j = 0, 1)$ are the matrix elements of the initial state ρ . The diagonal terms of the initial density matrix remain invariant under the phase damping channel while the off-diagonal terms decay with probability $(1-p)$. It should also be noted that

the trace of the state ρ' is preserved under the phase damping channel. In terms of the Bloch vector of a single qubit state, the transformation can be visualized as

$$(r^x, r^y, r^z) \rightarrow ((1-p)r^x, (1-p)r^y, r^z). \quad (2.15)$$

This implies that the Bloch sphere uniformly contracts around xy plane and no change occurs along the z -direction.

2.2.4 Amplitude damping channel

The amplitude damping channel is a model for the decay of an excited state of a two-level atom due to spontaneous emission of photons. Detection of the emitted photon (“observation of the environment”), via a positive operator valued measurement, gives us information about the initial preparation of the atom.

The unitary representation for the amplitude damping channel is given as

$$\begin{aligned} |0\rangle_S|0\rangle_E &\rightarrow |0\rangle_S|0\rangle_E \\ |1\rangle_S|0\rangle_E &\rightarrow \sqrt{(1-p)}|1\rangle_S|0\rangle_E + \sqrt{p}|0\rangle_S|1\rangle_E, \end{aligned} \quad (2.16)$$

where an atom initially in the ground state $|0\rangle_S$ remains in the ground state with unit probability. On the other hand, it remains in excited state $|1\rangle_S$ with probability $1-p$ and decays to the ground state from the excited state with probability p . In this process the environment changes its state from being in the ground state $|0\rangle_E$ to the excited state $|1\rangle_E$ as it receives a photon due to the decay of the atom. The Kraus operators can again be obtained by taking partial trace over the environment basis $\{|0\rangle_E, |1\rangle_E\}$. Two Kraus operators are enough to represent the action of the amplitude damping channel on a single qubit and are given as

$$K_0 = \begin{pmatrix} 1 & 0 \\ 0 & \sqrt{1-p} \end{pmatrix}, K_1 = \begin{pmatrix} 0 & \sqrt{p} \\ 0 & 0 \end{pmatrix}. \quad (2.17)$$

After substituting these Kraus operators in Eq. (2.4) the initial qubit state ρ transforms to

$$\rho' = \begin{pmatrix} \rho_{00} + p\rho_{11} & \sqrt{1-p}\rho_{01} \\ \sqrt{1-p}\rho_{10} & (1-p)\rho_{11} \end{pmatrix}, \quad (2.18)$$

where p is the rate of decay. Unlike the phase damping channel, both diagonal and off-diagonal terms get affected by this channel. It is interesting to note that under the amplitude damping channel, the identity \mathbb{I} matrix does not transform to an identity

matrix. A quantum channel with the property $\mathcal{T}(\mathbb{I}) = \mathbb{I}$ is called an unital channel. The amplitude damping channel is, thus, an example of a nonunital channel. Under the amplitude damping channel, the Pauli matrices $(\sigma^x, \sigma^y, \sigma^z)$ and identity matrix evolves as follows

$$\begin{aligned}\mathcal{T}(\sigma^x) &= \begin{pmatrix} 0 & \sqrt{1-p} \\ \sqrt{1-p} & 0 \end{pmatrix}, \mathcal{T}(\sigma^y) = \begin{pmatrix} 0 & -i\sqrt{1-p} \\ i\sqrt{1-p} & 0 \end{pmatrix}, \\ \mathcal{T}(\sigma^z) &= \begin{pmatrix} 1+p & 0 \\ 0 & -(1-p) \end{pmatrix}, \mathcal{T}(\mathbb{I}) = \begin{pmatrix} 1+p & 0 \\ 0 & (1-p) \end{pmatrix}.\end{aligned}\quad (2.19)$$

From Eq. (2.19), the transformation of a single quantum bit under the amplitude damping channel can be obtain as

$$\mathcal{T}(\rho) = \frac{1}{2}(\mathcal{T}(\mathbb{I}) + r^x\mathcal{T}(\sigma^x) + r^y\mathcal{T}(\sigma^y) + r^z\mathcal{T}(\sigma^z)).\quad (2.20)$$

That gives the following transformation for the Bloch vector, \vec{r} ,

$$(r^x, r^y, r^z) \rightarrow (\sqrt{1-p} \ r^x, \sqrt{1-p} \ r^y, p + (1-p) \ r^z).\quad (2.21)$$

This implies that each point on the Bloch sphere shifts towards the north pole, i.e., towards the position of the $|0\rangle$ state in the Bloch sphere.

2.2.5 Depolarizing channel

The errors which happen to an arbitrary pure qubit, say $|\Psi\rangle$, when interacting with its environment, can be categorized into bit flip error, which transforms $|\Psi\rangle$ into $\sigma^x|\Psi\rangle$, phase flip error, which transforms $|\Psi\rangle$ into $\sigma^z|\Psi\rangle$, and bit-and-phase-flip error. Here $\sigma^x, \sigma^y, \sigma^z$ are the three Pauli matrices. If an arbitrary qubit ρ is sent through a depolarizing channel, the state remains unchanged with probability $(1 - p')$ while the above three kinds of error occur with probability $\frac{p'}{3}$ each.

The unitary representation for the depolarizing channel is given by

$$|\psi\rangle_S|0\rangle_E \rightarrow \sqrt{1-p'}|\psi\rangle_S|0\rangle_E + \sqrt{\frac{p'}{3}}(\sigma^x|\psi\rangle_A|1\rangle_E + \sigma^y|\psi\rangle_S|2\rangle_E + \sigma^z|\psi\rangle_S|3\rangle_E).\quad (2.22)$$

The initial state of the system-environment remain intact with probability $1 - p'$ and error occurred with probability $\frac{p'}{3}$. The process of occurrence of error is

random and once a measurement is performed on the environment in the basis $\{|0\rangle_E, |1\rangle_E, |2\rangle_E, |3\rangle_E\}$, it is possible to infer about the type of error that has occurred. The Kraus operators are given as $K_0 = \sqrt{1-p'}\mathbb{I}$, $K_a = \sqrt{\frac{p'}{3}}\sigma^a$ for $a = x, y, z$.

Substituting these Kraus operators in Eq. (2.4), the transformation of the state ρ through the depolarizing channel is given as

$$\rho \rightarrow \rho' = (1-p')\rho + \frac{p'}{3}(\sigma^x \rho \sigma^x + \sigma^y \rho \sigma^y + \sigma^z \rho \sigma^z). \quad (2.23)$$

By putting $p' = \frac{3p}{4}$, we obtain

$$|i\rangle\langle j| \rightarrow \frac{p}{2}\mathbb{I}\text{tr}(|i\rangle\langle j|) + (1-p)|i\rangle\langle j|. \quad (2.24)$$

Here, $0 \leq p' \leq \frac{3}{4}$ and $0 \leq p \leq 1$. Note that for $p' = \frac{3}{4}$, the qubit output state in Eq. (2.23) will be proportional to the identity matrix, \mathbb{I} , while the same for the noisy state obtained via Eq. (2.24) occurs at $p = 1$. The effect of the depolarizing channel can be obtained from the knowledge of the action of Eq. (2.23) on \mathbb{I} , σ^x , σ^y , and σ^z . The depolarizing channel scales the Bloch vector \vec{r} uniformly to

$$\vec{r}' = \left(1 - \frac{4p}{3}\right)\vec{r}, \quad (2.25)$$

where \vec{r}' is the Bloch vector of the single qubit state after it has passed through the depolarizing channel.

2.3 Chapter summary

In this chapter, we have discussed the operator-sum representation formalism of quantum operations to describe the dynamics of a quantum system. This formalism is quite general and also characterizes irreversible processes such as the measurement process. We have also discussed about several paradigmatic quantum channels. We will the latter in chapter 5 to study the robustness of macroscopic quantum superposition states.

Quantum correlations

Quantum correlations form an important resource for performing different tasks in quantum information and computation. Development in experimental techniques has made it possible to realize many quantum communication and computation tasks that utilize quantum correlations. Characterization of quantum correlations is one of the main challenges in the quantum information theory, that includes detection, quantification, and manipulation of quantum correlations. These concepts have been understood up to a certain extent in the bipartite case. In particular, various measures have been proposed that quantify the amount of quantum correlation present in bipartite quantum states, a few of which are tractable at least numerically. The problem to characterize quantum correlations for a general multipartite state is much more involved. However, for pure multipartite states, the generalized geometric measure (GGM) is a computable measure that captures the genuine multipartite entanglement of multipartite quantum states. In this chapter, we discuss bipartite and multipartite quantum correlations, and some of their quantifiers.

3.1 Bipartite entanglement

One of the main tasks in quantum information theory is to characterize entanglement of composite quantum systems, i.e., to find whether a composite state is entangled or not, and if it is entangled, to find the amount of entanglement in that state, and consider its manipulations. The simplest case, where this question has been studied somewhat extensively is the case of bipartite systems. In this section, we discuss about certain aspects of quantum entanglement of bipartite quantum states, i.e., quantum states shared between two parties. Consider, therefore, two observers

(parties) A and B who are in possession of two quantum systems, represented by Hilbert spaces \mathcal{H}_A and \mathcal{H}_B respectively. The composite system is then represented by the Hilbert space $\mathcal{H}_{AB} = \mathcal{H}_A \otimes \mathcal{H}_B$. The dimension of the Hilbert space of party A is d_A and similarly the dimension of the Hilbert space of party B is d_B . The dimension of the Hilbert space of the combined system is $\dim(\mathcal{H}_{AB}) = d_{AB} = d_A d_B$. An arbitrary pure state, $|\Psi\rangle_{AB}$, of the composite system is a vector in the Hilbert space \mathcal{H}_{AB} . Let $\{|\phi_i\rangle_A \otimes |\psi_j\rangle_B\}$ be an orthonormal basis of \mathcal{H}_{AB} . The state $|\Psi\rangle_{AB}$ can be written as

$$|\Psi\rangle_{AB} = \sum_{i=0}^{d_A-1} \sum_{j=0}^{d_B-1} c_{ij} |\phi_i\rangle_A \otimes |\psi_j\rangle_B, \quad (3.1)$$

where $C = [c_{ij}]$ is the coefficient matrix of the expansion and $\sum_{ij} |c_{ij}|^2 = 1$. The density matrix corresponding to the state $|\Psi\rangle_{AB}$ is $\rho_{AB} = |\Psi\rangle_{AB} \langle \Psi|$. The state of the subsystem, $A(B)$, can be obtained from the density matrix, ρ_{AB} , by tracing out the degrees of freedom of subsystem $B(A)$.

To understand the entanglement of an arbitrary pure bipartite quantum state, it is customary to represent the state in the Schmidt form. The Schmidt form is a representation of a pure bipartite state in terms of eigenvectors of density matrices of the local subsystems. Among other things, this representation is mathematically convenient to perform calculations. For example, it is handy to calculate the reduced density matrices of either of the subsystems from the Schmidt representation. For a bipartite state given in Eq. (3.1), the corresponding Schmidt representation is given as

$$|\Psi\rangle_{AB} = \sum_{i=1}^n \sqrt{\lambda_i} |i\rangle_A \otimes |\tilde{i}\rangle_B, \quad (3.2)$$

where $\{|i\rangle_A\}$ and $\{|\tilde{i}\rangle_B\}$ are orthonormal sets of \mathcal{H}_A and \mathcal{H}_B respectively, and λ_i 's are positive real numbers. Here $n \leq \min\{d_A, d_B\}$.

With this, we now introduce the notion of entanglement for pure quantum states. The state $|\Psi\rangle_{AB}$ is called entangled if and only if it cannot be expressed as a product of two vectors belonging to the local Hilbert spaces \mathcal{H}_A and \mathcal{H}_B , i.e.,

$$|\Psi\rangle_{AB} \neq |\phi\rangle_A \otimes |\psi\rangle_B. \quad (3.3)$$

Otherwise, the state $|\Psi\rangle_{AB}$ is called an unentangled state. In terms of Schmidt representation, a state is called entangled if the Schmidt decomposition has more than one term. Examples of entangled states are the so-called Bell states given by

$$\begin{aligned}
|\Phi^\pm\rangle_{AB} &= \frac{1}{\sqrt{2}}(|00\rangle_{AB} \pm |11\rangle_{AB}) \\
|\Psi^\pm\rangle_{AB} &= \frac{1}{\sqrt{2}}(|01\rangle_{AB} \pm |10\rangle_{AB}),
\end{aligned} \tag{3.4}$$

where $|00\rangle_{AB} = |0\rangle_A \otimes |0\rangle_B$, etc. Here, the Bell states are already written in the Schmidt decomposition. As there are two nonzero eigenvalues of the local density matrix, the states in Eq. (3.4) are entangled states. Operationally, it is possible to prepare the product state, $|\phi\rangle_A \otimes |\psi\rangle_B$, without allowing the parties A and B to ever come into contact with one another, while the only way to prepare an entangled state is to apply a *global* unitary transformation to a product state.

Let us now consider the more general situation of mixed states. This requires the concept of local operations and classical communications (LOCC). See Appendix A for a formal description of LOCC. The more general quantum state shared by A and B , that can be prepared by LOCC between A and B , is of the form [254]

$$\varrho_{AB} = \sum_{a=1}^k p_a \varrho_A^a \otimes \varrho_B^a, \tag{3.5}$$

where ϱ_A^a and ϱ_B^a are quantum states defined on local Hilbert spaces, \mathcal{H}_A and \mathcal{H}_B respectively, and where $\{p_a\}$ form a probability distribution. It can be shown that $k \leq (\dim(\mathcal{H}_{AB}))^2$ [255, 256]. An important example of a class of mixed bipartite state is given by the Werner states,

$$\rho_{AB} = \lambda |\Phi^+\rangle\langle\Phi^+|_{AB} + \frac{1}{4}(1 - \lambda)\mathbb{I}, \tag{3.6}$$

where $|\Phi^+\rangle$ is one of the Bell states mentioned in Eq. (3.4). For $\lambda = 1$, the state is pure, while for $\lambda = 0$, the state is maximally mixed. Here, \mathbb{I} is the identity operator on $\mathcal{H}_A \otimes \mathcal{H}_B$. States which can be written in the form given by Eq. (3.5) are called separable. States which are not separable are entangled. Peres [86] noticed that a transposition on only one of the subsystems transforms a separable state into another valid quantum (separable) state, while entangled states may be transformed into operators that does not represent a quantum state. A transpose operation, \mathcal{T} , acting on a Hilbert space \mathcal{H} is defined as

$$\mathcal{T} : |i\rangle\langle j| \rightarrow (|i\rangle\langle j|)^T = |j\rangle\langle i|. \tag{3.7}$$

Given a density matrix of bipartite system, $\rho_{ij,\mu\nu}$, the partial transposition, with

respect to part A , is defined as

$$\mathcal{T}_A(\rho_{ij,\mu\nu}) = \rho_{\mu j, i \nu}. \quad (3.8)$$

Here, i, μ are the indices for the A part and j, ν are the indices for the B part, and the partial transpose act only on the A -part. A similar operation can also be defined for the B -part. Peres has shown that if a state ρ_{AB} has decomposition similar to the one given in Eq. (3.5), then the eigenvalues of the states after taking the partial transposition with respect to, say A , remains positive. However, if the state is entangled, then after taking the partial transposition, the final density matrix may have negative eigenvalues. For example, the singlet state, after partial transposition has a negative eigenvalue. In this way, it is possible to separate the states with positive partial transpose (PPT) with the one with nonpositive partial transpose (NPT), and provide us a sufficient criterion for detecting entanglement. It was shown by Horodecki *et al.* [87] that the criterion is also necessary in $\mathbb{C}^2 \otimes \mathbb{C}^2$ and $\mathbb{C}^2 \otimes \mathbb{C}^3$.

We can now apply this “positive partial transpose (PPT) criterion” to detect the entanglement of the Werner state. Applying this criterion to the Werner state, given in Eq. (3.6), we obtain that the density matrix, after taking the partial transposition with respect to A , is positive provided $\lambda \leq \frac{1}{3}$.

Now we consider a few measures of entanglement that quantify the amount of entanglement present in the state ρ . The necessity to quantify entanglement is connected, for example, to the resource theory of entanglement where entanglement is seen as a resource in different quantum communication and other tasks.

3.1.1 Concurrence

In two-qubit states, concurrence is a useful entanglement measure [82]. Concurrence for a pure two-qubit state, $|\Psi\rangle$, is given by

$$C(|\Psi\rangle) = |\langle \Psi | \tilde{\Psi} \rangle|, \quad (3.9)$$

where the tilde represents the “spin-flip” operation defined as

$$|\tilde{\Psi}\rangle = (\sigma^y \otimes \sigma^y) |\Psi^*\rangle. \quad (3.10)$$

Here $|\Psi^*\rangle$ is the complex conjugate of $|\Psi\rangle$ in the standard basis $\{|00\rangle, |01\rangle, |10\rangle, |11\rangle\}$, and σ^y is the Pauli operator, given by $\sigma^y = i(-|0\rangle\langle 1| + |1\rangle\langle 0|)$. For the pure state

$|\Psi\rangle = a|00\rangle + b|01\rangle + c|10\rangle + d|11\rangle$, the concurrence is given by $C(|\Psi\rangle) = 2|ad - bc|$. Here a , b , c , and d are complex numbers such that $|a|^2 + |b|^2 + |c|^2 + |d|^2 = 1$. For $ad = bc$, the state is in product form in its subsystems, and the concurrence is zero.

The concurrence of a mixed state, ρ_{AB} , of two qubits is defined as the minimal average concurrence over ensembles of pure states representing ρ_{AB} , i.e.,

$$C(\rho_{AB}) = \inf \sum_j p_j C(|\Psi_j\rangle), \quad (3.11)$$

where $\rho_{AB} = \sum_j p_j |\Psi_j\rangle\langle\Psi_j|$ and the infimum is over all such decompositions of ρ_{AB} . For a two-qubit mixed state, ρ_{AB} , it is possible to perform the optimization, and the concurrence of the state is given as

$$C(\rho_{AB}) = \max[0, \lambda_1 - \lambda_2 - \lambda_3 - \lambda_4], \quad (3.12)$$

where $\lambda_1, \lambda_2, \lambda_3, \lambda_4$ are the square roots of the eigenvalues of $\rho_{AB}\tilde{\rho}_{AB}$ in decreasing order and $\tilde{\rho}_{AB} = \sigma^y \otimes \sigma^y \rho_{AB}^* \sigma^y \otimes \sigma^y$, with the complex conjugation being taken in the computational basis. The measure is non-zero for all entangled two-qubit states, and is zero for the separable ones.

The variation of concurrence of the Werner state against the parameter λ (see Eq. (3.6)) is shown in Fig. 3.1. It is observed that the concurrence is zero for $\lambda \leq \frac{1}{3}$ and then increase monotonically with λ . It is equal to unity for $\lambda = 1$, i.e., $C(|\Phi^+\rangle) = 1$.

3.1.2 Logarithmic negativity

Logarithmic negativity [84, 85, 89] is another measure of entanglement of a bipartite quantum state, ρ_{AB} , shared between two parties A and B . The definition of logarithmic negativity is based on negativity, $N(\rho_{AB}) = \frac{1}{2}(\|\rho^{\mathcal{T}_A}\|_1 - 1)$. The negativity of a two-party state is therefore the sum of the absolute values of the negative eigenvalues of the partial transposed density matrix [86, 87] of the bipartite state ρ_{AB} . Here \mathcal{T}_A denotes the partial transpose of ρ_{AB} with respect to party A . The norm, $\|A\|_1 = \text{tr}\sqrt{A^\dagger A}$, denotes the trace norm of a Hermitian matrix A .

The logarithmic negativity (LN) is defined as

$$E_N(\rho_{AB}) = \log_2[2N(\rho_{AB}) + 1]. \quad (3.13)$$

For two qubit states, LN is positive if and only if the state is entangled [87]. The

measure is however defined and computable for bipartite states, for pure or mixed, of arbitrary dimensions. But for entangled states which have a positive partial transpose [256,257], the measure is vanishing. Also, it does not reduce to the entropy of entanglement (Appendix B) on pure states.

3.2 Bipartite quantum correlations

We in the preceding section have discussed about entanglement and its measures for bipartite quantum states. In this section, we will discuss about quantum correlations beyond entanglement. Separable states have zero entanglement, by definition. The question is whether all separable states represent classical situations. The motivation for such a query is the existence of phenomena of multiparty systems which are nonclassical and yet does not involve shared entanglement. Such phenomena include problems in local indistinguishability [27,28,30,32,34–36] and deterministic quantum computation with a single qubit [26,42] (cf. [258]). Mixed bipartite states of the form

$$\rho_{AB}^{cc} = \sum_{i,j=1} p_{ij} |i\rangle\langle i|_A \otimes |j\rangle\langle j|_B, \quad (3.14)$$

where $\{|i\rangle^A\}$ and $\{|j\rangle^B\}$ are orthogonal sets in \mathcal{H}_A and \mathcal{H}_B respectively, and where $\{p_{ij}\}$ forms a probability distribution, are separable states. However, they constitute a special class within separable states which are formed by mixing states of a biorthogonal basis of $\mathcal{H}_A \otimes \mathcal{H}_B$, and their correlations can be considered as truly classical. They are referred to as classically correlated states.

There have been several attempts at conceptualizing quantum correlations from information-theoretic perspectives that assign zero values to classically correlated states, instead of assigning zero values to separable states as for entanglement measures. We discuss below about two such measures, viz, quantum discord and quantum work-deficit.

3.2.1 Quantum discord

Quantum discord [46,47] is an information-theoretic measure of quantum correlation. One of the ways to motivate the definition of quantum discord is to note that two equivalent quantities that define mutual information in classical information theory turn out to be different in their quantized version. For two random variables X and Y , classical mutual information can be defined as

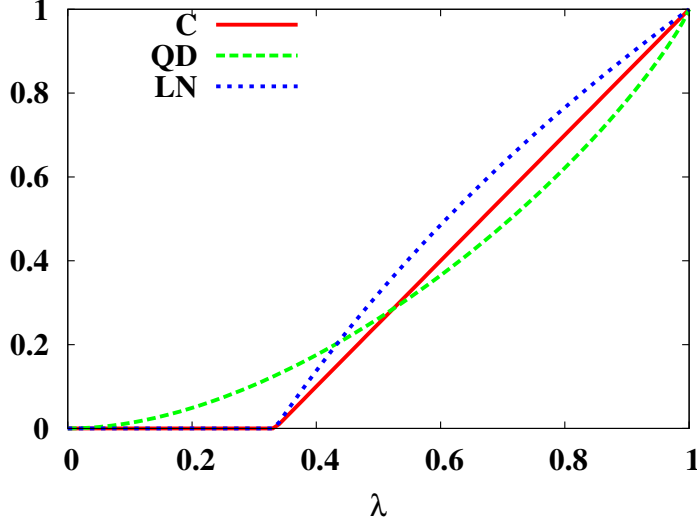


Figure 3.1: Concurrence (C), quantum-discord (QD) and logarithmic negativity (LN) of the Werner state (Eq. 3.8) against the parameter λ .

$$\mathcal{I}(X : Y) = H(X) + H(Y) - H(X, Y), \quad (3.15)$$

as well as

$$\mathcal{J}(X : Y) = H(X) - H(X|Y). \quad (3.16)$$

Here $H(X) = -\sum_x p_{X=x} \log_2 p_{X=x}$ is the Shannon entropy of the random variable X , and $p_{X=x}$ is the probability that the random variable X takes the value x . $H(X, Y)$ is the joint entropy of the variables X and Y . The conditional entropy, $H(X|Y)$, is defined as

$$H(X|Y) = \sum_y p_{Y=y} H(X|Y = y), \quad (3.17)$$

where $p_{Y=y}$ is the probability that the random variable Y takes the value y , and $H(X|Y = y)$ is the entropy of the variable X given that the variable Y takes the value y . Note that $H(X|Y = y) = -\sum_x p_{x|y} \log_2 p_{x|y}$, where $p_{x|y}$ is the probability that $X = x$ given that $Y = y$.

Using the Bayes' rule for the random variables X and Y , i.e., $p_{X=x|Y=y} = p_{X=x, Y=y}/p_{Y=y}$, it can be shown that $H(X|Y) = H(X, Y) - H(Y)$. This implies the equality of \mathcal{I} and \mathcal{J} . However, it was noticed that the two definitions are not same, when generalized to the quantum domain.

It has been argued that \mathcal{I} can be generalized to the quantum case, for a two-party quantum states, ρ_{AB} , as $I(\rho_{AB}) = S(\rho_A) + S(\rho_B) - S(\rho_{AB})$, where $S(\varrho) = -\text{tr}[\varrho \log_2 \varrho]$ is the von Neumann entropy of the quantum state ϱ , and ρ_A and ρ_B are the reduced density matrices of ρ_{AB} . The quantity \mathcal{J} can be generalized for ρ_{AB} as $J(\rho_{AB}) = S(\rho_A) - S(\rho_{A|B})$. Here $S(\rho_{A|B}) = \min_{\{\Pi_i^B\}} \sum_i p_i S(\rho_{A|i})$ is the conditional entropy of ρ_{AB} , where $\{\Pi_i^B\}$ are rank-1 projection-valued measurements performed on the B -part of the system, with $\rho_{A|i} = \text{tr}_B[(\mathbb{I}_A \otimes \Pi_B^i) \rho_{AB} (\mathbb{I}_A \otimes \Pi_B^i)]$, $p_i = \text{tr}_{AB}[(\mathbb{I}_A \otimes \Pi_B^i) \rho_{AB} (\mathbb{I}_A \otimes \Pi_B^i)]$, and with \mathbb{I}_A being the identity operator on the Hilbert space of A . Quantum discord of a bipartite quantum state, ρ_{AB} , is defined as

$$\mathcal{D}(\rho_{AB}) = I(\rho_{AB}) - J(\rho_{AB}). \quad (3.18)$$

It is shown in [46], that quantum discord defined in this way is nonnegative, and is equal to zero on quantum-classical states only, which are states of the form $\rho_{AB}^{qc} = \sum_j p_j \rho_A^j \otimes (|j\rangle\langle j|)_B$, where $\{p_j\}$ is a probability distribution, ρ_A^j are states on \mathcal{H}_A , and $\{|j\rangle_B\}$ is an orthonormal set in \mathcal{H}_B . Instead of party A , one can also perform the measurement in party B , and the quantum discord in that case will be denoted as $\mathcal{D}(\rho_{BA})$. Quantum discord is not symmetric with respect to interchange of subsystems A and B , i.e., in general, $\mathcal{D}(\rho_{AB}) \neq \mathcal{D}(\rho_{BA})$.

The quantum discord of the Werner state is shown in Fig. (3.1). The quantum discord is zero only for $\lambda = 0$ and it remain nonzero for all other values of the λ . The measurement operators, Π^i ($i = 1, 2$), used to evaluate J , are defined, in the computational basis, as

$$\Pi^1 = \begin{pmatrix} \cos^2 \frac{\theta}{2} & \frac{1}{2} e^{-i\phi} \sin \theta \\ \frac{1}{2} e^{i\phi} \sin \theta & \sin^2 \frac{\theta}{2} \end{pmatrix},$$

and

$$\Pi^2 = \begin{pmatrix} \sin^2 \frac{\theta}{2} & -\frac{1}{2} e^{-i\phi} \sin \theta \\ -\frac{1}{2} e^{i\phi} \sin \theta & \cos^2 \frac{\theta}{2} \end{pmatrix},$$

The minimization over all measurements involved in J is carried out by scanning over the parameter space for $\theta \in [0, \pi]$ and $\phi \in [0, 2\pi]$.

3.2.2 Quantum work-deficit

Another information-theoretic measure of quantum correlation is the quantum work-deficit, which is defined as the difference between the amount of work extractable

from a shared state by global and local quantum heat engines [48–51]. It is possible to quantify the amount of work that can be extracted from a bipartite state ρ_{AB} by global operations as

$$I_G(\rho^{AB}) = N - S(\rho_{AB}), \quad (3.19)$$

where N is the logarithm (base 2) of the dimension of the Hilbert space on which ρ_{AB} is defined. It can be interpreted as the number of pure qubits that can be extracted from ρ_{AB} by global operations on the state, and that consists of an arbitrary sequence of unitary and dephasing operations. Such operations are called “closed global operations”. Let us now define “closed local operations and classical communication (CLOCC)”. It consists of local unitaries, local dephasing, and sending the dephased state from one party to other. The number of pure qubits that can be extracted by CLOCC is given by,

$$I_L(\rho_{AB}) = N - \inf_{\Lambda \in \text{CLOCC}} [S(\rho'_A) + S(\rho'_B)], \quad (3.20)$$

where $S(\rho'_A) = S(\text{tr}_B[\Lambda(\rho_{AB})])$ and $S(\rho'_B) = S(\text{tr}_A[\Lambda(\rho_{AB})])$. The quantum work-deficit is defined as

$$W_D(\rho_{AB}) = I_G(\rho_{AB}) - I_L(\rho_{AB}). \quad (3.21)$$

This quantity is difficult to calculate, even numerically, and we will therefore, restrict ourselves to local dephasing on only one of the parties. If the measurement is on the B -part, the resulting “one-way” quantum work-deficit is defined as $W_D(\rho_{AB})$, while it is denoted as $W_D(\rho_{BA})$ if the measurement is on the A -part.

3.3 Multipartite entanglement

Multiparty quantum correlations is much less understood than its bipartite counterpart. We will restrict ourselves here to multiparty entanglement. There are several motivations to study multiparty quantum correlations, including multiparty entanglement. In particular, quantum many-body systems provide a suitable playground to study entanglement and quantum correlations in real materials. Most of the studies in these systems are concentrated on few body entanglement, e.g., bipartite entanglement [52, 53], tripartite entanglement [259–261] (See [6, 262–264] for measures based on monogamy of quantum correlations in general), and quantum discord [55]. See [20, 21, 147] for reviews. Instances where multipartite entanglement measures, e.g., geometric measure [226, 226, 265–269] and global entangle-

ment [270], (see also [271, 272]), have been used to describe many-body phenomena include Refs. [269, 273–282]. However, one of the main obstacles in investigating multipartite entanglement is the lack of computable measures. We will focus on pure multipartite quantum states and discuss about a measure of multipartite entanglement for such states. We call a pure multipartite quantum state as genuinely multipartite entangled if it is not a product across any bipartition of the sites involved. We will now discuss about a measure of genuine multipartite entanglement.

3.3.1 Generalized geometric measure

As a measure of genuine multipartite entanglement measure, we will employ the generalized geometric measure (GGM) [269] (cf. [265]). In case of quantum systems composed of more than two subsystems, the quantification of entanglement is much more involved in comparison to the bipartite case. This is because in a multipartite scenario, there are qualitatively different kinds of entangled states like biseparable, triseparable, etc., and there are also genuine multipartite entangled states. In order to quantify genuine multipartite entanglement, we use the GGM which is based on the distance between the n -party multipartite pure state, and an n -party pure state which is not genuinely multipartite entangled. More specifically, the GGM for an n -party pure quantum state, $|\psi_n\rangle$, is given by

$$\mathcal{E}(|\psi_n\rangle) = 1 - \max |\langle \phi_n | \psi_n \rangle|^2, \quad (3.22)$$

where the maximization is taken over all n -party pure quantum states, $|\phi_n\rangle$, that are not genuine multipartite entangled. It is possible to evaluate the maximization analytically for an arbitrary state $|\psi_n\rangle$ and is given by

$$\mathcal{E}(|\psi_n\rangle) = 1 - \max\{\eta_{\mathcal{A}:\mathcal{B}}^2 | \mathcal{A} \cup \mathcal{B} = \{1, \dots, N\}, \mathcal{A} \cap \mathcal{B} = \emptyset\}, \quad (3.23)$$

where $\eta_{\mathcal{A}:\mathcal{B}}$ is the maximal Schmidt coefficient of $|\psi_n\rangle$ in the bipartite split $\mathcal{A} : \mathcal{B}$. It can be shown that the GGM defined in this way is monotonically decreasing under LOCC [269].

As an illustration, let us consider the N -party GHZ state [95, 96] given by

$$|GHZ\rangle_{1,\dots,N} = \frac{1}{\sqrt{2}}(|0\dots 0\rangle + |1\dots 1\rangle). \quad (3.24)$$

The GGM for the N -qubit GHZ state is given by $\mathcal{E}(|GHZ\rangle) = \frac{1}{2}$.

3.4 Chapter summary

In this chapter, we have discussed about measures of entanglement and other quantum correlations. We first considered the concept of entanglement in the simplest case, i.e., the bipartite case. In this case, we defined measures like concurrence and logarithmic negativity, which are entanglement measures, as well as information-theoretic measures like quantum discord and quantum work-deficit. We also defined a measures of genuine multipartite entanglement for pure multipartite quantum states.

Macroscopic quantum superpositions

4.1 Introduction

Quantum superposition is one of the fundamental principles in quantum mechanics, and is considered to be the agent for various non-intuitive phenomena. According to this principle, if a quantum object exists in two or more distinct quantum states, then it can also exist in an arbitrary linear superposition of them. In other words, if $|\psi_1\rangle$ and $|\psi_2\rangle$ represents two different situations of a physical system, then the same system can also exist in $|\psi\rangle = c_1|\psi_1\rangle + c_2|\psi_2\rangle$, where c_1 and c_2 are arbitrary complex number upto an irrelevant phase and a normalization. The principle of quantum superposition in composite quantum systems, gives rise to another interesting feature of quantum mechanics, which is (quantum) entanglement.

One of the important questions about quantum superposition is its scalability to the macroscopic level. For a multiparty state to represent a macroscopic quantum superposition, it has to be composed of a large number of subsystems, say qubits, and simultaneously has to persist in a quantum superposition of at least two states, which are “macroscopically distinct” [92,283]. The original idea of using macroscopic superposition states was of Schrödinger in 1935 [22], where he introduced an entangled state composed of a microscopic and a macroscopic part. These micro:macro entangled states have since been found to be useful in technological pursuits, and are also fundamentally important, e.g., for understanding the quantum measurement problem and the quantum-to-classical transition [90,127,132,284,285]. These states also have applications in quantum computation. Feynman proposed that complex and large quantum systems can be efficiently simulated only by using a quantum computer [286]. Shor’s algorithm demonstrated that quantum algorithms can be

used to efficiently solve problems that may not be possible with classical ones [8]. Moreover, Steane proposed that to build a viable quantum computer that can compile and implement a quantum algorithm, which outperforms the ones running on classical machines, requires quantum coherence preserved in a system of about 10^3 qubits [287]. Such exciting developments on the theoretical front were accompanied by several experimental proposals and realizations, by using e.g. photons, ion traps, cold atoms, and nuclear magnetic resonance [15, 16, 18, 177, 288, 289]. These experimental successes have led to further theoretical discussions to develop tools to characterize such quantum superposition states.

In this chapter of the thesis, we discuss the Schrödinger’s cat state and its importance in quantum theory. We then move on to discuss a few notions used for quantifying the macroscopicity of quantum superposition states [92, 115, 124].

4.2 Schrödinger cat state

The Schrödinger cat state [22] is a quantum state of a composite system consisting of microscopic and macroscopic parts that is used to state the so-called Schrödinger cat “paradox”. The microscopic object is a radioactive atom and the macroscopic object is a cat. A schematic diagram of the Schrödinger cat paradox is shown in Fig. 4.1. In this figure, a cat is kept inside a chamber together with a radioactive atom and a flask of poison. The flask is attached to a hammer whose action on the poison flask is controlled by a switch. The “on” and “off” states of the switch are further controlled by whether the atom have decayed or not. If the atom is in its ground state, no decay will happen and the flask will not break. On the other hand, if the atom decays, the switch will be “on” and the flask will be broken with the stroke of the hammer.

The linearity of quantum theory predicts the existence of a quantum state of the combined micro:macro system that is

$$\frac{1}{\sqrt{2}} (|\text{up}\rangle|\text{alive}\rangle + |\text{down}\rangle|\text{dead}\rangle). \quad (4.1)$$

The undecayed state of the atom is denoted as $|\text{up}\rangle$, and the decayed state as $|\text{down}\rangle$, making up a two-dimensional complex Hilbert space (qubit). The $|\text{alive}\rangle$ and the $|\text{dead}\rangle$ states of the cat, on the other hand, was considered as a macroscopic system again forming a qubit. From Eq. (4.1), we find that the cat is in two different quantum mechanical states, in the closed chamber, depending on the decayed and

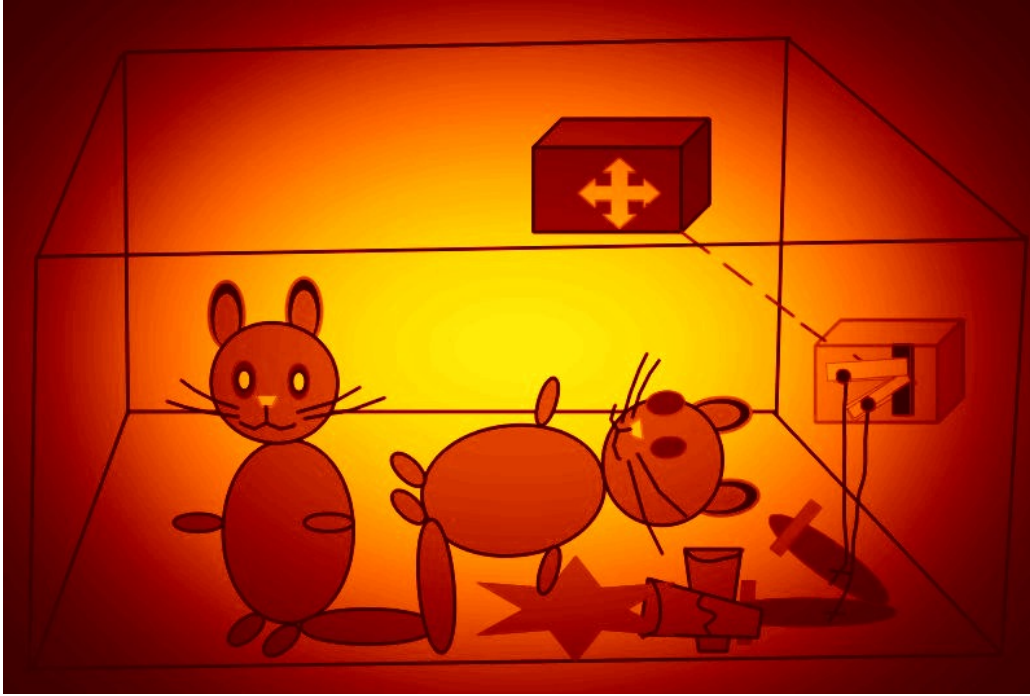


Figure 4.1: Schematic representation of Schrödinger's cat paradox experiment.

undecayed states of the atom. If the atom remains undecayed, the cat is in the $|\text{alive}\rangle$ state, so that the composite system is in the state $|\text{up}\rangle \otimes |\text{alive}\rangle$. On the other hand, if atom has decayed, the cat is in the $|\text{dead}\rangle$ state, with the composite system as $|\text{down}\rangle \otimes |\text{dead}\rangle$. However, if the state in Eq. (4.1) exists, quantum theory also allows the measurement of the atomic system in the basis $\{\frac{1}{2}(|\text{up}\rangle \pm |\text{down}\rangle)\}$ which leads to states of the cat which are formed by superposing $|\text{alive}\rangle$ and $|\text{dead}\rangle$ states of the cat.

A quantum state of a multiparty system that has been considered to be a realization of the Schrödinger cat state is the Greenberger-Horne-Zeilinger (GHZ) state [95], which in the present context, can be written as

$$|\text{GHZ}\rangle = \frac{1}{\sqrt{2}} \left(|0\rangle_{\mu} |0^{\otimes N}\rangle_{A_1 \dots A_N} + |1\rangle_{\mu} |1^{\otimes N}\rangle_{A_1 \dots A_N} \right). \quad (4.2)$$

The party denoted by μ represents the microscopic part, while the parties A_1 through A_N make up the macroscopic portion of the composite system. The microscopic part is a single qubit, and is spanned by the orthonormal states $|0\rangle$ and $|1\rangle$. The macroscopic portion is built out of N qubits, denoted as A_1, A_2, \dots, A_N , with each being spanned by the orthonormal states $|0\rangle$ and $|1\rangle$. Comparing this state with the original Schrödinger state, Eq. (4.1), $|0^{\otimes N}\rangle_{A_1 \dots A_N}$ can be thought of as representing the

alive cat and $|1^{\otimes N}\rangle_{A_1\dots A_N}$ as the dead cat. It is to be emphasised here that the $|\text{alive}\rangle$ and the $|\text{dead}\rangle$ cat states are macroscopically distinguishable. A question of concern, both from the point of theory and experiment, therefore, is the characterization of macroscopic distinguishability of the two macroscopic parts as a function of N . We will discuss this issue in the next section.

4.3 Characterization of macroscopic quantum superposition

If a quantum system is composed of N particles, then our interest in this section is to investigate whether the system can possess a quantum state of the form $|\Psi\rangle \propto |A_N\rangle + |B_N\rangle$, where [283]

1. N is sufficiently large, and
2. the states $|A_N\rangle$ and $|B_N\rangle$ are “macroscopically” distinguishable.

Leggett [92, 283] considered this question and proposed a measure, namely “disconnectivity”, to quantify genuine macroscopic quantum superposition. It is defined by using von Neumann entropies of local density matrices of the N -particle state. For a quantum state of N -particles, a quantity, $\delta_{N'}$, is defined as

$$\delta_{N'} = \frac{S(\rho_{N'})}{\min_M(S(\rho_M) + S(\rho_{N-M}))}, \quad (4.3)$$

where $S(\rho_{N'})$ is the von Neumann entropy of the reduced state $\rho_{N'}$ and $N' \leq N$. The disconnectivity D of a many-particle state is then defined as the largest N for which δ_N is smaller than some fraction a . The disconnectivity of the N -qubit GHZ state is N .

Dür, Simon, and Cirac [115] have investigated a method to characterize macroscopic quantum superposition of special types of multipartite states, given by

$$|\Psi_n\rangle = \frac{1}{\sqrt{K}}(|\phi_1\rangle^{\otimes n} + |\phi_2\rangle^{\otimes n}), \quad (4.4)$$

where $|\phi_1\rangle = |0\rangle$ and $|\phi_2\rangle = \cos(\epsilon)|0\rangle + \sin(\epsilon)|1\rangle$ and $K = 2 + \langle\phi_1|\phi_2\rangle^n + \langle\phi_2|\phi_1\rangle^n = 2(1 + \cos^n(\epsilon))$. Two different approaches were followed to identify what they called “the effective particle number”, N_{eff} , and found that for the states of the form in Eq. (4.4), $N_{eff} = n\epsilon^2$.

Lee and Jeong [124] has defined a measure of macroscopic quantumness for an arbitrary M -mode harmonic-oscillator system using phase space representation of states of the system. In particular, the states were expressed in terms of Wigner function of the phase space variable. The measure defined in this way quantifies both the degree of coherence and the effective size of the physical system that involves the superposition.

Motivated by the Leggett [92] approach of characterizing the macroscopic quantum superposition by devising methods to distinguish the macroscopic sectors in macroscopic quantum superposition states as the number of parties are increased, we consider the Schrödinger cat state given by

$$|\Psi_N\rangle \propto |0\rangle|A_N\rangle + |1\rangle|B_N\rangle, \quad (4.5)$$

where $|0\rangle$ and $|1\rangle$ are orthogonal states of the “minuscule” sector, similar to the sector spanned by the decayed and undecayed states of the atom in Eq. (4.1), while $|A_N\rangle$ and $|B_N\rangle$ are orthogonal states of the “large” sector, similar to the alive and dead state of the cat’s state. The aim here is to identify properties, if possible, of the two states of the large sector that show completely different characteristics with increasing the number of parties in that sector. We use the critical visibility, p_N^{crit} , associated with the states of the large sector, needed for the violation a Bell inequality. For an N - party state $|A_N\rangle$, consider a state of the form

$$\rho(p_N) = p_N|A_N\rangle\langle A_N| + (1 - p_N)\rho_{noise}^{(N)}, \quad (4.6)$$

where $\rho_{noise}^{(N)} = \frac{1}{2^N}\mathbb{I}$, with \mathbb{I} being the identity operator on the Hilbert space of which $|A_N\rangle$ is an element. The aim here is to find the status of the violation of local realism by the state, $\rho(p_N)$. For $p_N = 0$, the state is identical to a maximal noisy state and no violation of local realism occurs.

If the critical visibilities associated with two large states, $|A_N\rangle$ and $|B_N\rangle$, of the large sectors, differ significantly with the increasing number of parties, N , then the two sectors are macroscopically distinguishable. It is to be noted that for the N -party GHZ state, the above method does not distinguish the two states of the large sector, $|0\rangle^{\otimes N}$ and $|1\rangle^{\otimes N}$. However, if for example one of the large sector states is the N -party W_N state, $|W_N\rangle = \frac{1}{\sqrt{N}}\sum |10^{\otimes N-1}\rangle$ and the other is $|0\rangle^{\otimes N}$, then, it can be shown that the critical visibility of the two large sector states differ drastically [141, 144]. Therefore, a state of the form $|\Psi_N\rangle \propto (|0\rangle_\mu|W_N\rangle_{A_1\dots A_N} + |1\rangle_\mu|0^{\otimes N}\rangle_{A_1\dots A_N})$ could represent a valid macroscopic quantum superposition. Our claim that the characterization

of macroscopic superposition, presented here, in terms of Bell inequality violations subsequent to local measurement, is a sufficient and not a necessary one.

In chapter 5, we characterize the macroscopicity of a class of multipartite states by using the above method, and compare their macroscopicity with the N party GHZ and other multipartite states.

The Bell inequality violation for the multipartite state that we use is the following. Given a symmetric multipartite state $|\Psi_N\rangle$ of N parties, we perform measurements at $N - 2$ parties, and consider the violation of Bell inequality and the corresponding critical visibility to white noise of the post-measurement two-party state. In our case, the two-party state is a two-qubit state, and we consider the Clauser-Horne-Shimony-Holt (CHSH) inequality [290–292] for finding the extent of violation of local realism of the two-qubit state. The Bell inequality violation of the multipartite state is then defined as the violation amount for the two-qubit state maximized over the measurement bases and measurement outcomes at the $N - 2$ parties. For asymmetric states, we need to perform an additional maximization over all choices of the $N - 2$ parties, among the N parties, where the measurements are carried out. Note that this is a multipartite measure of local realism violation for the state $|\Psi_N\rangle$. This is similar to the post-measurement Bell inequality violation considered in [293], and is akin to the concept of localizable entanglement [294]. Relating violation of Bell inequalities with macroscopicity was probably first done in Ref. [93], where N -qubit GHZ states were shown to violate Bell inequalities by an amount that increases exponentially with N . A different angle was explored in Ref. [295] (see also [283]), where “macroscopic realism” was used as a premise in the derivation of a Bell-type inequality.

4.4 Chapter summary

Quantum superposition is one of the fundamental concepts in quantum mechanics. However, its existence at macroscopic scale remains debatable. The question of existence of macroscopic quantum superposition was put forward by Schrödinger to understand the consequences of the postulates of quantum mechanics at the macroscopic scale. Current experimental techniques have made it possible to create a superposition of multipartite states in different experimental setups, e.g., ion-trap, photon, SQUID, etc. In this chapter, we have discussed about macroscopic superpositions. We have identified a measure to characterize the macroscopicity of a quantum state. It is motivated by an idea of Leggett on macroscopic quantum

superpositions. We have used the violation of local realism by the states of large systems to characterize macroscopic superpositions. The new results presented here and in the next chapter are mainly based on the publications

1. *Quantum superposition in composite systems of microscopic and macroscopic parts resistant to particle loss and local decoherence*, **Utkarsh Mishra**, Aditi Sen(De), and Ujjwal Sen, Phys. Rev. A **87**, 052117 (2013).
2. *Local decoherence-resistant quantum states of large systems*, **Utkarsh Mishra**, Aditi Sen(De), and Ujjwal Sen, Phys. Lett. A **379**, 261 (2015).

A family of robust macroscopic quantum superposition states

5.1 Introduction

In this chapter, we identify a class of quantum states, each of which consists of a microscopic(minuscule) and a macroscopic(large) sector, that are effectively decoherence-free when each particle is locally passed through a noisy quantum channel. The states under consideration are of the form $|0\rangle|A_N\rangle + |1\rangle|B_N\rangle$, where $|0\rangle$ and $|1\rangle$ are orthogonal states of the minuscule sector, while $|A_N\rangle$ and $|B_N\rangle$ are orthogonal states of the large part of the state. N is the number of parties in the large part. We will show that it is possible to choose the states $|A_N\rangle$ and $|B_N\rangle$ in such a way that the resulting state is macroscopic in the sense of their drastic difference in visibilities to Bell inequality violation. The quantumness of the considered state under decoherence is calculated using measures of quantum correlations. The robustness of entanglement [20] and other quantum correlations [21] of the state is considered in the partition of the entire system into the minuscule and the large parts. The large part contains, in general, a relatively larger number of particles than the minuscule part. For specificity, we consider quantum states which has unit amount of entanglement in the minuscule to large bipartition.

We refer to the quantum states in the class that we investigate as the $H_{C_N}^m$ states, which have k particles in its minuscule part and N in its large part. The large sector is built by using W states [142, 144, 145], or more generally, Dicke states [146] with m excitations, and by an orthogonal product state. For the case when the large sector is built by the W state and the product state, we call the entire state as the

H-cat state and denote it by $|H_C\rangle$. The large part of the $H_{C_N}^m$ states can be shown to be “macroscopic” in a sense discussed in chapter 4. To study the behavior of quantumness of the state, we consider the effect of environment on each qubit of the state. The environment is modeled by quantum channels, discussed in chapter 2. We consider five kinds of noise models: local bit flip, local bit-phase flip, local phase damping, local amplitude damping, and local depolarizing channels. While performing quantum information processing using multipartite quantum states, different kind of decoherence effects may arise. For example, when using photons as a carrier of information, along with the environmental effects considered above, loss of particles is also a source of decoherence. The effect of loss of photons as a source of decoherence was, e.g., investigated in the teleportation protocol by Park *et al.* [296]. We consider also the effect of particle loss from the large sector of the state, as a source of decoherence.

We first investigate the quantum correlations properties of the decohered H-cat state under the noise models. In particular, we report the the effect of loss of a finite particle in the large sector, local depolarizing channel to each qubit, and their simultaneous effect on the H-cat state. We show that the H-cat state is robust, i.e. can preserve quantum coherence in the form of quantum correlations between its minuscule to large sector bipartition, against loss of a finite fraction of its particles and against local depolarizations on all its particles, and with the simultaneous action of both these noise effects. We then compare the robustness of this state with other quantum states of large systems including the N -party GHZ state. In particular, we find that for a finite number of particles in the macroscopic part, the H-cat state is more robust to local depolarizing noise than the GHZ state. It is important to mention here that it is not the multipartite entanglement of the noise-affected H-cat state that we consider. Instead, we consider the bipartite quantum correlations between the micro and the macro sectors of the noisy state. This is because it is this quantity that affects the state’s ability to produce macroscopically distinct superpositions in the large sector by measurements in the minuscule one.

We then discuss the effect of decoherence on the quantum correlation properties of the $H_{C_N}^m$ state given in Eq. (5.1). We observe that the content of entanglement and other quantum correlations in the microscopic to macroscopic partition of this class of states is independent of the number of particles in their macroscopic sectors, when all the particles suffer passage through local amplitude and phase damping channels. Decay of quantum correlations – entanglement as well as quantum discord – of this class of states in the minuscule to large partition is also much lower in

the case of all the local quantum channels, as compared to the other macroscopic superposition states.

5.2 The $H_{C_N}^m$ state as macroscopic quantum states

We define here a class of quantum states, each consisting of a minuscule and a large part. We denote it by $|H_{C_N}^m\rangle$, and is given by

$$|H_{C_N}^m\rangle = \frac{1}{\sqrt{2}}[|0^{\otimes k}\rangle_{\mu}|W_N^m\rangle_M + |1^{\otimes k}\rangle_{\mu}|0^{\otimes N}\rangle_M], \quad (5.1)$$

where

$$|W_N^m\rangle = \frac{1}{\sqrt{\binom{N}{m}}} \sum |1^{\otimes m}0^{\otimes N-m}\rangle. \quad (5.2)$$

The sum in the last equation denotes the equal superposition of all the $\binom{N}{m}$ combinations of m $|1\rangle$'s and $(N - m)$ $|0\rangle$'s. Here $\binom{N}{m} = \frac{N!}{m!(N-m)!}$. The suffix μ denotes the microscopic part while the suffix M is for the macroscopic sector of the state. We assume that $1 \leq m < N$. The case $m = 0$ is uninteresting, as then the $\mu : M$ partition is unentangled. The $H_{C_N}^m$ state becomes a GHZ state for $m = N$, which is considered separately in the succeeding section. We will generally be interested in the cases where $1 \leq k \ll N$, i.e., where the number of particles (qubits) in the microscopic part is much smaller than that of the macroscopic part. For $k = 1$ and $m = 1$, this reduces to the H-cat state [141, 297].

The state $|H_{C_N}^m\rangle$ has unit entanglement in the $\mu : M$ partition, and is of the form of the Schrödinger cat state, i.e., $|\bar{0}\rangle_{\mu}|\text{alive}\rangle_M + |\bar{1}\rangle_{\mu}|\text{dead}\rangle_M$, where $|\bar{0}\rangle_{\mu}$ and $|\bar{1}\rangle_M$ are orthonormal states of the microscopic part, and $|\text{alive}\rangle_M$ and $|\text{dead}\rangle_M$ are orthonormal states of the macroscopic (cat) part. In the case of $H_{C_N}^m$, the “alive” and “dead” states are modeled by $|W_N^m\rangle$ and $|0^{\otimes N}\rangle$, with the latter pair being macroscopically distinct in terms of their violation of Bell inequalities [144]. Following [144], we have computed the critical visibility for the state $|W_N^m\rangle$ beyond which the state violates local realism. The critical visibility in this case is given by

$$p_N^{\text{crit}}(m) = \frac{\binom{N}{m}}{(\sqrt{2} - 1)2^{N-1} + \binom{N}{m}} \quad (5.3)$$

which tends to zero as $N \rightarrow \infty$. It is in this sense that the states $|W_N^m\rangle$ and $|0^{\otimes N}\rangle$ of the large part of the H-cat state are macroscopically different. The Bell inequality

violation for the multipartite state that we use here is discussed in chapter 4.

For investigating the quantum coherence of this class of quantum states, each qubit of the $H_{C_N}^m$ state is sent through a noisy quantum channel. We then investigate the behavior of entanglement and quantum discord in the minuscule to large bipartition.

5.3 Effect of local decoherence on the H-cat state

First of all, we will study the effects of decoherence on the coherence properties of the H-cat state [141]. The H-cat state is obtained from the $|H_{C_N}^m\rangle$ state by substituting $m = 1$ and $k = 1$. The H-cat state, shared between $N + 1$ particles, is given by

$$|H_C\rangle_{\mu A_1 \dots A_N} = \frac{1}{\sqrt{2}} \left(|0\rangle_{\mu} |W_N\rangle_{A_1 \dots A_N} + |1\rangle_{\mu} |0^{\otimes N}\rangle_{A_1 \dots A_N} \right). \quad (5.4)$$

Here we consider its coherence properties after it has been subjected, *simultaneously* as well as separately, to local decoherence channels, in the form of local depolarizing channels, on all its constituent particles (in the micro as well as the macro sectors) and to loss of a finite fraction of its particles (in the macro part). The initial density matrix, i.e. the density matrix of the H-cat state before it passes through the local depolarizing channels and is affected by particle loss, is denoted here by $\rho_{N+1}^{in} = |H_C\rangle\langle H_C|$.

5.3.1 Effect of particle loss on the quantum correlations of the H-cat

We have already discussed that in various information processing tasks, using photons as a carrier of quantum information, it is essential to consider the loss of particles to account the effect of decoherence. In this section, we consider loss of particles as a channel of decoherence in characterizing macroscopic quantumness of the H-cat state. We begin with by considering a situation where the system loses a certain number of particles from its macroscopic part. Suppose ρ_{N+1}^{in} loses l particles from among the N particles constituting the macroscopic portion of the system. The resultant density matrix will then be an $(N - l + 1)$ party system having the following

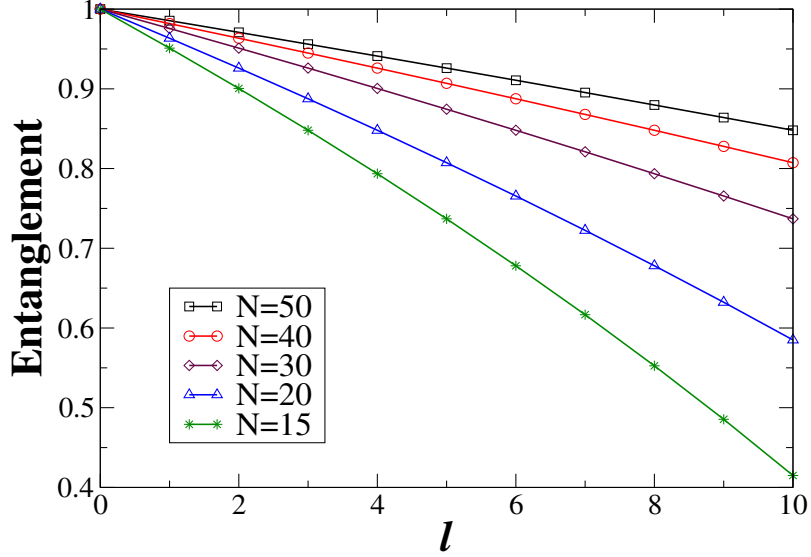


Figure 5.1: Entanglement after particle loss in H-cat state. The horizontal axis represents the number of particles lost (l) from the macroscopic part of the H-cat state while the vertical one represents the entanglement between the micro and the macro parts of the H-cat state after particle loss. The entanglement with respect to l is plotted for different initial number of particles, N . The vertical axis is measured in ebits, while the horizontal one is in particles.

form:

$$\begin{aligned}
\rho_{N-l+1}^L = & \frac{1}{2} \left[\frac{(N-l)}{N} |0\rangle\langle 0| \otimes |W_{N-l}\rangle\langle W_{N-l}| \right. \\
& + \frac{l}{N} (|0\rangle\langle 0|)^{\otimes N+1-l} + |1\rangle\langle 1| \otimes (|0\rangle\langle 0|)^{\otimes N-l} \\
& \left. + \left(\sqrt{\frac{N-l}{N}} |0\rangle\langle 1| \otimes |W_{N-l}\rangle\langle 0^{\otimes N-l}| + \text{h.c.} \right) \right]. \quad (5.5)
\end{aligned}$$

Here, the tensor product notation has been retained between the microscopic part (one qubit) and whatever has remained ($N-l$ qubits) after the loss of m particles from the macroscopic part. To investigate the effect of particle loss on the quantum coherence of the H-cat state $|H_C\rangle_{\mu A_1 \dots A_N}$, we find the entanglement, as quantified by logarithmic negativity, of the resultant state (after particle loss) in the $\mu : A_1 \dots A_{N-l}$ bipartition. Note here that we have assumed, without loss of generality, that the particles $A_{N-l+1}, A_{N-l+2}, \dots, A_N$ are lost. After taking the partial transposition with respect to the microscopic sector of the system, the partial transposed state of ρ_{N-l+1}^L is seen to be block-diagonal. The negative eigenvalue of the partial transposed state is

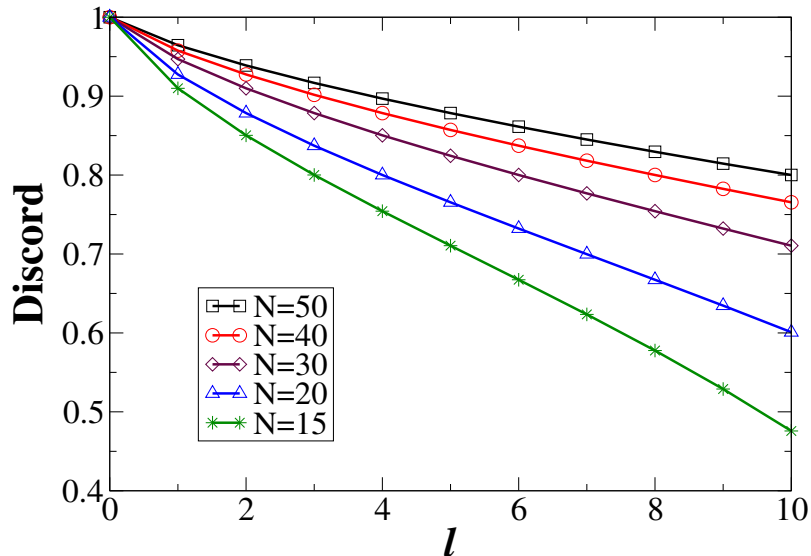


Figure 5.2: Quantum discord after particle loss in H-cat state. Other notations are the same as in Fig. 5.1.

$$\lambda_- = -\frac{1}{2} \left(1 - \frac{l}{N} \right). \quad (5.6)$$

Therefore, the entanglement of H-cat state after the loss of l particles is $E_N(\rho_{N-l+1}^L) = \log_2 \left(2 - \frac{l}{N} \right)$. If l and N are such that the ratio $\frac{l}{N}$ is a finite constant, then the entanglement between the microscopic and macroscopic parts will be less than unity, but can still be substantially higher than zero. The behavior of entanglement of the H-cat state with different rates of particle loss and for different total numbers of particles, is depicted in Fig. 5.1. The logarithmic decrease of entanglement with increasing numbers of particles lost, as seen from $E_N(\rho_{N-l+1}^L)$, is also clearly visible in Fig. 5.1.

We have also derived the quantum discord in the same situation, and found that the qualitative behavior is the same, except for slight changes in the curvature properties. In particular for $N = 50$, while about 85 % of the entanglement is retained after 10 particles are lost, it is about 80 % for quantum discord. See Fig. 5.2. It is worth to mention here that, for calculating the quantum discords of various states, we first find the corresponding state analytically, and then the optimization in the definition of quantum discord is performed numerically.

5.3.2 Effect of depolarizing channel on the quantum correlations of the H-cat

The depolarizing channel destroys off-diagonal elements of a quantum density matrix, destroying quantum coherence in the state, and is the usual model for decoherence phenomena [2]. Note that this is a *local* noise model, which is a natural choice for multiparty experimental situations, and our interest is in analyzing the coherence retained, after the action of this local noise on all the qubits building up the state. The form of the depolarizing channel, that we have used in this section, is given by Eq. (2.23) in chapter 2. We now investigate the quantum correlation properties of the H-cat state under local decoherence effects on all the $N + 1$ constituent particles. To this end, each particle, whether from the microscopic or the macroscopic sector, of the initial state ρ_{N+1}^{in} , is fed to a depolarizing channel, D_p . The output state, after this process, can be expressed as $D_p^1 \otimes D_p^2 \otimes \dots \otimes D_p^{N+1} \rho_{N+1}^{in} \equiv \rho_{N+1}^{D_p}$, where $D_p^1, D_p^2, \dots, D_p^{N+1}$ are $N + 1$ depolarizing channels acting on the $N + 1$ particles in the initial state. The entanglement and quantum discord of the locally decohered H-cat state can now be analyzed in the micro : macro bipartition. The mathematical form of the entanglement will be presented in a more general context below, and so we refrain from presenting it here. The results for entanglement are depicted in Fig. 5.3, where we also present the corresponding curves for the GHZ states. Interestingly, we obtain that the H-cat state is more resistant to local decoherence than the GHZ state, and for example, for 10 particles in the macroscopic part, the H-cat state can preserve entanglement up to 44% of local decohering noise, while the GHZ state remain entangled until 28% of the same noise. Quantum discord has a qualitatively similar behavior, and e.g. for $N = 7$, the quantum discord in the micro : macro partition for the GHZ state becomes $< 5 \times 10^{-4}$ for $p \approx 0.44$, while the same happens for the H-cat state for $p \approx 0.85$. See Fig. 5.4 for a depiction. The behavior of the entanglement of the H-cat state under local decoherence, for arbitrary N , can be read off from the formulas in Sec. 5.3.3 by setting $m = 0$. A plot of the entanglement for $N = 10^3$ is presented in Fig. 5.6. This is the $m = 0$ curve (continuous blue line) there.

5.3.3 Effect of both particle loss and local decoherence on the H-cat

We now consider the situation where the H-cat state is affected by local decoherence as well as by particle loss. We assume that l particles are lost (from the macro

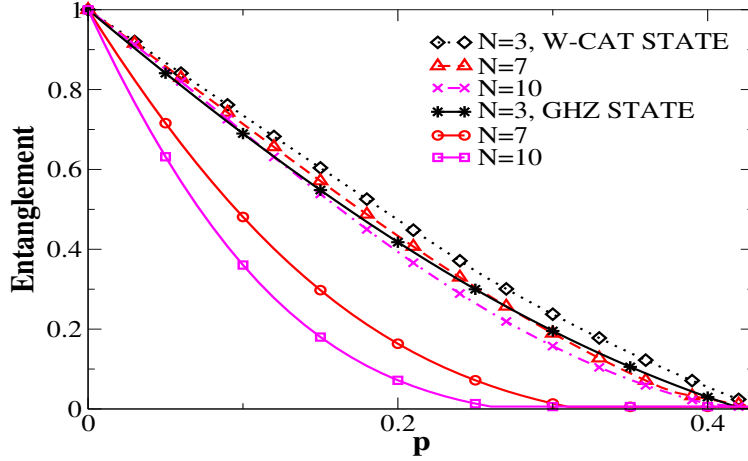


Figure 5.3: Entanglement of GHZ and H-cat states against local decoherence. While the continuous lines are for the GHZ states, the discontinuous ones are for the H-cat. The horizontal axis represents the dimensionless (decohering noise) parameter p , and the vertical axis is the entanglement in the micro : macro bipartition (in ebits).

part) and that the remaining $N - l + 1$ particles are all affected by local decoherence as modelled by the depolarizing channel. The entanglement in the micro : macro bipartition is analyzed for the resulting $(N - l + 1)$ -party state. There are two eigenvalues of the partial transposed state that make the maximum contribution. We denote them by $\lambda_-^{(1)}$ and $\lambda_-^{(2)}$, where $|\lambda_-^{(1)}| > |\lambda_-^{(2)}|$. Their explicit forms are given by

$$\lambda_-^{(1)} = \frac{1}{4} \left\{ c + (N - l - 1)d + a - \sqrt{4(N - l)b^2 + (c + (N - l - 1)d - a)^2} \right\}, \quad (5.7)$$

where

$$\begin{aligned} a &= \gamma_1 \tilde{p} + \frac{l}{N} \tilde{p}^{N-l+1} + \frac{p}{2} \tilde{p}^{N-l}, \\ b &= \frac{1}{\sqrt{N}} (1 - p)^2 \tilde{p}^{N-l-1}, \\ c &= \alpha_1 \frac{p}{2} + \frac{l}{N} \left(\frac{p}{2} \right)^2 \tilde{p}^{N-l-1} + \frac{p}{2} \tilde{p}^{N-l}, \\ d &= \frac{1}{N} \frac{p}{2} (1 - p)^2 \tilde{p}^{N-l-2}, \end{aligned}$$

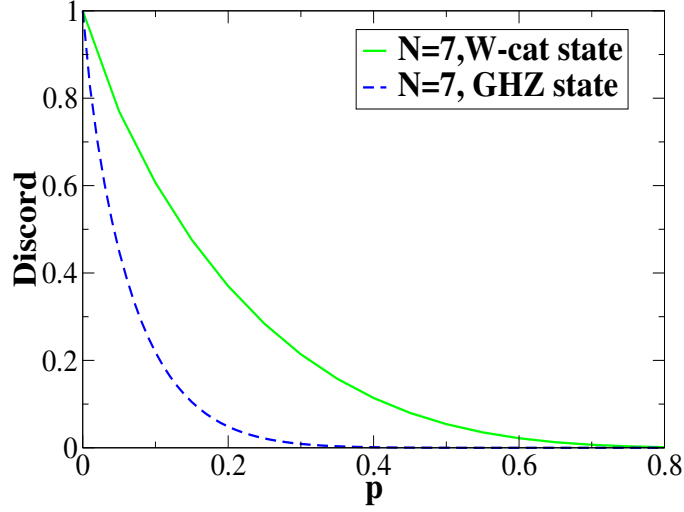


Figure 5.4: Quantum discord of GHZ and H-cat states against local decoherence. We plot the quantum discord (in ebits) on the vertical axis against the depolarizing parameter p (dimensionless) on the horizontal axis. The dashed line is for the GHZ state, while the continuous one is for the H-cat. The system is of 8 particles, so that $N = 7$. The states are led into local depolarizing channels at all the parties. The quantum discord of the output state is calculated in the micro : macro partition, where the measurement is carried out in the micro part.

with $\alpha_1 = \frac{1}{N} \left(\tilde{p}^{N-l} + (N-l-1) \left(\frac{p}{2}\right)^2 \tilde{p}^{N-l-2} \right)$, $\gamma_1 = \left(\frac{N-l}{N}\right) \left(\frac{p}{2}\right) \tilde{p}^{N-l-1}$, $\tilde{p} = 1 - \frac{p}{2}$, and

$$\lambda_-^{(2)} = \frac{1}{4} \left\{ (a_1 - b_1 + f + \tilde{N}g) - \sqrt{4(\tilde{N} + 2)e^2 + (-a_1 + b_1 + f + \tilde{N}g)^2} \right\}, \quad (5.8)$$

where

$$\begin{aligned} a_1 &= \left(\frac{p}{2}\right)^2 \tilde{p}^{N-l-1} + \frac{l}{N} \frac{p}{2} \tilde{p}^{N-l} + \gamma_2 \tilde{p}, \\ b_1 &= \frac{1}{N} (1-p)^2 \tilde{p}^{N-l-1}, \\ e &= \frac{1}{\sqrt{N}} (1-p)^2 \frac{p}{2} \tilde{p}^{N-l-2}, \\ g &= \frac{1}{N} (1-p)^2 \left(\frac{p}{2}\right)^2 \tilde{p}^{N-l-3}, \\ f &= \left(\frac{p}{2}\right)^2 \tilde{p}^{N-l-1} + \frac{l}{N} \left(\frac{p}{2}\right)^3 \tilde{p}^{N-l-2} + \alpha_2 \frac{p}{2}, \end{aligned}$$

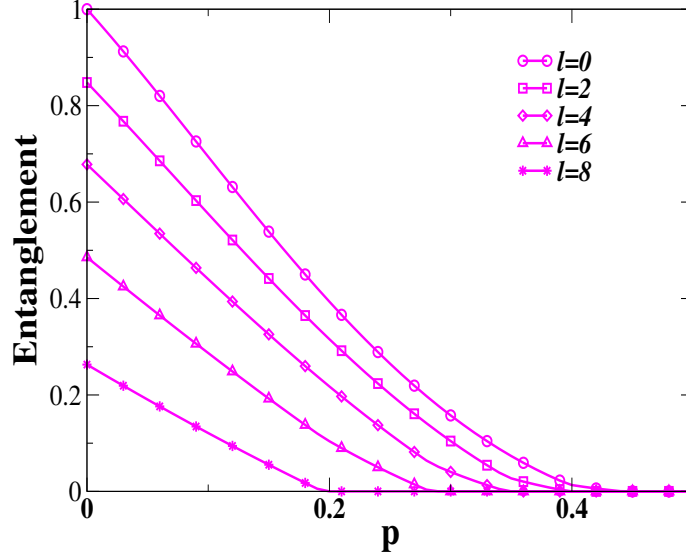


Figure 5.5: Effect of local decoherence and particle loss on H-cat state. Entanglement (measured in ebits) in the micro : macro bipartition is plotted on the vertical axis against a base of the dimensionless depolarizing parameter p , and the number of lost particles (l). The H-cat state under consideration is of 11 qubits, so that $N = 10$.

with $\alpha_2 = (1/N)[2\tilde{p}^{N-l-1}(p/2) + (N-l-2)(p/2)^3\tilde{p}^{N-l-3}]$, $\gamma_2 = \frac{1}{N}(\tilde{p}^{N-l} + (N-l-1)\left(\frac{p}{2}\right)^2\tilde{p}^{N-l-2})$, $\tilde{N} = N-l-4$.

The remaining eigenvalues make a contribution to the logarithmic negativity that is rather insignificant, and so for $N = 8$, $l = 1$ and $p = 0.1$, their contribution to the entanglement is less than 10^{-2} . Note here that by setting $l = 0$, we can obtain the entanglement expressions for the case when decoherence occurs without particle loss.

The entanglements are plotted in Figs. 5.5 and 5.6. In particular, in 5.6, we consider the case when the macroscopic system is constituted out of $N = 10^3$ particles, and we find that the entanglement in the micro : macro bipartition remains almost at its initial maximal value even with the loss of about 10% of its particles. Entanglement remains nonzero even when the remaining 90% particles are fed to local depolarizing channels until $p \lesssim .03$.

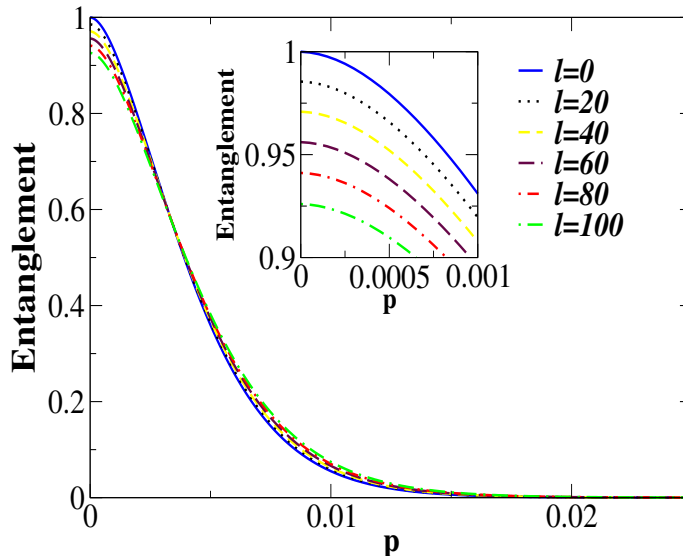


Figure 5.6: Effect of local decoherence and up to 10% particle loss on a H-cat state of $10^3 + 1$ qubits. All other considerations except the values of N and l are the same as in Fig. 5.5. The inset shows the details near $p = 0$.

5.4 Noise effects on entanglement of other micro:macro states

In this section, we compare other potential cat states with the H-cat state. We consider some other micro:macro states, and compare their ability to withstand particle loss. We begin by considering the state

$$|\Psi_1\rangle_{\mu A_1 \dots A_N} = \frac{1}{\sqrt{2}} \left(|0\rangle_{\mu} |W_N\rangle_{A_1 \dots A_N} + |1\rangle_{\mu} |\widetilde{W}_N\rangle_{A_1 \dots A_N} \right), \quad (5.9)$$

where

$$|\widetilde{W}_N\rangle_{A_1 \dots A_N} = \sigma_x^{\otimes N} |W_N\rangle_{A_1 \dots A_N}, \quad (5.10)$$

with $\sigma_x = |0\rangle\langle 1| + |1\rangle\langle 0|$. The state $|\Psi_1\rangle$ is the G state of Ref. [145]. This state is a cat-like state in the sense that the states $|W\rangle$ and $|\widetilde{W}\rangle$ are macroscopically distinct in terms of their σ^z -magnetizations, just like in the case of the GHZ state. This state, however, becomes separable if, for any N , we lose more than two particles.

Another state that can be considered as the micro:macro state is apparently quite similar to the H-cat state, with only the N -qubit W state state replaced by the state

$|\widetilde{W}_N\rangle$. This state therefore is

$$|\Psi_2\rangle_{\mu A_1 \dots A_N} = \frac{1}{\sqrt{2}} \left(|0\rangle_{\mu} |\widetilde{W}_N\rangle_{A_1 \dots A_N} + |1\rangle_{\mu} |0 \dots 0\rangle_{A_1 \dots A_N} \right). \quad (5.11)$$

This state is a cat-like state in the same sense as the H-cat state – the Bell inequality violations of $|\widetilde{W}_N\rangle$ and $|0 \dots 0\rangle$ are drastically different. Moreover, the states $|\widetilde{W}_N\rangle$ and $|0 \dots 0\rangle$ are also macroscopically different in terms of their σ^z -magnetizations. This state becomes separable if, for any N , we lose more than one particle.

An interesting generalization of the GHZ state is the concatenated GHZ [138] state

$$|\Psi_3\rangle = \frac{1}{\sqrt{2}} \left(|GHZ_p^+\rangle^{\otimes(N+1)} + |GHZ_p^-\rangle^{\otimes(N+1)} \right), \quad (5.12)$$

where

$$|GHZ_p^{\pm}\rangle = \frac{1}{\sqrt{2}} \left(|0\rangle^{\otimes p} \pm |1\rangle^{\otimes p} \right). \quad (5.13)$$

Here, there are $N+1$ logical qubits, and each logical qubit is built by using p physical qubits. Loss of all physical qubits from a logical qubit renders this state separable, like the GHZ state. Also, loss of some physical qubits from different logical qubits leads to separable states.

Yet another state is [92]

$$|\Psi_4\rangle = \frac{1}{\sqrt{2}} \left(|0\rangle |W_N\rangle + |1\rangle |W_N^{\perp}\rangle \right). \quad (5.14)$$

where

$$|W_N^{\perp}\rangle = \frac{1}{\sqrt{N}} \sum_{i=1}^N \omega^{i-1} |0 \dots 1_i \dots 0\rangle. \quad (5.15)$$

The index i denotes the position of $|1\rangle$, while the remaining positions are filled with $|0\rangle$ s. ω is an n^{th} complex root of unity. After a loss of l particles from the macroscopic sector of the state, the resulting state is a state of $N-l+1$ parties, and can be written as

$$\begin{aligned} \rho_{\Psi_4}^{N-l+1} &= \frac{1}{2} (\bar{N} |0\bar{1}\rangle \langle 0\bar{1}| + \bar{l} |0\bar{0}\rangle \langle 0\bar{0}| + \bar{N} |1\bar{1}\rangle \langle 0\bar{2}| \\ &\quad + \alpha |1\bar{0}\rangle \langle 0\bar{0}| + \text{h.c.}), \end{aligned} \quad (5.16)$$

where $|\bar{0}\rangle = |0 \dots 0\rangle$, $|\bar{1}\rangle = |W_{N-l}\rangle$, $|\bar{2}\rangle = |W_{N-l}^{\perp}\rangle$, and $\bar{N} = \frac{N-l}{N}$, $\bar{l} = \frac{l}{N}$, $\alpha = \sum_{i=1}^l \omega^{N-i}$. The eigenvalues of the partially transposed matrix in the micro : macro bipartition are $-\frac{\bar{N}}{2}$, $\frac{\bar{N}}{2}$, $\frac{\bar{N}}{2}$, $\frac{\bar{N}}{2}$, $\frac{l-2|\alpha|}{2N}$, $\frac{l+2|\alpha|}{2N}$. Since $0 \leq |\alpha| \leq 1$, there is only one

negative eigenvalue, namely $-\frac{\bar{N}}{2}$, for $l \neq 0$. We have seen in the case of H-cat state that the same eigenvalue contributes to the negativity, and hence in turn to the logarithmic negativity, which quantifies the entanglement in the micro : macro bipartition. So the behavior of $|\Psi_4\rangle$, under particle loss, is the same as of the H-cat state. However, the states $|W_N\rangle$ and $|W_N^\perp\rangle$ are neither macroscopically distinct in terms of their magnetizations nor in terms of their violations of Bell inequalities, or for that matter, any quantum correlation properties.

After discussion of the robustness of the H-cat state, we will now present the robustness of the $H_{C_N}^m$ state. The state $H_{C_N}^m$ can be considered a macroscopic quantum superposition in the sense defined in chapter 4 and Eq. (5.3). Thus, the $H_{C_N}^m$ state represent a class of macroscopic quantum superposition states for each value of m .

5.5 Effect of decoherence on the $H_{C_N}^m$ state

In this section, we discuss the effect of decoherence on the quantum correlations properties of $H_{C_N}^m$ when there are k particles in the microscopic sectors of the state. We then address two aspects of these states: (1) we consider the effects of local decoherence on these states and identify the state which is more robust against local noise than the other states, and (2) we study the scaling behavior of quantum correlations of this class of states with the increase in number of particles against noise.

5.5.1 Effect of local phase damping channel on the $H_{C_N}^m$ state

Let us begin with the situation when each qubit of the $H_{C_N}^m$ state is sent through a phase damping channel (Sec. 2.2.3). The block of the local phase damped $H_{C_N}^m$ state, after partial transposition, which contributes in the calculation of logarithmic negativity, in the micro : macro bipartition, is of the form

$$B_{H_{C_N}^m}^{lpdc} = \frac{1}{2} \begin{pmatrix} 0 & b & . & . & . & b \\ b & 0 & . & . & . & 0 \\ . & . & . & . & . & . \\ . & . & . & . & . & . \\ . & . & . & . & . & . \\ b & 0 & . & . & . & 0 \end{pmatrix},$$

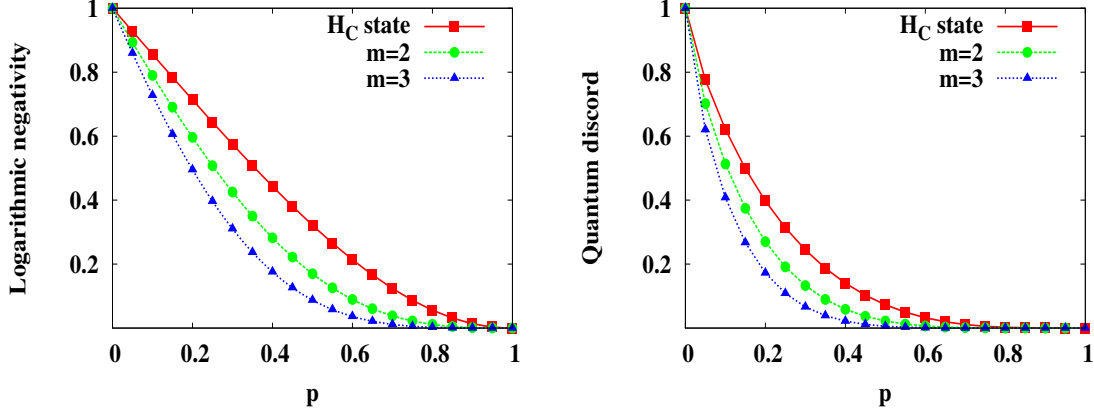


Figure 5.7: Entanglement and quantum discord of the local phase damped $H_{C_N}^m$ state. We plot the logarithmic negativity (in ebits) and quantum discord (in bits) on the vertical axes versus the decoherence parameter p (dimensionless) on the horizontal axes, for the $H_{C_N}^m$ state, after each of the qubits are affected by phase damping noise. The plots are displayed for $m = 1, 2$, and 3 . Note that for $m = 1$, the $H_{C_N}^m$ state is the same as the H_C state. All plots are for $N = 6$ and for $k = 1$. Here, and in the rest of the paper, we mostly plot the curves for the different quantities for a modest number of particles in the large sector (which, in the current case implies that we are dealing with a $2^7 \times 2^7$ matrix). This is despite the fact that in many cases, we can consider bigger system sizes and even have analytical results for arbitrary N . We however feel that the curves for the relatively modest system sizes will give the reader a feeling of the situation in a potential experimental realization of the phenomena considered.

where $b = \frac{1}{\sqrt{\binom{N}{m}}}(1-p)^{k+m}$. The block is obtained by considering the action of the LPDC on the off-diagonal elements of the state given in Eq. (5.1). We have to see how the term $(|0\rangle_\mu\langle 1|)^{\otimes k} \otimes |W_N^m\rangle_M\langle 0\dots 0| + (|1\rangle_\mu\langle 0|)^{\otimes k} \otimes |0\dots 0\rangle_M\langle W_N^m|$ transforms under the LPDC. To see it more closely, let us define $|0^{\otimes N}\rangle_M = |\bar{0}\rangle$, $|W_N^m\rangle_M = |\bar{1}\rangle$, and $|0^{\otimes k}\rangle_\mu = |\bar{0}\rangle$, $|1^{\otimes k}\rangle_\mu = |\bar{1}\rangle$. The diagonal terms transform as

$$\begin{aligned} |\bar{1}\rangle\langle\bar{1}| \otimes |\bar{0}\rangle\langle\bar{0}| &\mapsto |\bar{1}\rangle\langle\bar{1}| \otimes |\bar{0}\rangle\langle\bar{0}| \\ |\bar{0}\rangle\langle\bar{0}| \otimes |\bar{1}\rangle\langle\bar{1}| &\mapsto |\bar{0}\rangle\langle\bar{0}| \otimes D + |\bar{0}\rangle\langle\bar{0}| \otimes OD, \end{aligned} \quad (5.17)$$

where D is diagonal in the basis formed by the elements of the superposition $\sum |1^{\otimes m}0^{\otimes N-m}\rangle$ in Eq. (5.2), and OD consists of off-diagonal elements in the same basis. On the other hand, the off-diagonal terms transform as

$$\begin{aligned} |\bar{0}\rangle\langle\bar{1}| \otimes |\bar{1}\rangle\langle\bar{0}| &\mapsto (1-p)^{m+k} |\bar{0}\rangle\langle\bar{1}| \otimes |\bar{1}\rangle\langle\bar{0}| \\ |\bar{1}\rangle\langle\bar{0}| \otimes |\bar{0}\rangle\langle\bar{1}| &\mapsto (1-p)^{m+k} |\bar{1}\rangle\langle\bar{0}| \otimes |\bar{0}\rangle\langle\bar{1}| \end{aligned} \quad (5.18)$$

As we can see, the transformed diagonal terms do not interfere with the transformed off-diagonal terms, and therefore, only one independent block will contribute in the negativity and hence in the logarithmic negativity of the state given in Eq. (5.1) in its micro : macro bipartition under LDPC. The size of the block is $\binom{N}{m} + 1 \times (\binom{N}{m} + 1)$. The eigenvalues of this block are calculated analytically and only one negative eigenvalue is obtained. The negative eigenvalue is given by

$$\lambda_{H_{C_N}^m}^{lpdc} = -\frac{1}{2}(1-p)^{k+m}. \quad (5.19)$$

Therefore, the logarithmic negativity of the local phase damped state is given by

$$E_{H_{C_N}^m}^{lpdc}(k, m) = \log_2[2|\lambda_{\rho_{H_{C_N}^m}}^{lpdc}| + 1]. \quad (5.20)$$

An important point to note is that the entanglement does not depend on the total number of particles, N . That is, the effect on the $H_{C_N}^m$ state after all N qubits of the state are sent through phase damping channels, is independent of the size of the macroscopic part. As we will see below, (Sec. 5.5.2), this beautifully simple situation persists for the local amplitude damping channel. The case is richer for the local depolarization (Sec. 5.5.3), and the noise-affected state does depend on N , although the scaling of quantum correlations is better than in the noise-affected GHZ state. Coming back to local phase damping, when $m = 1$, $k = 1$, we obtain

$$E_{H_{C_N}^m}^{lpdc}(1, 1) = \log_2(\gamma^2 + 1), \quad (5.21)$$

with $\gamma = 1 - p$. This value of entanglement is the maximum among all other states in this class, i.e., among all $H_{C_N}^m$, as also observed in Fig. 5.7. Moreover, note that in the noiseless case, the entanglement is unity for all $H_{C_N}^m$.

Instead of entanglement, if one considers quantum discord, in the micro : macro bipartition, we again find that the $H_{C_N}^1$ state, with a single particle in the microscopic section, is maximally robust under this kind of noise than all the other states in this class (see Fig. 5.7). Moreover, numerical simulation indicates that quantum discord for this class of states is also independent of system-size of macroscopic part up to first order of magnitude (see Fig. 5.8). It is also observed that the independency of quantum discord on the number of parties in the macroscopic sector remains valid for higher values of k .

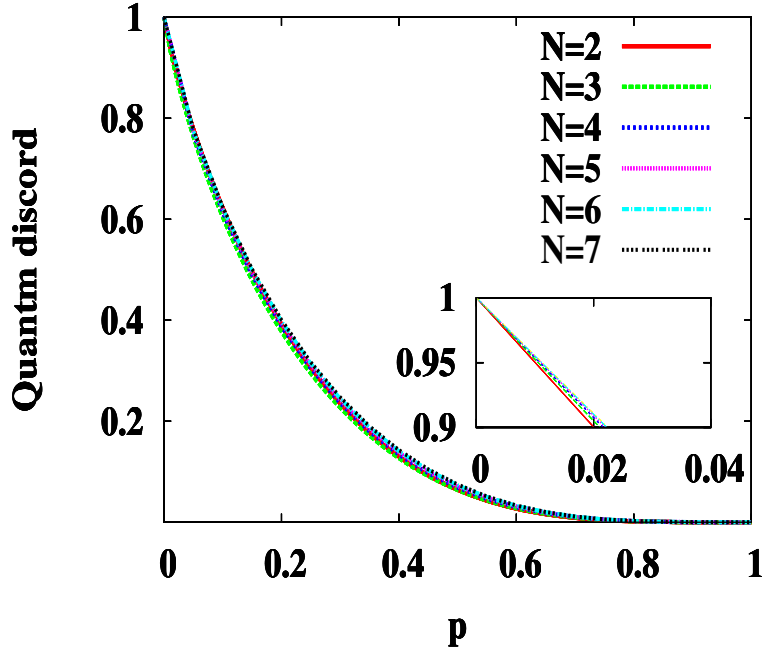


Figure 5.8: Independence of quantum discord of the local phase damped $H_{C_N}^1$ state on the number of particles in the macroscopic sector. Quantum discord (in bits) for the $H_{C_N}^1$ state (i.e., the H_C state) for different values of N after the state is local phase damped, is plotted on the vertical axis, against the decoherence parameter p (dimensionless) on the horizontal axis. Here, the microscopic part of the state consists of a single particle (i.e., $k = 1$). This shows that the quantum discord, like entanglement, is independent, up to numerical accuracy, of size of the macroscopic sector. A similar feature holds for higher values of k . The inset shows the same figure blown up near $p = 0$.

5.5.2 Effect of local amplitude damping channel on the $H_{C_N}^m$

Consider now the situation when all the qubits of the $H_{C_N}^m$ state are sent through amplitude damping channels. In this case, the block of the partially transposed local amplitude damped $H_{C_N}^m$ state, which gives negative eigenvalues contributing to entanglement in the micro : macro bipartition is an $\left(\binom{N}{m} + 1\right) \times \left(\binom{N}{m} + 1\right)$ matrix,

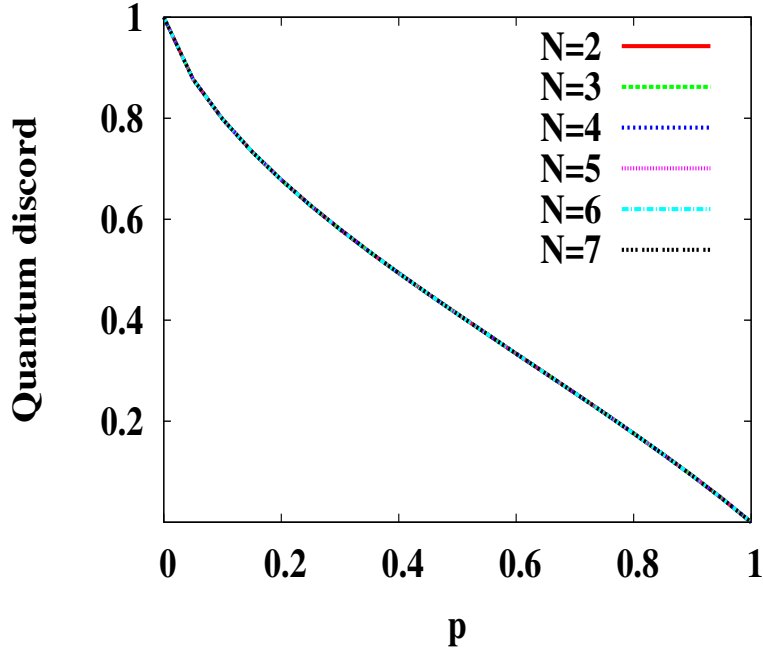


Figure 5.9: Independence of quantum discord of the local amplitude damped $H_{C_N}^m$ state on the number of particles in the macroscopic sector. All other considerations are the same as in Fig. 5.8, except that we do not have the inset here.

and is given by

$$B_{H_{C_N}^m}^{ladc} = \frac{1}{2} \begin{pmatrix} p^k + p^m & \frac{(1-p)^{\frac{m+k}{2}}}{\sqrt{\bar{N}}} & \dots & \frac{(1-p)^{\frac{m+k}{2}}}{\sqrt{\bar{N}}} \\ \frac{(1-p)^{\frac{m+k}{2}}}{\sqrt{\bar{N}}} & 0 & \dots & 0 \\ \cdot & \cdot & \dots & \cdot \\ \cdot & \cdot & \dots & \cdot \\ \cdot & \cdot & \dots & \cdot \\ \frac{(1-p)^{\frac{m+k}{2}}}{\sqrt{\bar{N}}} & 0 & \dots & 0 \end{pmatrix}.$$

Here, $\bar{N} = \binom{N}{m}$. We have used the same method as for the LPDC, to obtain the block contributing in the negativity of the state given in Eq. (5.1) under LADC. Here, after the channel has acted, the diagonal terms interfere with the off-diagonal terms, and therefore the first element of the block $B_{H_{C_N}^m}^{ladc}$ is non-zero. The negative eigenvalue of this matrix, denoted by $\lambda_{H_{C_N}^m}^{ladc}$, is given by

$$\lambda_{H_{C_N}^m}^{ladc} = \frac{1}{4} (p^k + p^m - \sqrt{(p^k + p^m)^2 + 4(1-p)^{k+m}}), \quad (5.22)$$

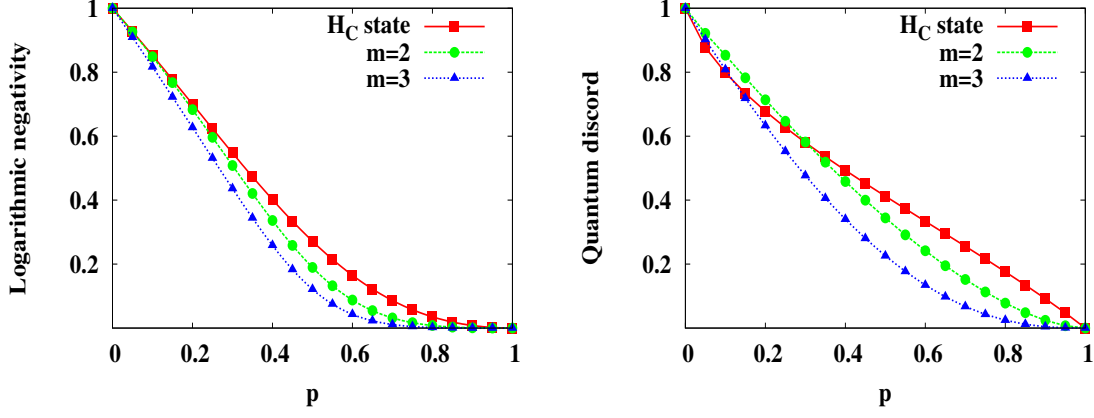


Figure 5.10: Logarithmic negativity and quantum discord against the noise parameter of amplitude damping channel, for the local amplitude damped $H_{C_N}^m$ state. All other considerations are the same as in Fig. 5.7.

and therefore the logarithmic negativity is

$$E_{H_{C_N}^m}^{ladc}(k, m) = \log_2[2|\min(0, \lambda_{H_{C_N}^m}^{ladc})| + 1]. \quad (5.23)$$

It is clear from Eqs. (5.22) and (5.23) that the logarithmic negativity is independent of N , just as for the local phase damping channel. Quantum discord, which is obtained numerically, is also independent of system size, as depicted in Fig. 5.9, for $k = 1$. The independency of quantum discord on N holds true also for higher values of k . For $k = 1$ and $m = 1$, the negative eigenvalue in Eq. (5.22) reduces to

$$\lambda_{H_{C_N}^m}^{ladc}(1, 1) = \frac{1}{2}(p - \sqrt{p^2 + (1-p)^2}). \quad (5.24)$$

Just like for the local phase-damping channel, the state $H_{C_N}^1$ can sustain more noise than any other states in this class for both the quantum correlation measures. Note here that quantum discord is non-zero for the entire range of the noise parameter, except at $p = 1$. Both the quantum correlations are plotted in Fig. 5.10 for different values of m .

5.5.3 Effect of local depolarizing channel on the $H_{C_N}^m$ state

We now consider the effect of the local depolarizing channel on the $H_{C_N}^m$ state. Unlike phase and amplitude damping channels, entanglement in this case does depend on the total number of particles, N , in the macroscopic part, and decreases with the increase of N . We also probe the behavior of entanglement with respect to m for

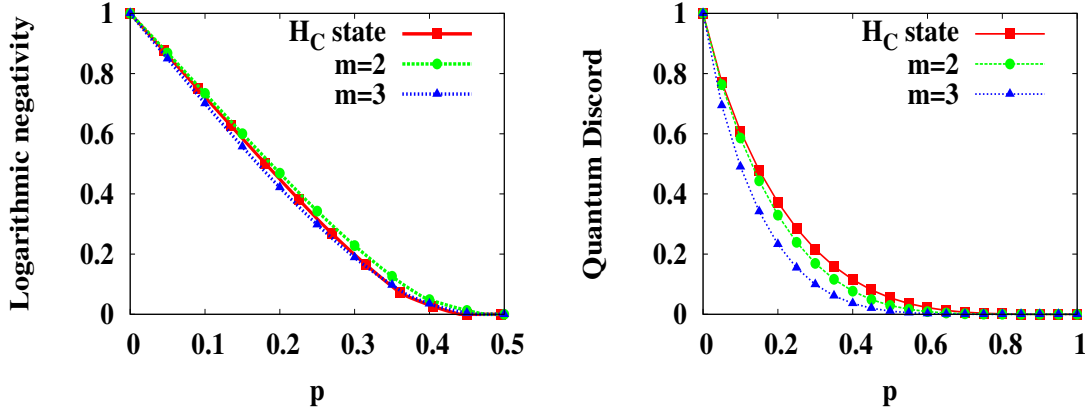


Figure 5.11: Logarithmic negativity and quantum discord for the local depolarized $H_{C_N}^m$ state against the noise parameter of the depolarizing channel. All other considerations are the same as in Fig. 5.7.

fixed total number of particles and also for a fixed number, k , of parties in the microscopic part.

As seen in Fig. 5.11 (left), the state with two excitations (i.e., $m = 2$), is more robust against local depolarizing channels than the state with one excitation (i.e., $m = 1$). Likewise, quantum discord decreases with the increase of excitations (see Fig. 5.11 (right)).

5.5.4 A comparison of the local decohering channels

It is interesting to find the channel, from the ones considered in this thesis, that is least destructive for the $H_{C_N}^m$. For fixed N , m , and k , we compared their effects on entanglement and discord of the state. An example of such comparison is presented in Fig. 5.12. It is observed that for both the quantum correlation measures, the local depolarizing channel is maximally destructive. The local amplitude damping channel is much less destructive in both cases. The local phase damping channel has, however a richer behavior. It is minimally destructive to logarithmic negativity, while surprisingly being almost maximally destructive to quantum discord.

5.6 Effect of decoherence on the GHZ state

Up to now, we have studied decoherence effects on the $H_{C_N}^m$ state for different models of decoherence. In this section, we study effects of these noise models on the well-known macroscopic state, the GHZ state. The GHZ state, consisting of k parties in

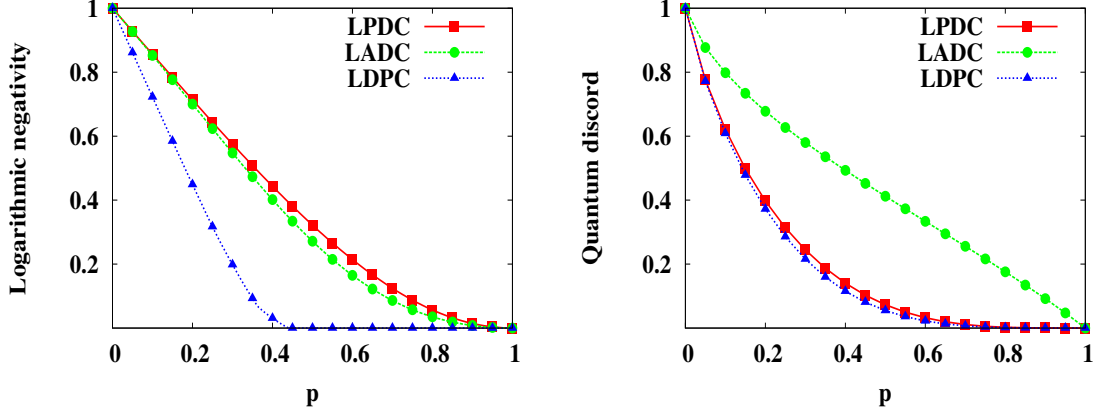


Figure 5.12: How much quantum correlation is retained against which noise? Logarithmic negativity and quantum discord for different noisy channels in the micro : macro bipartition for the $H_{C_N}^1$ state for $k = 1$. Here we have taken $N = 6$. The vertical axes are in ebits for logarithmic negativity and in bits for quantum discord. The dimensionless parameter p on the horizontal axes corresponds to the noise parameter in the LPDC, the LADC, or the LDPC.

the microscopic part and N in the macroscopic one, is given by

$$|\text{GHZ}\rangle_{N+k} = \frac{1}{\sqrt{2}}(|0^{\otimes k}\rangle_{\mu} \otimes |0^{\otimes N}\rangle_M + |1^{\otimes k}\rangle_{\mu} \otimes |1^{\otimes N}\rangle_M). \quad (5.25)$$

Just like the $H_{C_N}^m$ state, the $|\text{GHZ}\rangle_{N+k}$ state also possesses one ebit of entanglement which is the same as its quantum discord, in the microscopic to macroscopic bipartition. In this section, we will study the trends of quantum correlations of the $|\text{GHZ}\rangle_{N+k}$ state, against the three local noise models that we had considered for the $H_{C_N}^m$ state, and compare with those of the $H_{C_N}^m$ state. It has to be noted here that the macroscopic sector of the $H_{C_N}^m$ state consisting of N -qubit Dicke state has non-zero entanglement in any bipartition while both the states of the same sector of the GHZ state have zero entanglement to begin with.

5.6.1 Effect of local phase damping channel on the GHZ state

Let us begin by considering the effect of local phase damping channels on the GHZ state. After each qubit of the GHZ state is sent through a phase damping channel, the resulting state can be written as

$$\rho_{\text{GHZ}_{N+k}}^{lpdc} = \frac{1}{2} \left(P_0^{\mu \otimes k} \otimes P_{0\dots 0} + P_1^{\mu \otimes k} \otimes P_{1\dots 1} + A(P_{0,1}^{\mu \otimes k} \otimes P_{0\dots 0,1\dots 1} + h.c.) \right), \quad (5.26)$$

where $A = (1 - 2\beta)^{N+k}$, $\beta = \frac{p}{2}$, $P_0^\mu = |0\rangle\langle 0|$, $P_1^\mu = |1\rangle\langle 1|$, $P_{0,1}^\mu = \gamma|0\rangle\langle 1|$, $P_{0\dots 0} = |0\dots 0\rangle\langle 0\dots 0|$, $P_{1\dots 1} = |1\dots 1\rangle\langle 1\dots 1|$, $P_{0\dots 0,1\dots 1} = |0\dots 0\rangle\langle 1\dots 1|$. Here, $\gamma = 1 - p$. After performing the partial transpose on the state $\rho_{\text{GHZ}_{N+k}}^{\text{lpdc}}$ with respect to micro : macro bipartition, the matrix $B_{\text{GHZ}_{N+k}}^{\text{lpdc}}$, whose eigenvalues contribute to the entanglement of the noisy GHZ $_{N+k}$ state in the micro : macro bipartition, is found to be of the form

$$B_{\text{GHZ}_{N+k}}^{\text{lpdc}} = \begin{pmatrix} 0 & \frac{(1-2\beta)^{N+k}}{2} \\ \frac{(1-2\beta)^{N+k}}{2} & 0 \end{pmatrix},$$

and hence the entanglement is given by

$$E_{\text{GHZ}_{N+k}}^{\text{lpdc}} = \log_2[(1-p)^{N+k} + 1]. \quad (5.27)$$

It is clear from Eq. (5.27) that the entanglement of the state depends on the number of the particles in the macroscopic part. This is in sharp contrast to the situation in the case of the $H_{C_N}^m$ state, where quantum correlations do not depend on the number of particles in the macroscopic part of the state. Note that the exponential of the logarithmic negativity decreases as $(1-p)^{k+m}$ for the $H_{C_N}^m$ state (Eq. (5.20)), while as $(1-p)^{N+k}$ for the GHZ state (Eq. (5.27)). Since $m < N$, the entanglement of the $H_{C_N}^m$ state under a noisy environment, as modeled by local dephasing channels, is more than that of the GHZ $_{N+k}$ state, for any N , m , and k . The entanglements match for $m = N$. The $H_{C_N}^m$ and GHZ $_{N+k}$ states are equal up to local unitary transformations for $m = N$. But this does not imply equality of the entanglements for all channels, as the local unitary transformations and the local decohering channels may not commute. Note also that it is certainly possible to consider the case when $1 \leq m \ll N$, and in such cases, $(1-p)^{k+m}$ and $(1-p)^{k+N}$ are very different.

5.6.2 Effect of local amplitude damping channel on the GHZ state

In this case, all the qubits of the GHZ $_{N+k}$ state are sent through amplitude damping channels. The block of the total matrix, after partial transposition, which is responsible for non-zero logarithmic negativity is

$$B_{\text{GHZ}_{N+k}}^{\text{ladc}} = \frac{1}{2} \begin{pmatrix} p^k \gamma^N & \gamma^{\frac{N+k}{2}} \\ \gamma^{\frac{N+k}{2}} & p^N \gamma^k \end{pmatrix}.$$

Correspondingly, the eigenvalue which can be negative for some values of p , is given by

$$\lambda_{\text{GHZ}_{N+k}}^{\text{ladc}} = \frac{1}{4} \left(p^k \gamma^N + p^N \gamma^k - \sqrt{(p^k \gamma^N + p^N \gamma^k)^2 + 4\gamma^{N+k}(1-p^{N+k})} \right). \quad (5.28)$$

For fixed N , comparing Eqs. (5.22) and (5.28), we find that under the local amplitude damping channel, the $H_{C_N}^1$ state has higher entanglement than the GHZ_{N+k} state for all $N > 2$ and for $k \ll N$. See Figs. 5.13. Moreover, the ‘‘critical value’’ of the decohering parameter, p , at which the decohered state becomes separable, is always greater for the $H_{C_N}^1$ state than that for the GHZ_{N+k} state for all $N > 2$ and for $k \ll N$ (see also Table I). For higher values of m , i.e. for $m > 1$, the $H_{C_N}^m$ state has higher entanglement than the GHZ state, provided we choose sufficiently high N (See Figs. 5.13). Note that unlike the case of the local phase damping channel, the entanglements of the local amplitude damped $H_{C_N}^N$ and GHZ_{N+k} states do not match. However, the local amplitude damped $H_{C_N}^N$ can have only a lower entanglement than the local amplitude damped GHZ_{N+k} . This is clearly seen from Eqs. (5.22) (for $m = N$) and (5.28) (see also Fig. 5.13 for $m = 1, 10, 20, 30$).

5.6.3 Effect of local depolarizing channel on the GHZ state

Let us now study the effect of local depolarizing channels on the GHZ_{N+k} state. To calculate the entanglement, in the micro : macro bipartition, we have to find the negative eigenvalue of the matrix given by

$$B_{\text{GHZ}_{N+k}}^{\text{ldpc}} = \frac{1}{2} \begin{pmatrix} a & b \\ b & a \end{pmatrix},$$

where $a = \alpha^k \beta^N + \beta^k \alpha^N$, $b = \gamma^{N+k}$, $\gamma = (1-p)$ and $\alpha = (1 - \frac{p}{2})$. The eigenvalue of $B_{\text{GHZ}_{N+k}}^{\text{ldpc}}$, which is negative for some values of p , is given by

$$\lambda_{\text{GHZ}_{N+k}}^{\text{ldpc}} = \frac{1}{2} [\alpha^k \beta^N + \alpha^N \beta^k - \gamma^{N+k}]. \quad (5.29)$$

The logarithmic negativity, then, is given by

$$E_{\text{GHZ}_{N+k}}^{\text{ldpc}} = \log_2(2|\min(0, \lambda_{\text{GHZ}_{N+k}}^{\text{ldpc}})| + 1). \quad (5.30)$$

For six particles in the macroscopic sector and a single particle in the microscopic one, a comparison of entanglement and discord between the $|H_{C_N}^1\rangle$, $|H_{C_N}^2\rangle$, $|H_{C_N}^3\rangle$,

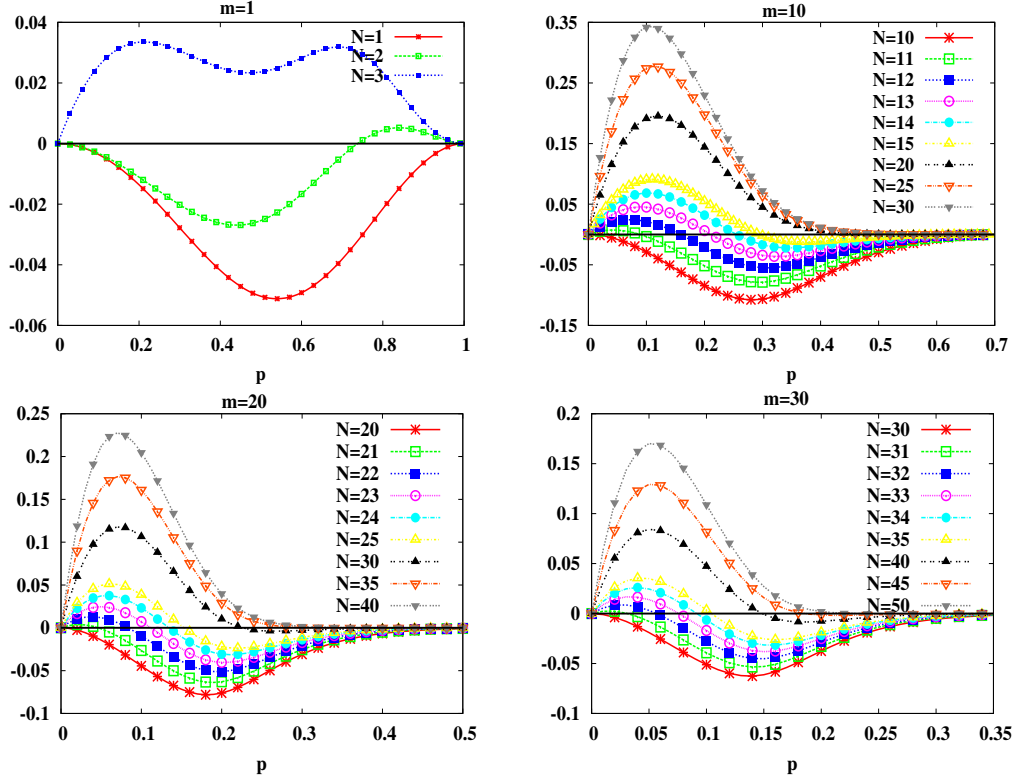


Figure 5.13: Comparison of the entanglements of the local amplitude damped $H_{C_N}^m$ and GHZ_{N+k} states. We plot here the difference, \mathcal{D} , between the logarithmic negativities (logarithmic negativity of the noisy $H_{C_N}^m$ state minus that of the noisy GHZ_{N+k} state) of the local amplitude damped $H_{C_N}^m$ and GHZ_{N+k} states for $k = 1$ and $m = 1, 10, 20, 30$, on the vertical axes, against the amplitude damping parameter, p , on the horizontal axes, for different number of qubits, N , in the macroscopic part. The logarithmic negativities are measures in ebits, while N is measured in qubits. p is a dimensionless parameter. The curves are plotted in the respective cases only up to a certain value of N , that depends on m . For higher N , the curves are always positive with respect to the vertical axis. The highest value of N , for a given m , that is plotted in a given panel, is however not necessarily the highest value of N , for which $\mathcal{D} \geq 0$ for all p . The $\mathcal{D} = 0$ line is marked on all the panels for ease of reference.

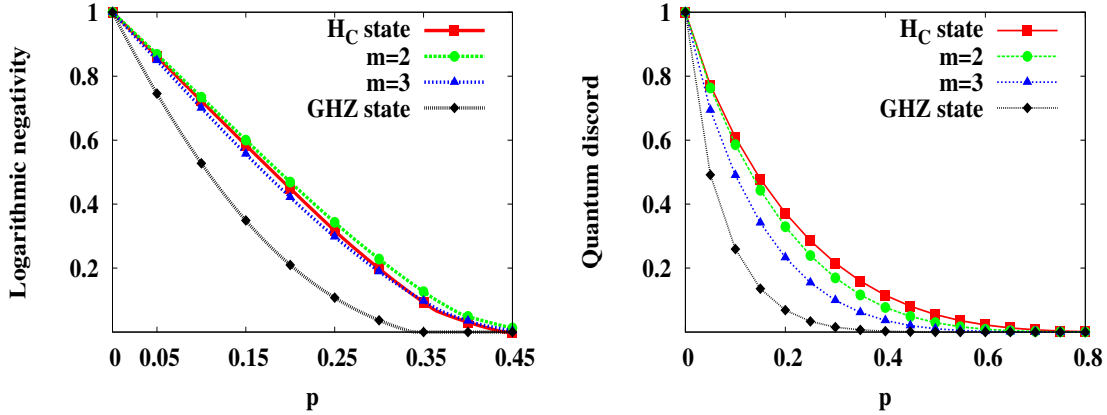


Figure 5.14: The panels are the same as in Fig. 5.11, except that there is an additional curve in each panel corresponding to the GHZ state for $k = 1$, $N = 6$. See Table I for numerical values.

and the GHZ states, after they are affected by local depolarizing channels, is presented in Fig. 5.14. We find that the $|H_{C_N}^1\rangle$, $|H_{C_N}^2\rangle$ and $|H_{C_N}^3\rangle$ can sustain about 43%, 46%, and 45% noises respectively, while the GHZ remains robust against up to 34% noise, for $k = 1$ and $N = 6$. When $k = 2$, the value of p at which logarithmic negativity vanishes is 0.445 for the $|H_{C_N}^1\rangle$ state while it is 0.43 for the GHZ state. When $k = 3$ these values are 0.42 and 0.48 for the $|H_{C_N}^1\rangle$ and GHZ states, respectively. A comparison between the $|H_{C_N}^1\rangle$ and GHZ states, after they are affected by local depolarizing channels, is presented in Fig. 5.15 for different values of k . A comparison with respect to robustness of entanglement and quantum discord, between the different noise models, of the GHZ state is presented in Fig. 5.16. The latter comparison reveals a picture that is quite different from that obtained in a similar comparison in Fig. 5.12 for the $H_{C_N}^m$ state. See Figs. 5.12 and Fig. 5.16 for more details.

5.7 Effect of local bit and bit-phase flip channels on the GHZ and the $H_{C_N}^m$ states and their comparison

In this section, we will compare the effects on the quantum correlations of the $H_{C_N}^m$ state with those of the GHZ state, in their $\mu : M$ bipartitions when each qubit of the states is sent through the bit flip or the bit-phase flip channel with error probability p . In case of the bit flip, logarithmic negativity of the $H_{C_N}^m$ state is decreasing

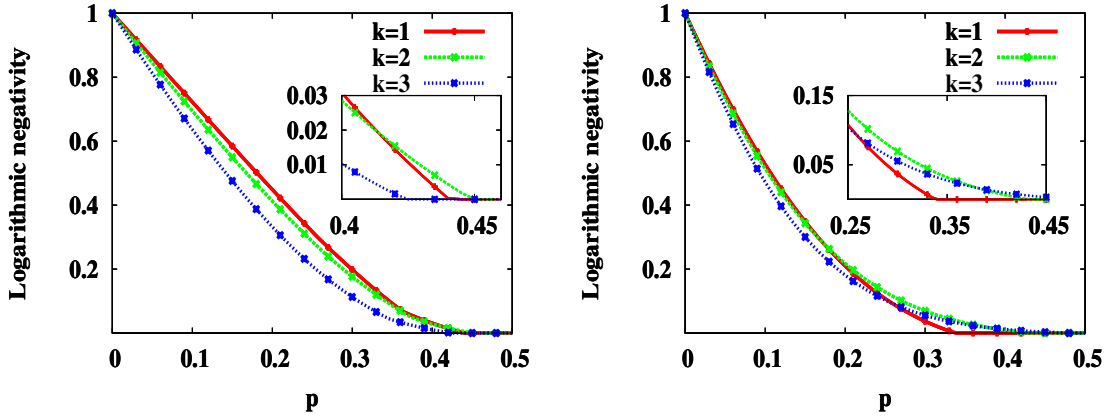


Figure 5.15: $H_{C_N}^1$ (left panel) and GHZ (right panel) after being affected by local depolarizing channels for different number of particles in the macroscopic sectors. The vertical axes represent logarithmic negativity (in ebits) in the micro : macro bipartition, the horizontal axes correspond to the depolarizing parameter, p (dimensionless). We choose $N = 6$. As is clear from the panel on the right, increase of k for a fixed N leads to increase in logarithmic negativity for the GHZ state. The insets reveal the situations where the entanglements vanish. The axes of the insets represent the same quantities as of the corresponding parent figures.

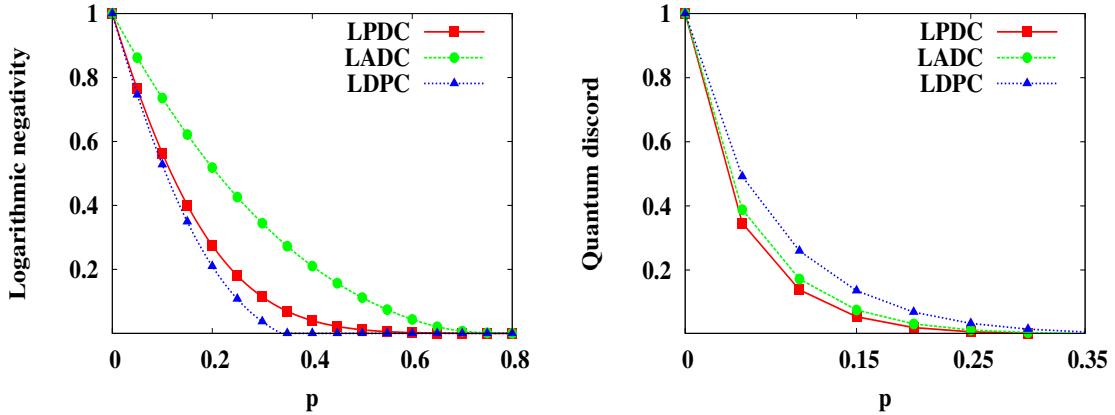


Figure 5.16: The panels are the same as in Fig. 5.12, except that all the curves correspond now to the noise-affected GHZ states instead of the $H_{C_N}^1$ states. Comparing the panels here with those of Fig. 5.12, we see that the noise-affected GHZ states behave very differently from the corresponding noise-affected $H_{C_N}^1$ states. This is especially true for the entanglements of the local phase damped states and for the quantum discords of the states after being affected by any type of noise.

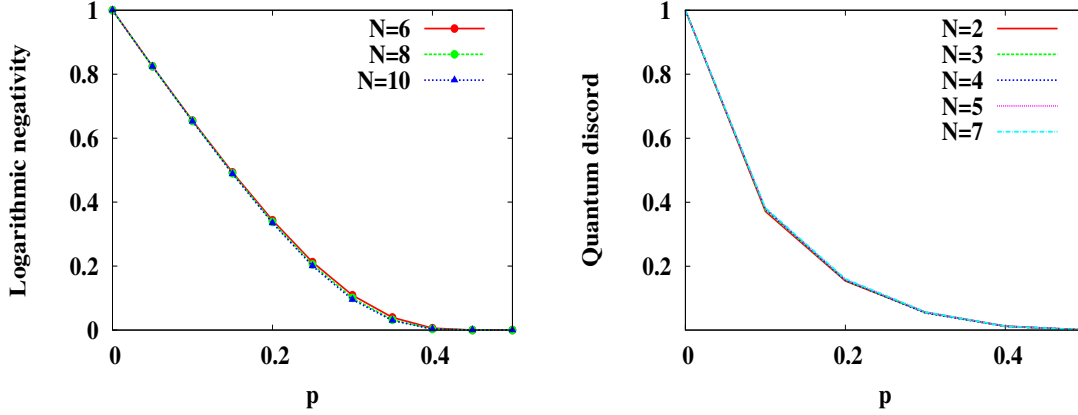


Figure 5.17: Effect of local bit flip error on the $H_{C_N}^m$ state for $N = 6, 8, 10$, $m = 1$, and $k = 1$ with respect to its logarithmic negativity and quantum discord in the $\mu : M$ bipartition. Other considerations are the same as in Fig. 5.7.

with respect to the error probability p . It is also decreasing with increasing number of qubits in the large sector (see Fig. 5.17). The decrease in entanglement with respect to N is very small and therefore we can say, up to numerical precision, that the logarithmic negativity remains independent of N . Quantum discord of the bit-flipped $H_{C_N}^m$ state for different number of qubits in the large sector is shown in the right panel of Fig. 5.17 for $m = 1$ and $k = 1$. The quantum discord, up to numerical accuracy, also remains unaffected with the increase in N . The quantum discord is obtained numerically with the measurements done on the minuscule sectors. The entanglement of the GHZ state, in the $\mu : M$ bipartition increases with N for fixed p . It can be calculated exactly for arbitrary N [298]. Quantum discord for GHZ state, after being affected by the local bit flip error channel is also increasing with N , although the increase is very small as compared to that for entanglement.

To see the role of m on the quantum correlations of bit flip error affected $H_{C_N}^m$ state, we have calculated the logarithmic negativity and quantum discord for the $N = 6$ qubit $H_{C_N}^m$ state for different values of m ranging from $m = 1$ to 5. We find that as we increase m , the entanglement of the $H_{C_N}^m$ state increases and reaches a value close to that of the GHZ state. Quantum discord of the $H_{C_N}^m$ state also increases with increasing m and becomes almost equal to that for the GHZ state for $m \approx 3$.

The situation for the bit-phase flip error affected $H_{C_N}^m$ state is very similar.

Table for critical values of decoherence parameter for different states under different noisy channels.

| Channel | $H_{C_N}^1$ | $H_{C_N}^2$ | $H_{C_N}^3$ | GHZ | G | $H_{C_N}^{N-1}$ | $H_{C_N}^N$ |
|---------|-------------|-------------|-------------|------|-----|-----------------|-------------|
| LPDC | 97.5 | 92 | 86 | 67.5 | 81 | 73 | 67.5 |
| LADC | 97 | 91 | 84 | 78 | 87 | 73.5 | 75 |
| LDPC | 43 | 46 | 45 | 33 | 43 | 39 | 33 |

Table 5.1: Comparison of “critical values” of decoherence at which the entanglement vanishes for different states under different noisy channels. The critical point has been taken at the value of decoherence parameter where logarithmic negativity becomes less or equal to 10^{-4} . The values are exhibited as percentages of the noise level that the corresponding state can sustain before becoming separable. The states considered to construct this Table consists of one qubit in its minuscule sector and six qubits in its large sector. The first column shows the type of local noise acting on the state. The second, third, fourth, fifth, sixth, seventh, and eighth columns exhibit the critical values for the $H_{C_N}^1$, $H_{C_N}^2$, $H_{C_N}^3$, GHZ, G , $H_{C_N}^{N-1}$, and $H_{C_N}^N$ states respectively. The G state appears in Eq. (5.31). Note that the critical values for the GHZ and $H_{C_N}^N$ states are the same for the LPDC and LDPC, while they differ for the LADC.

5.8 Effect of local decoherence in other macroscopic quantum states

In this section, we will discuss the effects of noise on quantum correlations of some further macroscopic states. We then compare their results with those of the $H_{C_N}^m$ and GHZ_{N+k} states.

5.8.1 G state

Consider the state

$$|G\rangle_{\mu A_1 \dots A_N} = \frac{1}{\sqrt{2}} \left(|0\rangle_{\mu} |W_N\rangle_{A_1 \dots A_N} + |1\rangle_{\mu} |\widetilde{W}\rangle_{A_1 \dots A_N} \right), \quad (5.31)$$

introduced in [145], where

$$|\widetilde{W}\rangle_{A_1 \dots A_N} = \sigma_x^{\otimes N} |W_N\rangle_{A_1 \dots A_N}, \quad (5.32)$$

with $\sigma_x = |0\rangle\langle 1| + |1\rangle\langle 0|$. This state is a cat-like state in the sense, that the states $|W\rangle$ and $|\widetilde{W}\rangle$ are macroscopically distinct in terms of their σ^z -magnetizations, similar to the case of the GHZ state. In the absence of noise, this state also possesses maximum entanglement in the micro : macro bipartition.

Let us begin by considering the effect of local phase damping channels on the state $|G\rangle_{\mu A_1 \dots A_N}$. In this case, the block which gives the negative eigenvalues has dimension $2N \times 2N$, and is given by

$$B_G^{lpdc} = \frac{1}{2} \begin{pmatrix} 0_{N \times N} & B_{N \times N} \\ B_{N \times N} & 0_{N \times N} \end{pmatrix},$$

where

$$B_{N \times N} = \begin{pmatrix} \gamma^{N-1} & \gamma^{N-1} & \cdot & \cdot & \gamma^{N-1} & \gamma^{N+1} \\ \gamma^{N-1} & \gamma^{N-1} & \cdot & \cdot & \gamma^{N+1} & \gamma^{N-1} \\ \cdot & \cdot & \cdot & \gamma^{N+1} & \cdot & \cdot \\ \cdot & \cdot & \cdot & \cdot & \cdot & \cdot \\ \cdot & \cdot & \cdot & \cdot & \cdot & \cdot \\ \gamma^{N+1} & \gamma^{N-1} & \cdot & \cdot & \gamma^{N-1} & \gamma^{N-1} \end{pmatrix},$$

and $0_{N \times N}$ is an $N \times N$ matrix with all entries being 0. The block is obtained by generalizing the explicit calculation of negativity, for the state given in Eq. (5.31) under LPDC for $N = 3, 4, 5$, to general N , by using the same approach as employed in Sec. 5.5.1. The eigenvalues are calculated using induction technique. The results are cross-checked matching with numerical simulations for $N = 3, 4, 5, 6, 7$ qubit states. The negative eigenvalues so obtained are

$$\frac{1}{2N} \gamma^{N-1} (\gamma^2 - 1) \text{ with multiplicity } (N - 1), \quad (5.33)$$

and

$$\frac{1}{2N} (-(N - 1) \gamma^{N-1} - \gamma^{N+1}) \text{ with multiplicity } 1. \quad (5.34)$$

From the eigenvalues, it is clear that the entanglement of the G state in the micro : macro bipartition, after it is affected by the local phase damping channels, depends on the size of macroscopic sector (see Fig. 5.18). For $N = 6$, the G state can sustain 81% local phase damping noise, which is lower than that of the $H_{C_N}^m$ for any N and for $m = 1, 2, 3$ (see Table I).

We now consider the effect of local amplitude damping channels on the state. The block which gives the negative eigenvalues, after partially transposing the noisy

state, is of dimension $2N \times 2N$, and is given by

$$B_G^{ladc} = \frac{1}{2} \begin{pmatrix} l_1 & \cdot & \cdot & \cdot & l_1 & l_2 & \cdot & \cdot & \cdot & l_2 \\ \cdot & \cdot \\ \cdot & \cdot \\ \cdot & \cdot \\ l_1 & \cdot & \cdot & \cdot & l_1 & l_2 & \cdot & \cdot & \cdot & l_2 \\ l_2 & \cdot & \cdot & \cdot & l_2 & l_3 & l_4 & \cdot & \cdot & l_4 \\ \cdot & \cdot \\ \cdot & \cdot \\ \cdot & \cdot \\ l_2 & \cdot & \cdot & \cdot & l_2 & l_4 & l_4 & \cdot & \cdot & l_3 \end{pmatrix},$$

where $l_1 = \frac{1}{N}p\gamma^{N-1}$, $l_2 = \frac{1}{N}\gamma^{\frac{N+1}{2}}$, $l_3 = \frac{(N-1)}{N}\gamma^2p^{N-2}$, and $l_4 = \frac{1}{N}\gamma^2p^{N-2}$. Here also we have done extensive analyses for small numbers of parties, and then extended the results for general N , by identifying that the off-diagonal elements, after passing through the LADC, form a block and the diagonal elements interfere in this block. The eigenvalue calculation is again based on the induction method. The negative eigenvalues are

$$\lambda_{G,1}^{ladc} = \frac{1}{4}[(Nl_1 + l_3 + (N-1)l_4) - \sqrt{4N^2l_2^2 + (-Nl_1 + l_3 + (N-1)l_4)^2}], \quad (5.35)$$

and

$$\lambda_{G,2}^{ladc} = \frac{1}{4}[a_1 + c_1 + (2N-4)d_1 - \sqrt{2N(N-1)b_1^2 + (-a_1 + c_1 + (2N-4)d_1)^2}] \quad (5.36)$$

where $a_1 = p^{N-1}\gamma$, $b_1 = \frac{2}{N}\gamma^{\frac{N-1}{2}}p$, $c_1 = \frac{2}{N}p^2\gamma^{N-2}$, and $d_1 = \frac{1}{N}p^2\gamma^{N-2}$. Fig. 5.18 clearly shows that the entanglement, as quantified by the logarithmic negativity, of the G state decreases with the increase in the number of particles in the macroscopic section, unlike in the case of the $H_{C_N}^m$ state, for both local phase and local amplitude damping channels. A comparison of the logarithmic negativities and quantum discords for the G state under different local noisy channels is presented in Fig. 5.19 where we additionally consider the local depolarizing channel. For a fixed N , from the perspective of the robustness of entanglement, the local amplitude damping channel is the best among the channels considered, while the local depolarizing channel is the worst. The situation is rather similar for quantum discord – local amplitude damping is still the best, but the local phase damping is marginally worse

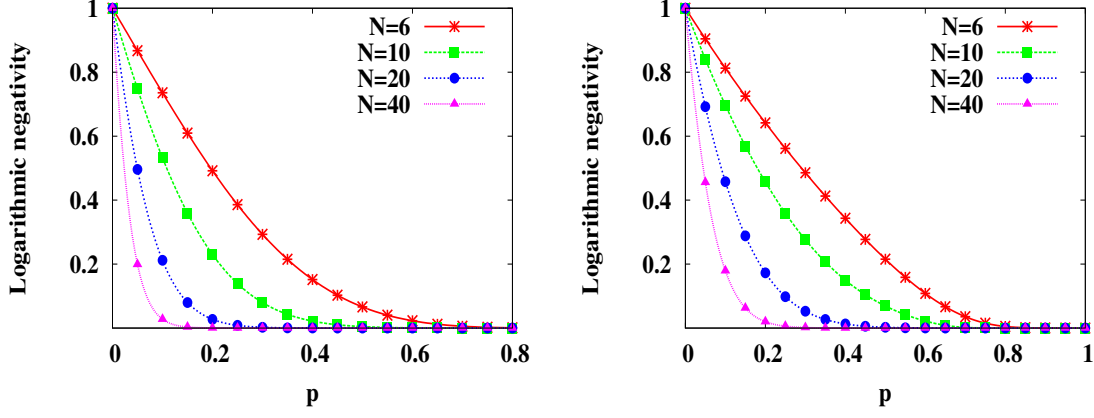


Figure 5.18: Entanglement of the noisy G state depends on the number of particles in the macroscopic sector. The logarithmic negativity (in ebits) of the noisy G state is plotted on the vertical axes against the decohering parameter p (dimensionless) on the horizontal axes, for different values of N . The left panel is for the local phase damping channels while the right one is for the local amplitude damping channels.

than local depolarizing. Note the qualitative similarity of this situation with that for the $H_{C_N}^m$ state (see Fig. 5.12) and the dissimilarity with that for the GHZ state (see Fig. 5.16). In Fig. 5.20, we compare the entanglement of the local depolarized G state with those in the local depolarized $H_{C_N}^m$ states. We find that the critical value for the G state is rather similar to those of the $H_{C_N}^m$ states. See Table I for further details. Note that the plots of logarithmic negativity and quantum discord of the G state are shown here for $N = 6$ under the different noisy channels. The corresponding analytic expressions of logarithmic negativity, for local phase damping and local amplitude damping, for arbitrary N , are given in the text. For the case of the local depolarizing channel, the logarithmic negativity is calculated numerically. The optimization for quantum discord is performed numerically in all the cases.

5.8.2 $H_{C_N}^{N-1}$ state

Let us introduce another multiparticle state which is quite similar to the $H_{C_N}^1$ state, with only the W_N^1 replaced by W_N^{N-1} , where W_N^{N-1} is obtained from Eq. (5.2) by putting $m = N - 1$. The state, therefore, is given by

$$|H_{C_N}^{N-1}\rangle_{\mu A_1 \dots A_N} = \frac{1}{\sqrt{2}}(|0\rangle_{\mu} |W_N^{N-1}\rangle_{A_1 \dots A_N} + |1\rangle_{\mu} |0 \dots 0\rangle_{A_1 \dots A_N}). \quad (5.37)$$

This state is a cat-like state in the same sense as the $H_{C_N}^1$. Moreover, the states $|W_N^{N-1}\rangle$ and $|0 \dots 0\rangle$ are macroscopically different in terms of their σ^z -magnetizations.

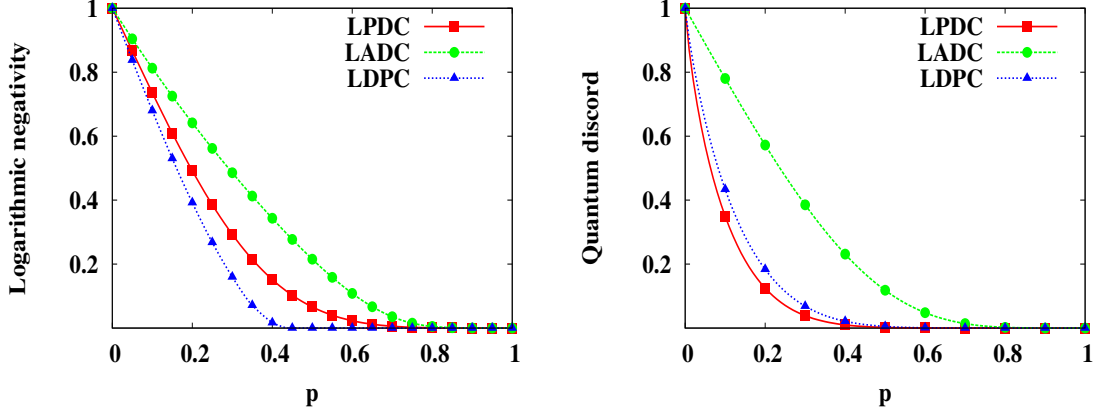


Figure 5.19: The panels here are the same as in Fig. 5.12, except that the curves here pertain to the noisy G states. For numerical values, see Table I.

The effects of local phase and amplitude damping channels, for this case can be obtained by putting $m = N - 1$ in Eqs. (5.20) and (5.23). (See Fig. 5.21.) Let us now investigate the effect of the local depolarizing channels on the state. The blocks which give the negative eigenvalues are of dimension $(N + 1) \times (N + 1)$, and are

$$B_{H_{C_N}^{N-1}}^1 = \frac{1}{2} \begin{pmatrix} a & b & b & . & . & . & b \\ b & c & d & . & . & . & .d \\ b & d & c & . & . & . & d \\ . & . & . & . & . & . & d \\ . & . & . & . & . & . & . \\ . & . & . & . & . & . & . \\ . & . & . & . & . & . & . \\ b & d & d & . & . & . & c \end{pmatrix}$$

and

$$B_{H_{C_N}^{N-1}}^2 = \frac{1}{2} \begin{pmatrix} \tilde{a} & \tilde{b} & \tilde{b} & . & . & . & \tilde{b} \\ \tilde{b} & \tilde{c} & \tilde{d} & . & . & . & .\tilde{d} \\ \tilde{b} & \tilde{d} & \tilde{c} & . & . & . & \tilde{d} \\ . & . & . & . & . & . & \tilde{d} \\ . & . & . & . & . & . & . \\ . & . & . & . & . & . & . \\ . & . & . & . & . & . & . \\ \tilde{b} & \tilde{d} & \tilde{d} & . & . & . & \tilde{c} \end{pmatrix},$$

respectively, where $a = \beta\alpha^N + \frac{1}{N}\alpha^2\beta^{N-1}$, $b = \frac{1}{\sqrt{N}}\gamma^N\alpha$, $c = \alpha^2\beta^{N-1} + \frac{1}{N}(\beta\alpha^N + (N - 1)\beta^3\alpha^{N-2})$, $d = \frac{1}{N}\beta\gamma^2\alpha^{N-2}$, and $\tilde{a} = \alpha\beta^N + \beta^2\alpha^{N-1}$, $\tilde{b} = \frac{1}{\sqrt{N}}\beta\gamma^N$, $\tilde{c} = \beta^2\alpha^{N-1} +$

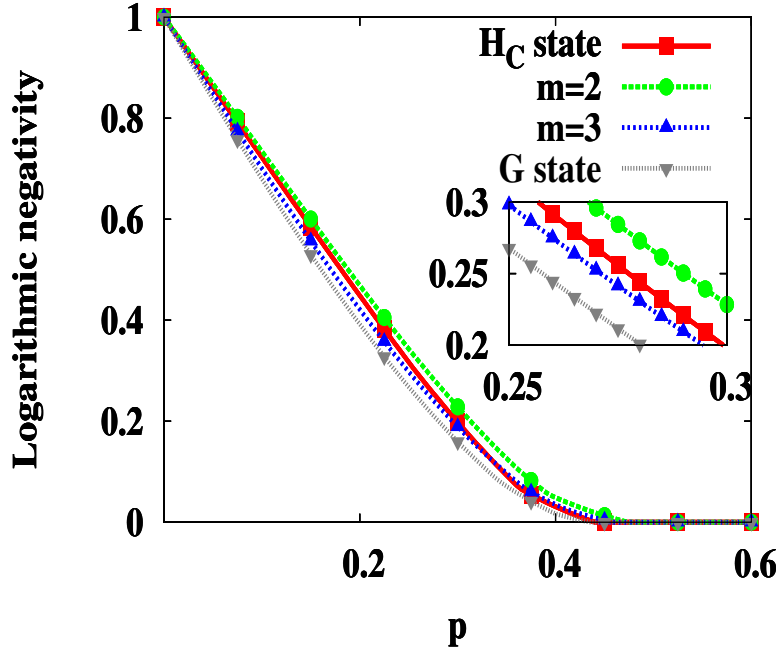


Figure 5.20: The plot here is the same as the left panel in Fig. 5.14, except that the curve for the GHZ state is replaced by that for the G state. The inset shows a magnified view of the curves in an intermediate zone. The numerical values of p at which the entanglements vanish, for the different states, are given in Table I.

$\frac{1}{N}(\alpha\beta^N + (N-1)\alpha^3\beta^{N-2})$, $\tilde{d} = \frac{1}{N}\alpha\gamma^2\beta^{N-2}$. The blocks are calculated by using the same methods as employed in the Sec. 5.5.1. Induction method is used to calculate the eigenvalues of the blocks. The negative eigenvalues are

$$\lambda_{H_{C_N}^{N-1},1}^{ldpc} = \frac{1}{2}(a + c + (N-1)d - \sqrt{(4Nb^2 + (-a + c + (N-1)d)^2)}) \quad (5.38)$$

and

$$\lambda_{H_{C_N}^{N-1},2}^{ldpc} = \frac{1}{4}(\tilde{a} + \tilde{c} + (N-1)\tilde{d} - \sqrt{(4N\tilde{b}^2 + (-\tilde{a} + \tilde{c} + (N-1)\tilde{d})^2)}) \quad (5.39)$$

respectively. The logarithmic negativity of the local depolarized state is therefore given by

$$E_{H_{C_N}^{N-1}}^{ldpc} = \log_2[2(|\min(0, \lambda_{H_{C_N}^{N-1},1}^{ldpc})| + 2|\min(0, \lambda_{H_{C_N}^{N-1},2}^{ldpc})| + 1)]. \quad (5.40)$$

The comparison among local amplitude damping, local phase damping, and local depolarizing channels, for the $H_{C_6}^5$ state, is presented in Fig. 5.22. It is clear from the figure that the effect of the local amplitude damping channel, on the $H_{C_N}^{N-1}$ state

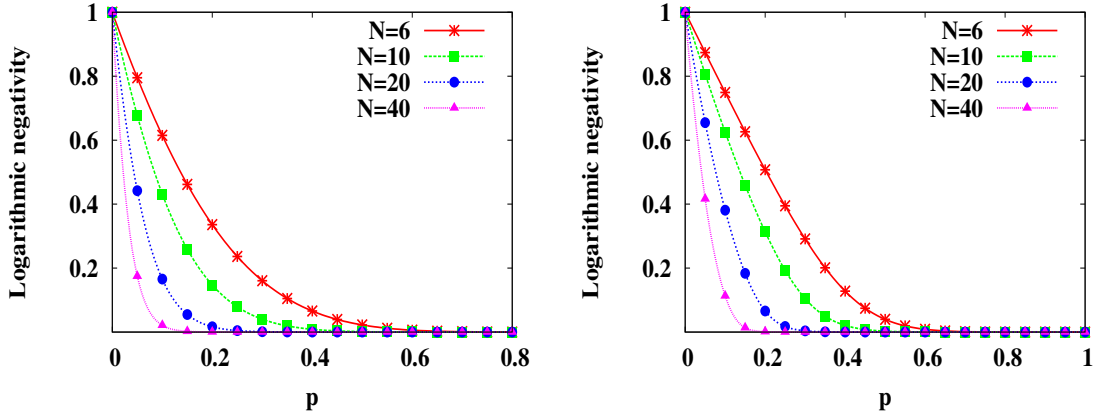


Figure 5.21: The panels in this figure are the same as in Fig. 5.18, except that here they are for the $H_{C_N}^{N-1}$ state.

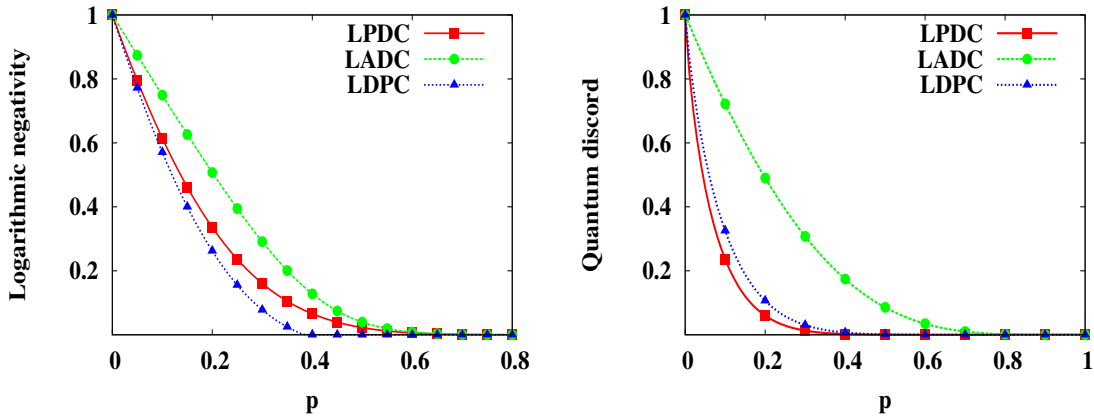


Figure 5.22: The panels in this figure are the same as in Fig. 5.12, except that here they pertain to the $H_{C_N}^{N-1}$ state, for $N = 6$.

is much less pronounced as compared to local phase damping and local depolarizing channels. For fixed noise models, the percentage of noise that the individual states can sustain, before it becomes separable in the microscopic to macroscopic partition, is given in Table I.

5.9 Chapter summary

Studying macroscopic quantum superposition states under environmental noise is important from a variety of perspectives ranging from fundamental concepts, like the quantum-to-classical transition, to robustness of quantum information processing and computational tasks. We have studied a class of multipartite quantum states consisting of a microscopic and a macroscopic part and are akin to Schrödinger cat

state. The microscopic part is assumed to be formed by a few qubits, while the macroscopic one is built by a large number of the same. We have investigated the effect of several paradigmatic models of *local* environmental noise on the multiparty states, by calculating quantum correlations between their microscopic and macroscopic sectors, after the states are affected by the local noise. We have considered five different types of local noisy channels, viz. the local phase damping, the local amplitude damping, and the local depolarizing channels. In addition, we also consider loss of finite fraction of particles from the macroscopic sector as effect of decoherence. In studying the quantum correlations, we considered both entanglement measures as well as information theoretic quantum correlation measures.

We find that the quantum correlations of all the states from the class considered here remain independent of the size of the macroscopic sector under local phase damping and local amplitude damping channels. We identify the state in this class which remains maximally robust for a given local noise. Interestingly, we observe that for all the quantum states in the class, entanglement is almost equally robust against local amplitude damping and local phase damping noise, while being much worse off against local depolarization. In contrast, quantum discord is much more robust against local amplitude damping than local depolarization or local phase damping noise. Finally, we find that the quantum correlations in the proposed class of multiparty quantum states is better preserved than that in the other macroscopic superposition states against all the local noise models. The findings may help us to identify a potential candidate for quantum memory devices.

The results of chapters 4 and 5 are published as

1. *Quantum superposition in composite systems of microscopic and macroscopic parts resistant to particle loss and local decoherence*, **Utkarsh Mishra**, Aditi Sen(De), and Ujjwal Sen, Phys. Rev. A **87**, 052117 (2013).
2. *Local decoherence-resistant quantum states of large systems*, **Utkarsh Mishra**, Aditi Sen(De), and Ujjwal Sen, Phys. Lett. A **379**, 261 (2015).

Behavior of quantum correlations under time evolution of spin models: Ergodicity

6.1 Introduction

In this chapter, we consider the question of validity of the statistical mechanical description of quantum correlation measures of anisotropic Heisenberg models in one-dimension ($1D$), ladder and two-dimension ($2D$) by investigating their ergodic properties in these models under sudden quenching in one of the system parameters. These studies are important in order to understand the behavior of quantum correlations in realistic materials. Spin models have been established as promising substrates in different physical systems for implementing many quantum information protocols which include, for example, one-way quantum computation [10] and quantum communication tasks [299–305]. Moreover, application of measures of quantum correlations of both the paradigms have proven advantageous in investigations of cooperative physical phenomena observed in many-body systems [52–65, 147]. Due to the paucity of analytical as well as numerical methods to solve quantum spin models, most of these considerations are restricted to the ground state or the thermal state of the system. While it is important to understand the quantum correlation properties of these “static states” of the system, the time-evolution of the system is an integral part of several quantum information processing protocols, a prominent example being the one-way quantum computer [10].

Quantum Heisenberg models, e.g., have created lots of interest due to their rich physical properties and the possibility of realizing such systems in artificial materials as well as in inorganic compounds. However, investigations into the dynamics of such

models, for example, under the influence of time-dependent magnetic fields, are limited by the fact that the system cannot be diagonalized analytically. We investigate the time dynamics of quantum correlations of the anisotropic Heisenberg model in a time-dependent magnetic field, in one-dimensional, ladder, and two-dimensional lattices. The characterization, quantification, and realization of quantum correlations in many-body systems are some of the main challenges in quantum information and of interest in current research [20, 21, 54, 147].

Properties like magnetization, susceptibility, classical and quantum correlations in the static states of the isotropic Heisenberg model have been studied extensively, both theoretically and experimentally [54, 147, 306, 307]. The model can be exactly solved by the Bethe ansatz [308]. Variation of different physical parameters in this model leads to the appearance of rich phases [309, 310], like spin-liquid, resonating valence bond states, etc. Moreover, such models can now be created in the laboratories in a controlled way by using e.g., photons [311], trapped ions [312], and cavity QED [313]. However, numerical simulations or approximate methods are the only techniques that can be used to investigate properties of the time-evolved states of this model. Here we investigate the behavior of quantum correlations of the evolved state as well as the equilibrium state in the anisotropic Heisenberg model in low-dimensional systems, under the influence of time-dependent magnetic fields and temperature. We find that quantum correlation measures in the entanglement-separability paradigm are ergodic in these systems irrespective of system parameters. However, information-theoretic quantum correlation measures exhibit a transition from nonergodic to ergodic behavior with the change of interaction strength in the direction of the magnetic field. We also observe that the transition point changes drastically as we go from one-dimensional and ladder lattices to the two-dimensional one.

We then move to study the time-dynamics of quantum correlations in the quantum transverse anisotropic XY spin chain of infinite length at zero as well as finite temperatures. The evolution occurs due to the instantaneous quenching of the coupling constant between the nearest-neighbor spins of the model, which is either performed within the same phase or across the quantum phase transition point connecting the order-disorder phases of the model [148, 149]. We characterize the time-evolved quantum correlations, entanglement and quantum discord, which exhibit varying behavior depending on the initial state and the quenching scheme. We show that the system is endowed with enhanced bipartite quantum correlations compared to that of the initial state, when quenched from ordered to the deep disordered phase.

However, bipartite quantum correlations are almost washed out when the system is quenched from disordered to the ordered phase with the initial state being at the zero-temperature. Moreover, we identify the condition for the occurrence of enhanced bipartite correlations when the system is quenched within the same phase. Finally, we investigate the bipartite quantum correlations when the initial state is a thermal equilibrium state with finite temperature, which reveals the effects of thermal fluctuation on the phenomena observed at zero-temperature. Specifically, we show that if the coupling constant of the driving Hamiltonian is fixed at a value that corresponds to the disordered phase, then the entanglement remains non-zero, irrespective of the choice of the initial state. In fact, the bipartite entanglement at large time is enhanced significantly compared to that of the initial state, if the initial state corresponds to the ordered phase and the system is quenched into the disordered phase. On the other hand, if the coupling constant of the driving Hamiltonian is fixed at a value that belongs to the ordered phase of the corresponding Hamiltonian, then the dynamics show rich features. Moreover, we mention two important scenarios. First, the quenching is performed across the quantum critical point with the initial and the final values of the interaction strength chosen from two sides of the quantum phase transition point, with the initial state belonging to the disordered phase. In this case, the large time entanglement of the evolved state always vanishes irrespective of the choice of the initial state with finite entanglement. Second, the initial and the final values of the interaction strength are chosen from the ordered phase. In this case, entanglement always survives. Additionally, we identify quenching strategies via which the long time evolved entanglement of the system is enhanced compared to that of the initial state. We also perform analogous investigations for the quantum discord. Further, we extend our analysis to finite temperature of the initial thermal equilibrium state. In general, we find that, as it may be expected, quantum discord is more robust against thermal fluctuations in comparison to entanglement.

6.2 The model

We consider a system of N quantum spin- $\frac{1}{2}$ particles arranged in a lattice with unequal nearest-neighbor interactions along x , y , and z directions. It is therefore the antiferromagnetic anisotropic Heisenberg model or the XYZ model, and is given by

$$H_{int} = \frac{1}{4} \sum [J_x \sigma_i^x \sigma_j^x + J_y \sigma_i^y \sigma_j^y + J_z \sigma_i^z \sigma_j^z], \quad (6.1)$$

where σ_i^a ($a = x, y, z$) are the Pauli spin matrices at the site i of the spin lattice, and J_x , J_y , and J_z represent the coupling constants in the x , y and z directions respectively. The summation in Eq. (6.1) runs over all nearest-neighbor pairs on the lattice. Periodic boundary conditions are assumed in all cases considered in this thesis. We will consider systems of quantum spins arranged in lattices in different low dimensions. Assigning different relations among J_x , J_y , and J_z , in the above Hamiltonian lead to various other well-known spin models, including the isotropic Heisenberg model for which $J_x = J_y = J_z$, and the anisotropic XY model for which $J_x \neq J_y$, $J_z = 0$. To check for ergodic properties of different physical quantities of these Heisenberg spin models, we will consider the initial state of the evolution to be the canonical equilibrium state at the initial instant (see discussion in the succeeding section). A non-trivial evolution of the system can be obtained in this case by introducing a magnetic field represented by H_{mag} , in such a way that $[H_{int}, H_{mag}] \neq 0$. Hence the total Hamiltonian can now be written as

$$H(t) = H_{int} - h(t)H_{mag}. \quad (6.2)$$

For the present paper, we choose $J_x = J(1 + \gamma)$, $J_y = J(1 - \gamma)$, $J_z = J\delta$ and $H_{mag} = \frac{J}{2} \sum \sigma_i^z$, with the summation running over all sites of the lattice. Here $J > 0$ is assumed to have the dimension of energy, while γ and δ are dimensionless system parameters. Here γ represent xy -anisotropy. For brevity, we will sometimes call it simply as ‘‘anisotropy’’. The time-dependence of the applied magnetic field is of the form

$$h(t) = \begin{cases} a, & t \leq 0 \\ 0, & t > 0, \end{cases} \quad (6.3)$$

where $a \neq 0$ is a dimensionless parameter. Here t represents the time. Therefore, the total Hamiltonian is given by

$$H(J, \gamma, \delta, h(t)) = \frac{J}{4} \sum [(1 + \gamma)\sigma_i^x\sigma_j^x + (1 - \gamma)\sigma_i^y\sigma_j^y + \delta\sigma_i^z\sigma_j^z] - \frac{J}{2}h(t) \sum \sigma_i^z. \quad (6.4)$$

When $h(t) = 0$ and $J_x = J_y = J_z$, the above Hamiltonian is exactly solvable by using Bethe ansatz [308] by which the ground state energy can be obtained [314]. However, there exists no such exact solution for the anisotropic Heisenberg model. Moreover, we wish to study the evolution of the system and hence require the single site- and two-site properties of the entire energy spectrum of the system at a given time. Hence, to study the statistical mechanical properties of such systems at finite temperature, we opt for exact diagonalization using numerical simulations.

6.3 Statistical mechanical properties

In this chapter, we aim to study the statistical mechanical properties of the anisotropic Heisenberg model in time-dependent external magnetic fields. The statistical mechanical notions like canonical equilibrium state, time-evolved state and ergodicity will be briefly defined in this section, mainly to set the terminology and the notations. In particular, we introduce a quantity called the “ergodicity score” which helps us to quantify the degree to which a physical quantity is possibly nonergodic.

6.3.1 Time-evolution

For the quantum spin system, described by the Hamiltonian in Eq. (6.4), we denote the canonical equilibrium state of the system, at time t , as ρ_β^{eq} , and is given by

$$\rho_\beta^{eq}(t) = \frac{\exp(-\beta H(t))}{\mathcal{Z}}, \quad (6.5)$$

where \mathcal{Z} is the partition function,

$$\mathcal{Z} = \text{tr}[\exp(-\beta H(t))],$$

and $\beta = \frac{1}{k_B T}$, with k_B being the Boltzmann constant. T represents the absolute temperature.

The canonical equilibrium state can evolve due to the application of external “disturbances”, like switching on of the magnetic field across the system. In our case, the evolution of the system is governed by the Hamiltonian given in Eq. (6.4). We assume that the system is in contact with a heat bath at temperature T' for a long time until $t = 0$. We assume that the contact is in the canonical sense, so that the system and the heat bath exchange energy (under the normal average energy constraint), but do not exchange particles. We assume that this contact leads the system to the canonical equilibrium state at $t = 0$, i.e., the state of the system at $t = 0$ is $\rho_\alpha^{eq}(0)$, where $\alpha = \frac{1}{k_B T'}$. For $t > 0$, the magnetic field is switched off, and we consider the situation where the contact with the heat bath is also cut off for all times $t > 0$. The system therefore starts evolving according to the Schrödinger equation governed by the Hamiltonian in Eq. (6.4), with the initial state of this evolution being $\rho_\alpha^{eq}(0)$, and we denote the corresponding evolved state as $\rho_\alpha(t)$. Note here that $\rho_\alpha^{eq}(t = 0) = \rho_\alpha(0)$.

6.3.2 Ergodicity and ergodicity Score

To check whether a given physical quantity \mathcal{Q} is ergodic, we consider the value of \mathcal{Q} in the evolved state at a “large time”. The time of evolution, t_l , is termed as large, for the physical quantity \mathcal{Q} , if (i) there are no fluctuations in the physical quantity \mathcal{Q} with respect to time for $t > t_l$, or if (ii) the fluctuation amplitude of \mathcal{Q} with respect to time is smaller than the required precision level, for $t > t_l$, or if (iii) the fluctuations of \mathcal{Q} with respect to time is of a constant amplitude. We are interested in the time-average of the physical quantity \mathcal{Q} at large-times. For the cases (i) and (ii), an explicit time-averaging is not required, as the system dynamics brings the quantity \mathcal{Q} to its time-averaged value. For the case (iii), an explicit time-averaging for times $t > t_l$ is required. We now ask whether there exists a temperature T' , at which the large-time time-averaged value of a physical quantity \mathcal{Q} in the evolved state is equal to the value of same physical quantity in the equilibrium state at temperature T at large-time. The physically relevant range of T can be considered as up to an order of magnitude of the initial temperature T' . This difference between T and T' is, for example, to allow for possible errors in an experimental realization of the physical system or some typical theoretical effective standard deviation in that system.

If the time-average of a physical quantity is the same as the ensemble average, the quantity is said to be ergodic. Such a study is therefore based on the comparison of the large-time time-averaged value, $\mathcal{Q}^\infty(T', a)$, with the canonical equilibrium value, $\mathcal{Q}^{can}(T, h(t = \infty))$. Note that these quantities also depend on the system parameters J , γ , and δ . The physical quantity \mathcal{Q} is therefore said to be ergodic if

$$\mathcal{Q}^\infty(T', a) = \mathcal{Q}^{can}(T, h(t = \infty)). \quad (6.6)$$

Otherwise, it is termed as nonergodic.

Let us now introduce a quantity which can quantify the degree to which a given physical quantity, \mathcal{Q} fails to be ergodic. We call it the “ergodicity score”, and define it as

$$\eta^D(\tilde{\delta}, \alpha) = \max[0, \mathcal{Q}^\infty(T', a) - \max_T \mathcal{Q}^{can}(T, h(t = \infty))] \quad (6.7)$$

where $\tilde{\delta}$ denotes the aggregate of all physical parameters required to define the Hamiltonian of the system under consideration. For the system considered here, $\tilde{\delta}$ consists of J , h , δ and γ . We remember that $\alpha = \frac{1}{k_B T'}$. The maximization over T is for all T that falls in the physically relevant range around T' , as discussed earlier. Note therefore that a non-zero value of η^D implies that \mathcal{Q} is nonergodic and that a vanishing

Q indicates ergodicity.

6.4 Single- and two-site density matrices of time-dependent Heisenberg Model

To analyze the ergodic properties of quantum correlations, let us now find the general form of the single- and two-site density matrices of equilibrium and evolved states of the Hamiltonian given in Eq. (6.4). The general single-site density matrix is given by

$$\rho_1 = \frac{1}{2}[\mathbb{I} + \vec{m} \cdot \vec{\sigma}], \quad (6.8)$$

where \mathbb{I} is the 2×2 identity matrix, and $\vec{m} = \text{tr}[\rho_1 \vec{\sigma}]$ is the magnetization vector. If the entire system is of N qubits, then the single-site density matrix can be obtained by tracing out $N - 1$ parties. For a periodic lattice, tracing out of any $N - 1$ qubits will lead to the same single-site density matrix. In the equilibrium state, since $\rho_\beta^{*eq}(t) = \rho_\beta^{eq}(t)$, where the complex conjugation has been taken in the computational basis, $m_x = 0$. Moreover, in this case, $m_y = 0$, since $[H, \otimes_i \sigma_i^z] = 0$. Therefore, the single-site density matrix for the equilibrium state reduces to

$$\rho_1^{eq}(t) = \frac{1}{2}[\mathbb{I} + m_z^{eq}(t) \sigma^z]. \quad (6.9)$$

where we have hidden the dependence on temperature in the notation. The single-site density matrix for the evolved state also turns out to be $\rho_1(t) = \frac{1}{2}(\mathbb{I} + m_z(t) \sigma^z)$.

The nearest-neighbor two-site density matrix can be written, in general, as

$$\rho_{12} = \frac{1}{4}[\mathbb{I} \otimes \mathbb{I} + \vec{m} \cdot \vec{\sigma} \otimes \mathbb{I} + \mathbb{I} \otimes \vec{m} \cdot \vec{\sigma} + \sum_{i,j=x,y,z} T_{ij}(\sigma^i \otimes \sigma^j)] \quad (6.10)$$

where $T_{ij} = \text{tr}[(\sigma^i \otimes \sigma^j) \rho_{12}]$ represent the two-site correlation functions. Since periodic boundary conditions are assumed, the nearest-neighbor state, ρ_{12} , is independent of which two neighboring sites are chosen for constructing the nearest-neighbor state. Due to the form of the single-site density matrices that has already been derived, the two-site density matrices for both equilibrium and evolved states reduces to

$$\rho_{12} = \frac{1}{4}[\mathbb{I} \otimes \mathbb{I} + m_z(\sigma^z \otimes \mathbb{I} + \mathbb{I} \otimes \sigma^z) + \sum_{i,j=x,y,z} T_{ij}(\sigma^i \otimes \sigma^j)]. \quad (6.11)$$

We observe numerically that all off-diagonal correlations vanish for the equilibrium state. However, for the evolved state, only xz - and yz -ones vanish.

6.5 Ergodicity of physical quantities in quantum XY model

In this section, we recapitulate some of the earlier attempts to investigate ergodicity in many-body systems. Much attention has been given to the XY Hamiltonian as it is exactly solvable [188–197, 199, 200] (see [315] for a discussion on exact diagonalization of XY model). P. Mazur [191] had investigated ergodicity of magnetization in the XY model and reported that the magnetization is a nonergodic quantity in the model. Later on, in a series of papers, Barouch *et al.* [189, 190] had investigated the time evolution of classical correlators, denoted as $T_{i,j}(i, j = x, y, z)$ in our notation, and magnetization, m_z , in the XY model with time-dependent magnetic field. From their detailed study, they infer that the classical correlators do not approach to a value, in the limit of infinite time, to an equilibrium value for any temperature T . Also the single-site magnetization do not approach to its equilibrium magnetization for any value of temperature T . This observation of magnetization has been argued to be connected with the observation by Mazur [191].

With the development in quantum information and computation theory, attempts have been made to study the time dynamics of quantum correlations in realistic systems. These studies were also motivated by experimental success in optical lattices, ion traps where complex many-body Hamiltonians can be realized and the interaction between the constituent subsystems can be controlled [147]. Entanglement dynamics under sudden quenching has been studied in the infinite XY model. It was observed that the two-site entanglement, evolved from the initial equilibrium state, does not approach its equilibrium value [188]. A systematic study of ergodicity in XY model and comparison of different physical quantities with respect to their ergodicity behavior is reported in [201]. The two-site entanglement is a function of single-site magnetization, m_z , and two-site classical correlators. A complementary behavior is observed between entanglement and classical correlators. Entanglement is found to be nonergodic while classical correlators show opposite behavior and remain ergodic in the XY model [201]. In later papers, a comparison was made between quantum correlations of both the paradigms with respect to their ergodic behavior in finite and infinite XY model [202]. In both the cases, it was observed that quantum correlations belonging to entanglement-separability paradigm remains always ergodic, irrespective of the value of anisotropic parameter and strength of field. On the other hand, information-theoretic quantum correlation measures shows rich behavior for an intermediate value of the magnetic field. For higher and lower value of the mag-

netic field the quantum discord, e.g., is observed to be ergodic, while for intermediate values of the field, quantum discord found to be nonergodic. Interestingly, the results match also for the system with finite size. The finite size observation is a key result for us as we have investigated the ergodicity of quantum correlations in the XYZ model where the model is not exactly solvable and one has to rely on numerical calculations. In the next section, we present the ergodicity of quantum correlations in the XYZ model with a time-dependent magnetic field.

6.6 Quantum Heisenberg XYZ spin chain with magnetic field

In this section, we investigate the statistical mechanical properties of quantum correlation measures in the one-dimensional quantum spin- $\frac{1}{2}$ lattice described by the Hamiltonian in Eq. (6.4). The isotropic antiferromagnetic Heisenberg model in one-dimension provides an understanding of the spin-spin correlation functions and suppression of long range magnetic order in spin-liquids. Moreover, some materials like Sr_2CuO_3 and SrCuO_2 mimic the Heisenberg spin chain [306]. Recently developed techniques make it possible to realize this model in physical systems like photons [311], trapped ions [312], and cavity QED [313]. Entanglement in the ground and the thermal states of the Heisenberg model have also been studied [316].

6.6.1 Quantum correlations in equilibrium and evolved states

For any system, that is in its canonical equilibrium state, all quantum correlations vanish when the temperature goes to infinity. Measures that are defined within the entanglement-separability paradigm typically vanish even for moderately high temperatures while information-theoretic measures like quantum discord goes to zero asymptotically with the increase of temperature. This feature is retained by the system described by the Hamiltonian in Eq. (6.4), on an one-dimensional lattice with periodic boundary conditions. This shows that information-theoretic quantum correlation measures are more robust to temperature when compared to entanglement-separability measures. Moreover, we observe that the entanglement of the nearest-neighbor reduced state of the canonical equilibrium state behaves differently with temperature in different ranges of γ and δ . See Figs. 6.1(a) and 6.1(b). In particular, we find that for fixed low values of the anisotropy, γ , the entanglement saturates to a value with increasing β , and this saturated value is more or less independent of

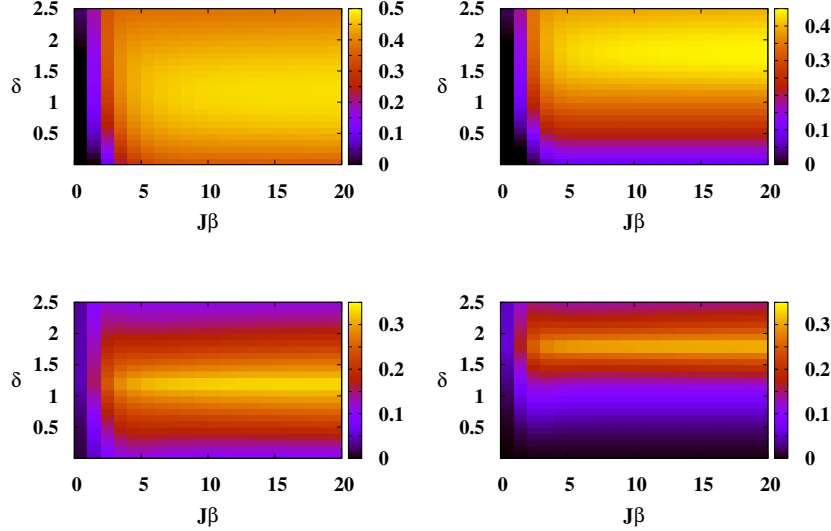


Figure 6.1: Behavior of quantum correlations in the equilibrium state. We plot quantum correlation measures of nearest-neighbor reduced states of the canonical equilibrium states, for a system of 12 quantum spin- $\frac{1}{2}$ particles arranged as a ring and described by the Hamiltonian H with respect to $J\beta$, and the relative strength of the zz -interaction, δ , for different values of γ . The left plots are for logarithmic negativity and the right ones are for quantum discord. The left plots are for $\gamma = 0.2$ while the right one are for $\gamma = 0.8$. Quantum discord is measured in bits. All other axes in the figures correspond to dimensionless parameters.

δ , the relative strength of the zz -interaction. However, when γ is relatively high, entanglement saturates to a low value for small δ , while for high δ , it saturates to a higher value. On the other hand, quantum discord saturates to a low value with decreasing temperature for small δ as well as for high δ , while it saturates to a high value for intermediate values of δ (see Figs. 6.1(c) and 6.1(d)). This behavior of quantum discord is true for all values of γ . However, with the increasing of the value of γ , the point where the maximum value of quantum discord is obtained, shifts to higher values of δ . We have performed calculations also for concurrence and quantum work-deficit, and they have qualitatively similar features as logarithmic negativity and quantum discord respectively.

Let us now discuss the time-dynamics of entanglement and other quantum correlations in the nearest-neighbor state. For the discussion, we choose $\gamma = 0.8$. However, the behavior remains the same for other moderate values of γ . The entanglement measures collapse and revive non-periodically with time, when δ is small. See Fig. 6.2(a), where we can view this feature for logarithmic negativity. For intermediate values of δ , revival of entanglement occurs less frequently (Fig. 6.2(b)). For very

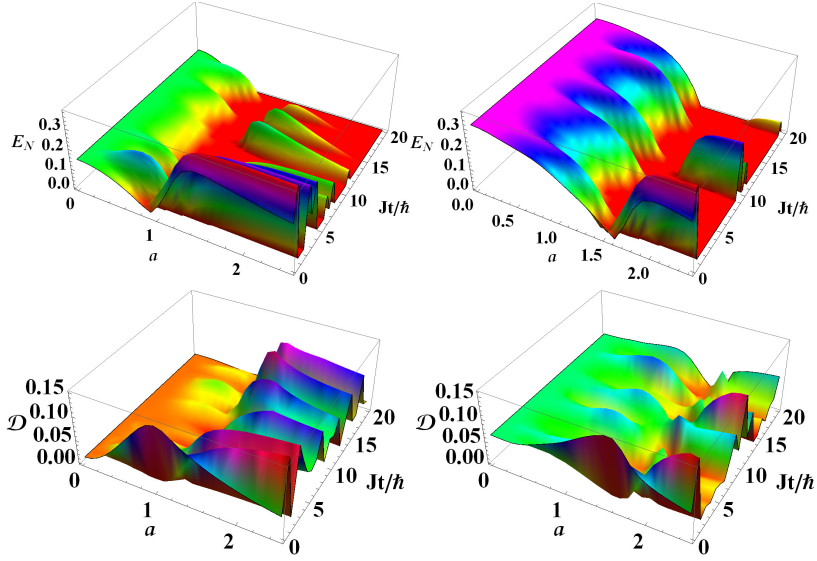


Figure 6.2: Quantum correlations of the time-evolved states. The system under consideration is the same as in Fig. 6.1, but for 8 spins. The evolution is assumed to begin in the equilibrium state at $t = 0$ and at an exemplary value of the temperature given by $J\alpha = 20$. Logarithmic negativity (top plots) and quantum discord (bottom plots) of the nearest-neighbor reduced states of the time-evolved states, are plotted against the initial magnetic field, a , and $\frac{Jt}{\hbar}$, for different values of δ . Here we choose $\gamma = 0.8$. The left plots are for $\delta = 0.2$ and the right ones are for $\delta = 0.8$. All axes correspond to dimensionless quantities except those for quantum discord, which is measured in bits.

high δ , the model is “Ising-like”, and the entanglement as well as other quantum correlation measures collapse and revive periodically with time. The non-periodic collapse and revival behavior persists up to moderate values of δ for the information-theoretic quantum correlation measures like quantum discord. See Figs. 6.2(c) and 6.2(d).

6.6.2 Statistical mechanical properties of quantum correlation measures

We now examine the ergodicity properties of the quantum correlation measures. From Figs. 6.1 and 6.2, by analyzing the behavior of the entanglements of the equilibrium and evolved states, we find that entanglement measures are ergodic for all values of δ , $\gamma (\neq 0)$, and a . We have analyzed this for logarithmic negativity as well as for concurrence. Hence, the ergodicity score is vanishing for all system parameters for all such measures.

Quantum discord and quantum work-deficit, both information-theoretic mea-

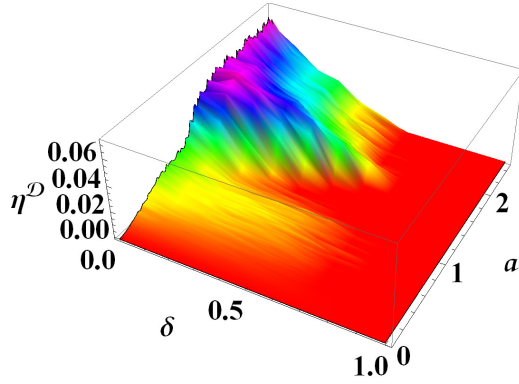


Figure 6.3: Ergodicity score for quantum discord. The ergodicity score for quantum discord of the anisotropic Heisenberg XYZ chain (with a magnetic field) of 8 spins, arranged in a ring, is plotted against δ and the applied initial magnetic field a , for a fixed $\gamma = 0.8$. The initial state of the time-evolution is the $t = 0$ canonical equilibrium state at a temperature given by $J\alpha = 20$. The ergodicity score is measured in bits. All other physical parameters used in the figure are dimensionless.

asures, also remain ergodic, when $\delta \geq \gamma$. However, for $\delta < \gamma$ these measures exhibit nonergodicity for a large range of the magnetic field. In Fig. 6.3, we plot $\eta^{\mathcal{D}}$ with respect to the δ and the field strength, a , for $\gamma = 0.8$, where we assume that the time-evolution starts off from the canonical equilibrium state for the Hamiltonian in Eq. (6.4) at $t = 0$ and for temperature given by $J\alpha = 20$. To plot $\eta^{\mathcal{D}}$, we choose $J\beta = 20$ for the equilibrium state, in the calculation of $\mathcal{Q}^{can}(T, h(t = \infty))$, since we find that the quantum discord of the equilibrium state is a monotonically increasing function with respect to $J\beta$ and saturates for a $J\beta$ much below $J\beta = 20$.

The trends, with respect to δ , of ergodicity scores of quantum discord and quantum work-deficit for different γ , are depicted in Fig. 6.4. For a fixed anisotropy γ , there always exists a certain value of δ , for which quantum discord changes from being nonergodic to being ergodic. We denote that critical value of δ as δ_c^γ , remembering that it pertains to quantum discord, and that there is a similar critical δ , at a possible different value, for quantum work-deficit. We observe that the δ_c^γ increases with the increase in γ , and in Fig. 6.4, $\delta_c^{\gamma=0.4} < \delta_c^{\gamma=0.6} < \delta_c^{\gamma=0.8}$ for both quantum discord and quantum work-deficit.

The general behavior, of the quantum correlation measures in this system, that is emerging, is as follows. Entanglement measures exhibit ergodic behavior in all relevant parameter domains. The picture is richer for information-theoretic quantum correlation measures, and in particular, for a given anisotropy γ and a given measure, there is a critical $\delta = \delta_c^\gamma$ at which the system transits from nonergodic to ergodic behavior for that measure.

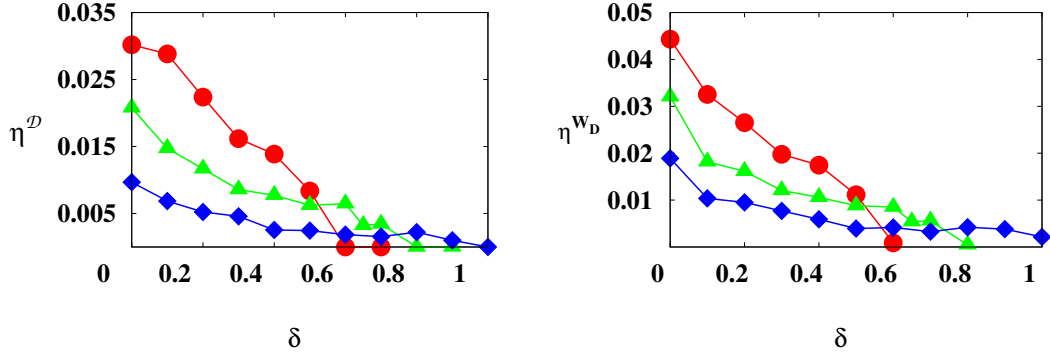


Figure 6.4: Comparing ergodicity scores for quantum discord and quantum work-deficit. The ergodicity score for quantum discord (left) and quantum work-deficit (right) of the nearest-neighbor reduced state of the time-evolved states of the anisotropic Heisenberg XYZ chain (with a magnetic field) of 12 spins, arranged in a ring, is plotted against δ , for different values of γ and a for fixed initial magnetic field $a = 0.6$. Here we choose $J\alpha = 20$ for the $t = 0$ canonical equilibrium state from which the evolution starts off. The depicted curves are for $\gamma = 0.4$ (red circles), $\gamma = 0.6$ (pink triangles), and $\gamma = 0.8$ (green squares). The ergodicity score for quantum discord is measured in bits, while that for quantum work-deficit is measured in qubits. All other quantities used in the figure are dimensionless.

6.7 Quantum Heisenberg XYZ spin ladder with magnetic field

It is interesting to study whether the two quantum correlation paradigms showing opposing statistical mechanical behavior persists in higher-dimensional systems. To find this, we first consider the spins in a ladder arrangement, which is made up of two Heisenberg XYZ spin- $\frac{1}{2}$ chains, coupled by the same interactions along the rungs [317]. There is the time-dependent z -field at all sites. Periodic boundary condition is assumed along the rails. Such systems can be found in solid state materials like Sr_2CuO_3 and $\text{Sr}_{14}\text{Cu}_{24}\text{O}_{41}$ [306]. Recently it was found that the entanglement spectrum [318] of the ground state of this model is related to the energy spectrum of its two single Heisenberg chain [319].

In this model, the quantum correlation measures of the evolved and equilibrium states behave in a similar fashion as for the XYZ chain. In particular, entanglement of the nearest-neighbor states remain ergodic in this case. And there exists a critical δ , above which the time-averaged value of the information-theoretic correlation measures, quantum discord and quantum work-deficit, of the nearest-neighbor reduced states of the evolved states match with the same measure of the equilibrium state,

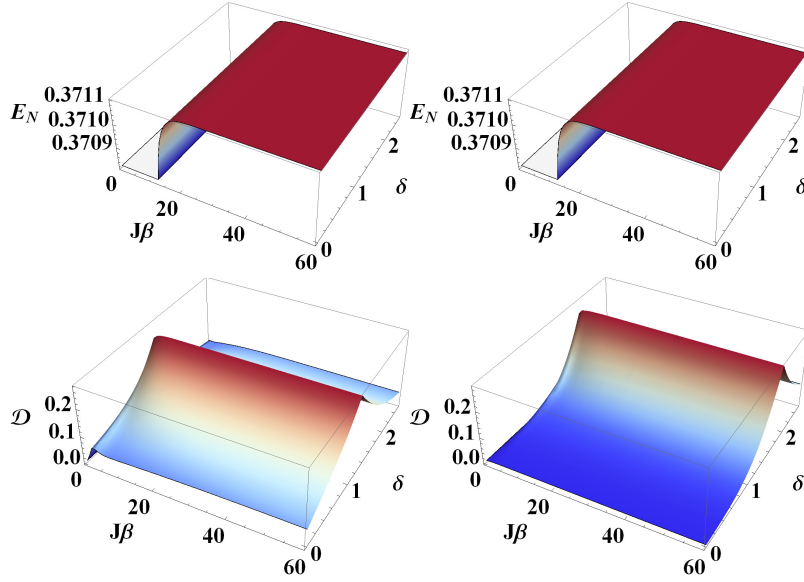


Figure 6.5: Behavior of quantum correlations in the equilibrium state. We plot quantum correlation measures of nearest-neighbor reduced states of the canonical equilibrium states, for a system of 8 quantum spin- $\frac{1}{2}$ particles arranged as a ladder and described by the Hamiltonian H with respect to $J\beta$, and the relative strength of the zz -interaction, δ , for different values of γ . The top plots are for logarithmic negativity and the bottom ones are for quantum discord. The left plots are for $\gamma = 0.2$ while the right one are for $\gamma = 0.8$. Quantum discord is measured in bits. All other axes in the figures correspond to dimensionless parameters.

for some β , in a given magnetic field and a given γ (see Fig. 6.6 for the states along the rails). Quantum discord of the long-time equilibrium state does not remain a monotonically increasing function with β like in the 1D model. See Fig. 6.5. To calculate $\eta^{\mathcal{D}}$, we choose $J\beta = 60$, at which the maximum value of $\mathcal{Q}^{can}(T, h(t = \infty))$ is attained, for all values of δ . δ_c^γ increases with the increase in γ , while it is independent of the choice of the initial applied magnetic field for a fixed γ . These qualitative features of quantum discord remain the same, when a rung of the ladder is considered. A similar feature is observed for quantum work-deficit of the rung and rail states. See Fig. 6.6(b) in this respect. We therefore again find that the strength of the zz -interaction, as quantified by δ , can be adjusted in such a way that the nonergodic nature of the information-theoretic measures, that persists in this system for low δ , gets washed off, and we obtain ergodic behavior for high δ .

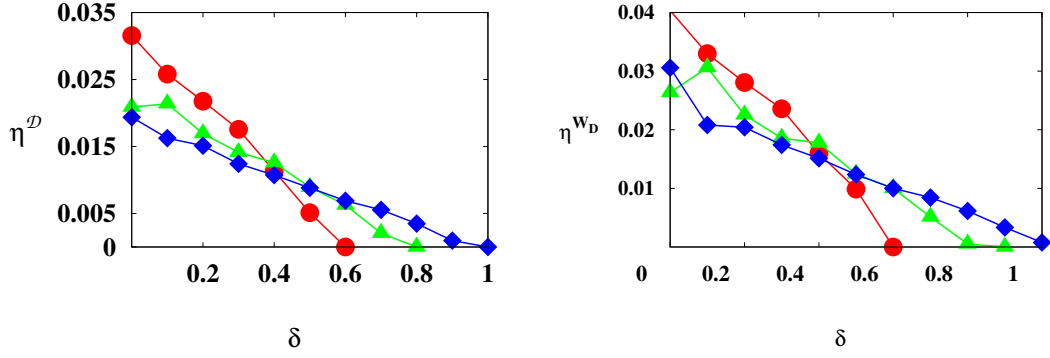


Figure 6.6: Ergodicity curves in the Heisenberg XYZ ladder. The ergodicity scores of quantum discord (left) and quantum work-deficit (right) of a nearest-neighbor reduced state, along a rail, of the time-evolved state, in the ladder, of 8 spins is plotted with respect to the relative strength of the zz -interactions. The transition points, where the system moves from nonergodic to ergodic behavior of the information-theoretic measures are qualitatively similar to those in one-dimension, for a fixed γ . The depicted plots are for $\gamma = 0.4$ (red circles), $\gamma = 0.6$ (pink triangles) and $\gamma = 0.8$ (green squares). For the evolved state, $a = 0.6$, $J\alpha = 20$. The units are the same as in Fig. 6.4.

6.8 2D Quantum Heisenberg XYZ model with magnetic field

The two-dimensional Heisenberg model describes important systems, including materials like $\text{SrCu}_2(\text{BO}_3)_2$ and CaV_4O_9 [320]. Experimental studies of the Heisenberg model in 2D lattices have been proposed e.g., in trapped ions [321] and optical lattices [322].

We consider a quantum Heisenberg XYZ spin model on a square lattice with antiferromagnetic interactions between the nearest-neighbor spins. Periodic boundary condition is assumed and hence, geometrically, the system forms a spin-arrangement on a torus. The time-dependent magnetic field is assumed to be active at all sites. Like in the ladder and 1D models, we again find that the entanglement measures are ergodic for all values of γ , δ , and the initial magnetic field a . Interestingly, unlike in the 1D and ladder systems, the transition from nonergodicity to ergodicity of the information-theoretic measures, occurs for relatively low values of the zz -interaction strength, i.e., for low values of δ (Fig. 6.7). For example, when γ and h are 0.6, in the ladder and 1D systems, both quantum discord and quantum work-deficit remain nonergodic till $\delta \approx 0.8$, while they both become ergodic in 2D at $\delta \approx 0.16$. These observations lead us to infer that information-theoretic measures are more sensitive

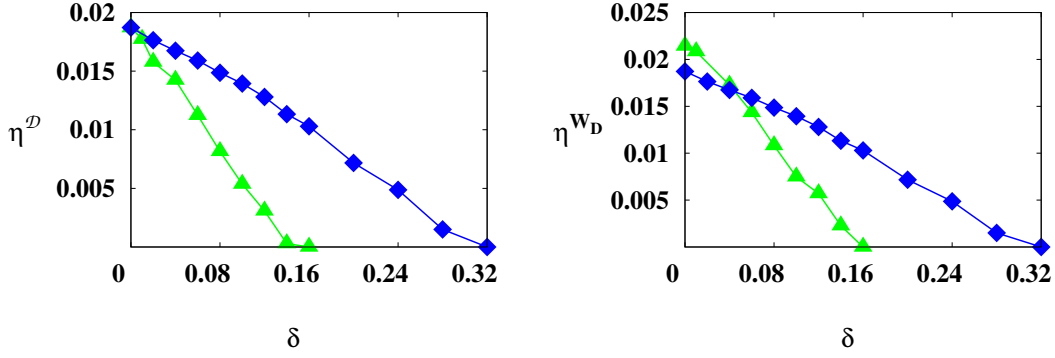


Figure 6.7: Ergodicity scores in the 2D Heisenberg XYZ model. The ergodicity scores of quantum discord (left) and quantum work-deficit (right) in the nearest-neighbor reduced state of the time-evolved state, with respect to the strength of the zz -interaction for the anisotropic Heisenberg XYZ model on a 2D square lattice, consisting of 12 spins in a torus. The plots are for $\gamma = 0.6$ (pink triangles) and $\gamma = 0.8$ (green squares). For the time-evolved state, $a = 0.6$, $J\alpha = 20$. The units are the same as in Fig. 6.4.

to the dimension of the lattice, than the entanglement measures, with respect to their statistical mechanical properties.

6.9 Behavior of quantum correlations under sudden quenching in coupling constant in XY spin chain

In a few preceding sections, we studied the dynamics of quantum correlations in the XYZ Hamiltonian with time-dependent quenching in the magnetic field. In this section, we investigate the dynamics of quantum correlations, in the XY spin chain, with time-dependent quenching in the coupling constant. The anisotropic quantum XY spin chain in presence of external transverse magnetic field is given by

$$H = \sum_i \frac{J(t)}{4} [(1 + \gamma)\sigma_i^x \sigma_{i+1}^x + (1 - \gamma)\sigma_i^y \sigma_{i+1}^y] - \frac{h}{2} \sum_i \sigma_i^z, \quad (6.12)$$

where $J(t)$ is the time dependent pairwise coupling strength between the nearest-neighbor spins, h is the external transverse magnetic field, and γ is the anisotropy constant. For case of nomenclature, we have made a slight change of notation here with reference to the Hamiltonian displayed in Eq. (6.4). The periodic boundary condition, i.e. $\sigma_{N+1}^i = \sigma_1^i (i = x, y, z)$, is considered. Note that, in the above Hamil-

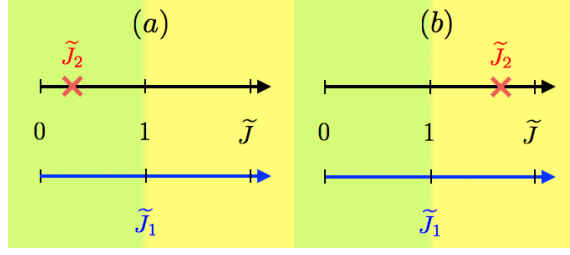


Figure 6.8: The quenching scheme employed in section 6.9. In case *A*, the final coupling constant is fixed in the disordered phase, i.e., $\tilde{J}_2 < 1$. In case *B*, the final coupling constant is fixed in the region of ordered phase, i.e., $\tilde{J}_2 > 1$. In both the cases, the initial coupling constant \tilde{J}_1 is varied from the values ranging from the disorder to the ordered phase. Such situations cover both the scenarios i.e., when \tilde{J}_1 and \tilde{J}_2 are in same phase or \tilde{J}_1 and \tilde{J}_2 are different phases. All quantities are dimensionless.

tonian, when $\gamma = 0$, the system corresponds to the XX model and when $\gamma = 1$, it corresponds to the Ising model.

The time-dependent coupling constant between the nearest-neighbor spins in the Hamiltonian is chosen as a step function, which is given by

$$J(t) = \begin{cases} J_1, & t \leq 0 \\ J_2, & t > 0. \end{cases} \quad (6.13)$$

The sudden change in the coupling constant, i.e., from J_1 at time $t \leq 0$, when the system is prepared in the canonical equilibrium state, $e^{-\beta H(J_1)}$ with $\beta = 1/\kappa_B T$, κ_B and T being Boltzmann constant and temperature respectively, to J_2 at time $t > 0$, when the system is unitary evolving under the influence of new Hamiltonian, $H(J_2)$, with coupling constant J_2 , is termed as quenching.

In order to characterize the bipartite quantum correlations present in the spin system whose Hamiltonian is given in Eq. (6.12), we need to find the two-site density matrices of the time evolved state of the system. The single- and two-site density matrix can be expressed in terms of magnetization and classical correlators and is given in Eq. (6.8) and Eq. (6.10) respectively. For the Hamiltonian given in Eq. (6.12), the magnetization, m_z , and the two-site diagonal correlations, T_{ii} , can be exactly calculated for the one-dimensional infinite XY spin model with external quenched transverse magnetic field [189, 190, 198]. The analytical expression for m_z and T_{ii} can also be obtained analogously if the quenching is considered in the nearest-neighbor couplings strengths. The exact analytical expressions and details of the calculations for this case are sketched in Appendix C.

6.10 Instantaneous quenching in the interaction strength

We now consider that the system, whose Hamiltonian is given in Eq. (6.12), starts evolving from the initial canonical state at zero temperature due to sudden quenching in the coupling constant, as given in Eq. (6.13), and study the behavior of bipartite quantum correlation measures, both concurrence and quantum discord, with respect to the evolution time. The evolution of the system is initiated at $t = 0$ by an instantaneous change in the nearest-neighbor interaction strength from some initial value, J_1 , to a final value, J_2 . Throughout the process of time evolution of the system, the external magnetic field is kept unaltered. Hence, we scale the coupling constants J by J/h , which is henceforth denoted as \tilde{J} . It is well known that the static XY Hamiltonian undergoes a quantum phase transition from a “disordered” phase with $\tilde{J} < 1$ to an “ordered” phase with $\tilde{J} > 1$ at the quantum critical point $\tilde{J} = 1$. The system is considered to be in equilibrium at $t = 0$ with Hamiltonian $H(\tilde{J}_1)$ and starts evolving after $t > 0$ with the new driving Hamiltonian $H(\tilde{J}_2)$.

The quantum XY spin chain with transverse magnetic field and time-dependent coupling constant described by the Hamiltonian given in Eq. (6.12) is exactly solvable by successive applications of Jordan-Wigner, Fourier, and Bogoliubov transformations (See Appendix C). The two-site density matrices (see Eq. (6.10)), for both initial and evolved states of this spin chain, can be obtained by using the analytical expressions of the magnetization and the two-site correlation, which are given in Appendix C. The bipartite quantum correlations for the initial and the evolved states can be computed using these two-site density matrices.

During quenching, the choice of the values for \tilde{J}_1 and \tilde{J}_2 can be considered in two different situations: (i) a situation where both \tilde{J}_1 and \tilde{J}_2 are chosen from the same phase (i.e., both $\tilde{J}_1 < 1$ and $\tilde{J}_2 < 1$ or both $\tilde{J}_1 > 1$ and $\tilde{J}_2 > 1$), and (ii) when both of them are chosen from the different phases. For simplification, we fix \tilde{J}_2 to be in either of the two phases and then probe the behavior of quantum correlations for different initial states by continuously varying the initial values of the coupling constant, \tilde{J}_1 , from the disordered phase to the ordered one. Fig. 6.8 depicts these two situations schematically.

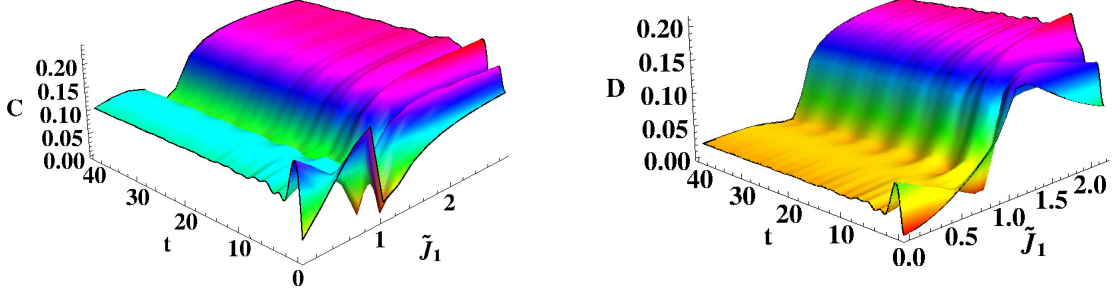


Figure 6.9: Dynamics of nearest neighbor concurrence (left) and quantum discord (right) in the evolved state of quantum XY model against time, t , and quenched coupling \tilde{J}_1 . The final coupling is fixed at $\tilde{J}_2 = 0.5$. We choose $\gamma = 0.5$. The base axes represent dimensionless quantities, while the vertical axis in the top (right) panel is in ebits (bits).

6.11 Dynamics of quantum correlations under quenching

Let us now discuss the behavior of quantum correlation measures, both concurrence and quantum discord, for two different cases depending on the choice of coupling constant \tilde{J}_2 , i.e., Case A: \tilde{J}_2 corresponds to the disordered phase (i.e., $\tilde{J}_2 < 1$) and Case B: \tilde{J}_2 corresponds to the ordered phase (i.e., $\tilde{J}_2 > 1$). These cases cover both the scenarios that were mentioned earlier. The characteristics of bipartite quantum correlations in each of these cases are considered separately.

Case A: \tilde{J}_2 corresponds to the disordered phase

Consider first the case when the quenched coupling constant, \tilde{J}_2 , at $t > 0$ is fixed at a value which corresponds to the disordered phase of the driving Hamiltonian, $H(\tilde{J}_2)$ (see Fig. (6.8)). The initial state at $t = 0$ corresponds to the zero-temperature state of the system governed by the Hamiltonian $H(\tilde{J}_1)$. Depending on the choice of \tilde{J}_1 , the initial state is tuned across the disordered and ordered phases. The external applied magnetic field is not altered to keep the uniform scaling of coupling constant throughout the evolution process. Using m_z and correlators, T_{ij} , we evaluate the concurrence and quantum discord for the nearest-neighbor spins.

In Fig. 6.9, we plot the concurrence (right panel) and quantum discord (left panel) for the system under evolution with respect to the coupling constant of the initial Hamiltonian $H(\tilde{J}_1)$ and time (t). The transverse magnetic field is kept constant, $h = 1$, and anisotropic constant, γ , is chosen to be as $\gamma = 0.5$. We choose $\tilde{J}_2 = 0.5$ and

vary both \tilde{J}_1 and time from zero to some higher values. We observe that the behavior of quantum correlations is qualitatively similar for any choice of \tilde{J}_2 , provided \tilde{J}_2 is less than unity. From Fig. 6.9, it is clear that the behavior of quantum correlations can be divided into three different regions in the $\tilde{J}_1 - t$ plane: Region 1 with $\tilde{J}_1 < 1$, region 2 close to $\tilde{J}_1 = 1$, and region 3 with $\tilde{J}_1 > 1$. In region 1 and 3, at moderate to high time scales, the value of quantum correlations, both concurrence and discord, have less variation with respect to time and hence tend to attain steady values at large time. However, in region 1, the value of concurrence is lower in comparison to the same in region 3, while quantum discord in region 1 possess a very small finite value, which is much less than that in the region 3, where it can reach the maximum value of approximately 0.2. At small values of time, in regions 1 and 3, the quantum correlations show noticeable irregularities in their behavior with respect to \tilde{J}_1 . Such irregular values of entanglement, at small times, can be attributed to the non-zero value of the correlator, t_{xy} , which eventually vanishes at large time. In region 2, as we vary \tilde{J}_1 from disorder to order phase, the concurrence sharply decreases, becomes minimum at $\tilde{J}_1 = 1$ and further increases until it saturates in region 3. For small time scales, in region 2, concurrence has irregular behavior and at moderate time scales, it saturates to a small value of the order of 10^{-2} . However, quantum discord in this region takes more time to reach the steady value. Note that, at large time, the system is always more entangled in the region where the choice of quenched coupling constants are from different phases, as described previously in situation (ii), in comparison to when the coupling constants chosen from the same phase, as described previously in situation (i).

Finally, a close look in Fig. 6.9 shows that in the region 3, bipartite quantum correlations at large time, where we may assume the system tends to reach steady state, is always greater than that of the initial state at time $t = 0$. However, in the region 1, such enhancement in the quantum correlations through the evolution process happens only if the coupling strength of the initial state, \tilde{J}_1 , is less than 0.5, which is equal to our choice of the coupling constant of the driving Hamiltonian, \tilde{J}_2 . We will follow up this scenario later with further discussions.

Case B: \tilde{J}_2 in ordered phase

Let us now fix \tilde{J}_2 of the driving Hamiltonian from the ordered phase. Again the initial state is chosen as the zero temperature state of $H(\tilde{J}_1)$.

In Fig. 6.10, we plot the concurrence (left panel) and quantum discord (right panel) for the system under evolution with respect to the coupling constant corre-

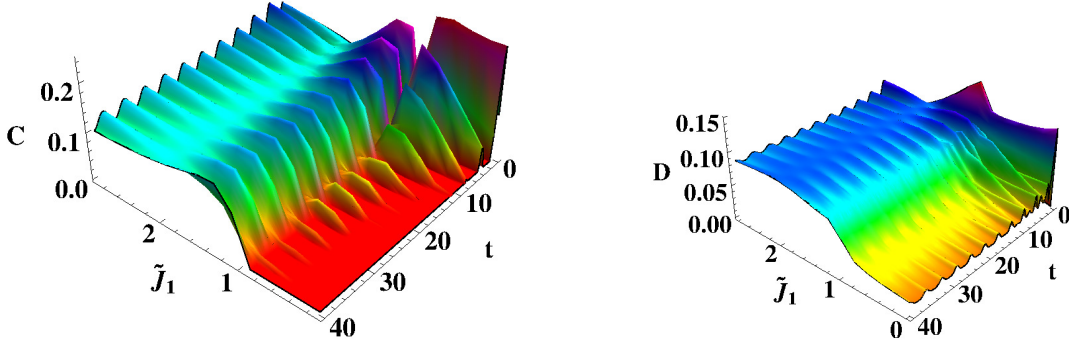


Figure 6.10: Variation of the nearest neighbour concurrence (left panel) and quantum discord (right panel) of the evolved state in XY model with respect to quenched coupling constant \tilde{J}_1 and t , where $\tilde{J}_2 = 2.0$ and $\gamma = 0.5$. The dimensions are the same as in Fig. 6.9.

sponding to the initial Hamiltonian $H(\tilde{J}_1)$ and time. The transverse magnetic field is kept constant, $h = 1$, and anisotropic constant, γ , is chosen to be as $\gamma = 0.5$. We choose $\tilde{J}_2 = 2.0$. Similar to the case A, the behavior of quantum correlations can again be analysed by dividing the J_1 - t plane into three distinct regions: Region 1 with $\tilde{J}_1 < 1$, region 2 close to $\tilde{J}_1 = 1.0$, and region 3 with $\tilde{J}_1 > 1$. Here we discuss concurrence and quantum discord individually as they have different characteristics.

In region 1, concurrence shows revival and collapse with respect to time. In particular, the amplitude and reviving regions of concurrence gradually decrease and finally vanish at large time. It is worth mentioning here that the number of revivals that appear in the region 1 depends on the value of anisotropic parameter γ . As we increase γ from zero to one, the number of revivals increases. In the region 3, entanglement oscillates between two non-zero values and the amplitude of oscillations being maximum at low time scales located close to region 2. However, as expected, at $\tilde{J}_1 = 2.0$ such oscillations vanish and the entanglement assumes constant non-zero value. In region 2, concurrence shows continuous revival and collapse with the increase in time. The collapse and revival of bipartite entanglement in XY spin chain with time-dependent field have been studied in [61].

At small time scales, irrespective of regions, quantum discord has large irregularities in its strength and as time increases, these irregularities vanish and regular oscillations occur. Comparing entanglement and discord, for at large t , we find that at $\tilde{J}_1 = 1$, entanglement shows much sharper transition from zero to a non-zero value while smooth transition is observed for quantum discord. Note that, at large times, the strength of quantum discord is much higher in region 3 than that of region 1,

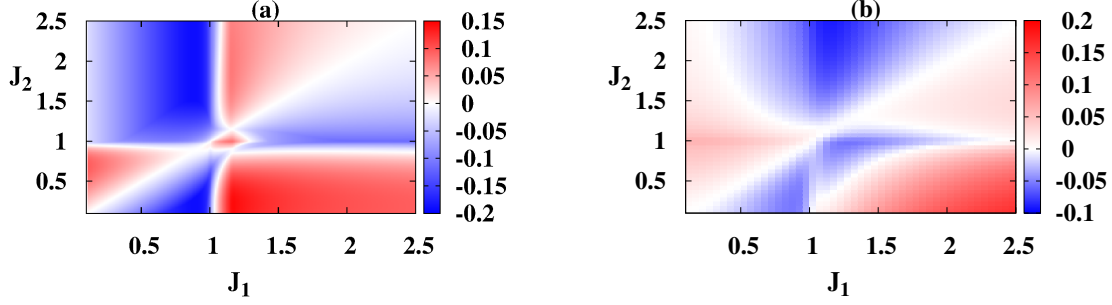


Figure 6.11: (a) Plot of the difference in entanglement between the final and the initial two-site states, δC , in the quantum XY spin chain against \tilde{J}_1 and \tilde{J}_2 . The negative values (the blue regime) in the difference indicates that the initial bipartite entanglement is more as compared to the final bipartite entanglement in the $J_1 - J_2$ plane, while the positive value (the red regime) reveals that bipartite entanglement is enhanced during dynamics compared to the initial state. Here $\gamma = 0.5$ and $h = 1.0$. (b) The plot of the difference in quantum discord between the final and the initial two-site states, δD . The dimensions are same as in Fig. 6.9.

where quantum discord survives with small values. In region 2, quantum discord shows smooth increasing trend from disorder to order phase of \tilde{J}_1 .

Dynamical enhancement

In previous section, we have elaborately discussed the features of quantum correlations measures for two specific cases, Case A and Case B, for two chosen values of the coupling constant, \tilde{J}_2 , corresponding to the driving Hamiltonian. We would now like to see whether such features are generic at large times, when the observables acquire steady state values. For this, we set $t \rightarrow \infty$ in the analytical expressions of the magnetization and the correlators and continuously vary the coupling constants \tilde{J}_1 and \tilde{J}_2 .

In Fig. 6.11(a), we plot the difference of final and the initial state entanglement, δC , where $\delta C = C(t \rightarrow \infty) - C(t = 0)$, as a function of quenched coupling constants \tilde{J}_1 and \tilde{J}_2 for $\gamma = 0.5$. Here the external magnetic field is set at unity, and we set $\tilde{J}_1 = J_1$ and $\tilde{J}_2 = J_2$.

In Fig. 6.11(a), depending on the ranges of the initial and final coupling constants, we divide the panel into four parametric regimes: (i) region 1: with J_1 and J_2 both less than unity, (ii) region 2: with $J_1 < 1$ and $J_2 > 1$, (iii) region 3: with $J_1 > 1$ and $J_2 > 1$, and (iv) region 4: with $J_1 > 1$ and $J_2 < 1$.

The white line along the diagonal in Fig. 6.11(a) corresponds to the case, when

$J_1 = J_2$. Obviously, in this case the system is not perturbed externally and the entanglement of the system at infinite time is same as in the initial time. One can immediately have two interesting observations when the system is quenched across the phase transition point. First, when the initial state is in the ordered phase, i.e., $J_1 > 1$, and the system is instantaneously quenched to deep in disordered phase, i.e., $J_2 \ll 1$, the nearest-neighbor bipartite entanglement is enhanced significantly than that of the initial state. For example, for $J_2 = J_1 = 1.4$, the bipartite entanglement of the initial unperturbed state measured by concurrence is approximately 0.066 ebit, which get enhanced to a value close to 0.186 ebit by quenching J_2 to its final value at $J_2 = 0.2$. Secondly, when the initial state is in the disordered phase, i.e., $J_1 < 1$, and the system is instantaneously quenched to ordered phase with $J_2 > 1$, the amount of entanglement is significantly decreased compared to the initial value. In fact, any finite entanglement present in the initial state is washed out completely if J_2 is chosen from deep ordered phase (see Fig. 6.12(a)). As for an example, the initial state has entanglement 0.143 ebit for $J_2 = J_1 = 0.6$, which vanishes for any driving Hamiltonian $H(J_2)$, with $J_2 > 1.3$.

However, when the system is quenched within the same phase, the steady state bipartite entanglement at infinite time may be enhanced or deteriorated compared to that of the initial state depending on the parametric range. In this situation, we observe that the enhancement occurs when $J_2 > J_1$.

Fig. 6.11(b) shows the difference between the final and the initial state quantum discord, δD , where $\delta D = D(t \rightarrow \infty) - D(t = 0)$, as a function of quenched coupling constants \tilde{J}_1 and \tilde{J}_2 for $\gamma = 0.5$. The features of quantum discord is approximately similar to the bipartite entanglement. However, unlike entanglement, quantum discord survives with small values when the system is quenched from the disordered to the ordered phase (see also Fig. 6.13(a)). We have checked that the qualitative behavior of the entanglement and the quantum discord remain same for other choices of the anisotropy constant, γ .

6.12 Effect of thermal fluctuations

In this section, we consider the thermal state at a given inverse temperature, β , as the initial state and investigate the effect of temperature of the bipartite quantum correlations of the evolved state at large times.

In Figs. 6.12(a-d), we plot the behavior of bipartite entanglement at $t \rightarrow \infty$ as a function of quenched coupling constants J_1 and J_2 for different temperatures. We

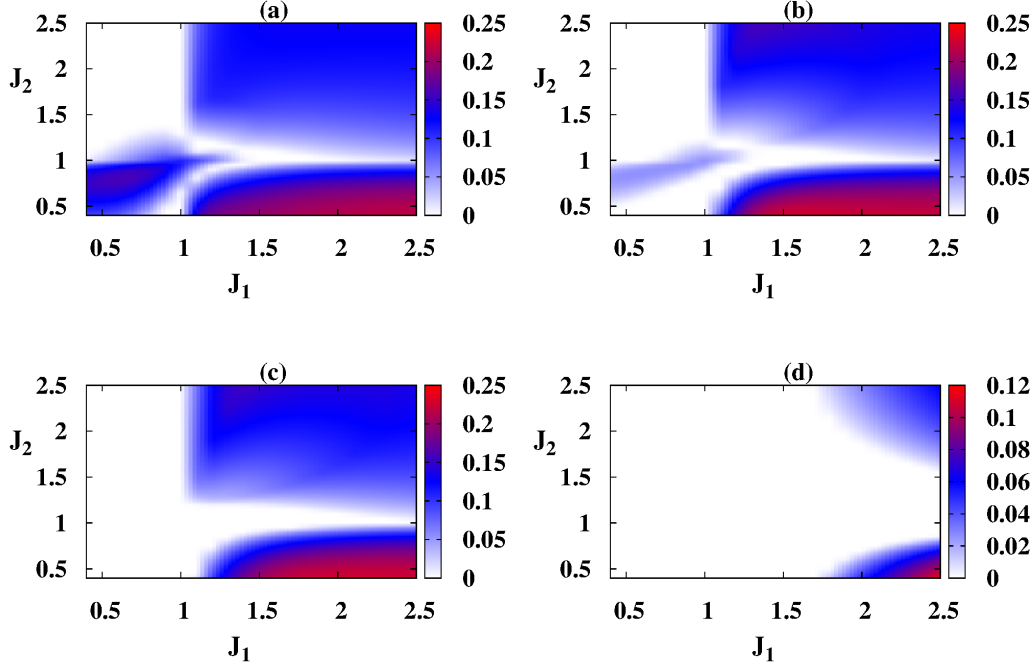


Figure 6.12: Long-time behavior of the nearest neighbor concurrence in the quantum XY model with sudden quenching in the couplings. The coupling strengths J_1 and J_2 are varied from 0 to 3. The anisotropy parameter of the Hamiltonian is fixed at $\gamma = 0.5$. The different plots are for different values of β of the initial quantum state. (a) $\beta \rightarrow \infty$, (b) $\beta = 3.0$. (c) $\beta = 2.0$, and (d) $\beta = 0.8$. All the quantities are dimensionless, except concurrence, which is in ebits.

choose (a) $\beta = \infty$, (b) $\beta = 3$, (c) $\beta = 2$, and (d) $\beta = 0.8$.

To start with, we review the behavior of the entanglement at zero-temperature, but now plot the final state entanglement itself at infinite time as a function of J_1 and J_2 . We again divide the panel into four parametric regimes as introduced in the previous section. In Fig. 6.12 (a), we observe that in region 1 the bipartite entanglement survives with moderate values. In region 2, it is fragile and is close to zero. In the entire region 3, the entanglement assumes non-zero value. In region 4, the entanglement is relatively more robust against perturbation, compared to other three regions. We monitor the effect of temperature of the initial thermal state on the entanglement starting from zero-temperature to a finite temperature. It is clear that, in all the regions, the entanglement decreases with the increase of temperature. Comparing Figs. 6.12(a)-6.12(d), we observe that entanglements in regions 1 and 2 vanish much faster than that of the regions 3 and 4.

Therefore, we conclude that the robustness of the entanglement with respect to

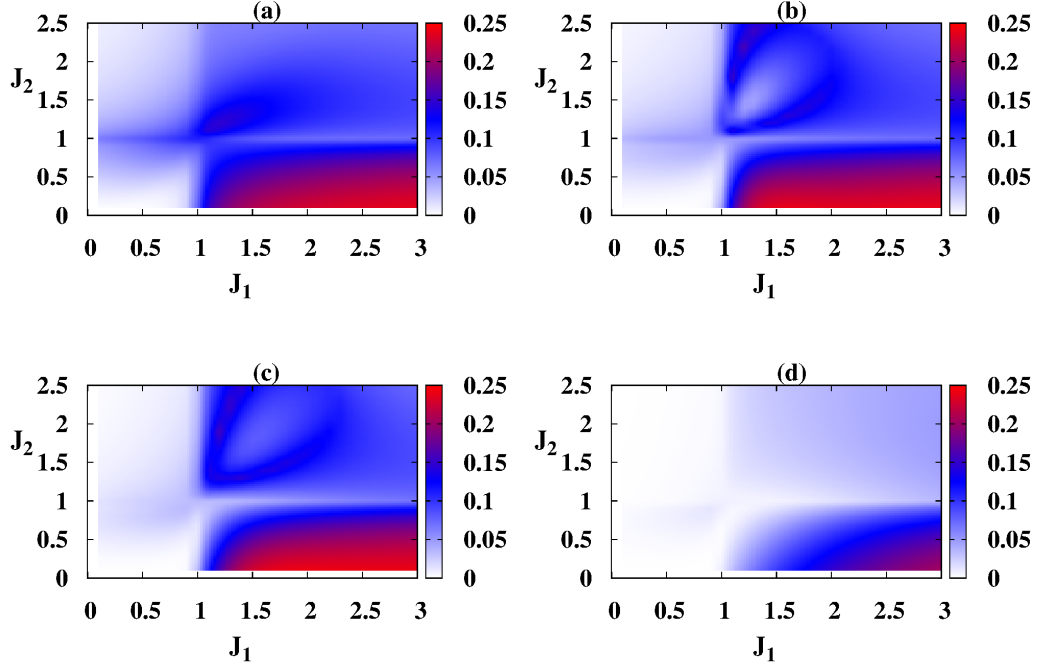


Figure 6.13: Long-time behavior of quantum discord of nearest-neighbour spins in the infinite quantum XY chain with sudden quenching in the couplings. Other details are same as in Fig. 6.12, except that quantum discord is measured in bits.

temperature depends both on J_1 as well as J_2 . The behavior of quantum discord is more or less similar to that of the entanglement, except that the quantum discord is more robust for the increase in temperature as depicted in Figs. 6.13(a-d). In particular, both quantum correlation measures survives with relatively high temperature when $J_1 > 1$ and $J_2 < 1$.

6.13 Chapter summary

Many-body systems provide a suitable playground to study quantum correlations and extract their properties. Also, using tools from quantum information theory, several properties of many-body systems of interacting particles have been investigated. This establish a strong connection between quantum information and many-body systems. In this chapter, we look for the evolution of quantum correlations in quantum Heisenberg models. Quantum Heisenberg models have created lot of interest due to their rich physical properties and the possibility of realizing such systems in artificial materials as well as in inorganic compounds. However, investigations into the dynamics of such models, for example, under the influence of time-dependent

magnetic fields, are limited by the fact that the system cannot be diagonalized analytically. Here, we have studied the behavior of quantum correlations, both from the entanglement-separability paradigm and the information-theoretic one, of the equilibrium state as well as the evolved state of the quantum Heisenberg anisotropic XYZ model, by numerical simulations. In particular, we found that although entanglement measures are ergodic irrespective of the system parameters, information-theoretic measures exhibit a rich picture, with respect to their statistical mechanical properties. Specifically, we find that the zz -interaction strength has a cross-over value, for a given xy -anisotropy and a given information-theoretic quantum correlation measure, that indicates a transition from nonergodic to ergodic behavior for that measure. The qualitative features of the measures in the entanglement-separability paradigm and the information-theoretic one are the same in the one-dimensional, ladder, and two-dimensional square lattices. However, in the square lattice, the information-theoretic measures are more sensitive to the change of the zz -interaction strength than in other dimensions. Such dimension-dependent change of ergodic behavior is absent for entanglement measures.

Controlled dynamics of isolated complex quantum systems, of many-particles, in presence of external perturbation has its importance in various fields of theoretical and experimental physics. Quantum correlations, on the other hand, are important resources, for various quantum information and computational tasks. However, they are usually believed to be fragile in presence of the external perturbation. We characterized the dynamics of quantum correlations, such as concurrence and quantum discord, in an infinite XY model between the nearest-neighbor spins due to sudden quenching of the interaction strength.

Two separate cases, where the coupling constant of the driving Hamiltonian, \tilde{J}_2 , is chosen either from the ordered phase, i.e., $\tilde{J}_2 > 1$ or the disordered phase, i.e., $\tilde{J}_2 < 1$, were considered in section 6.9. With such choices of \tilde{J}_2 , we continuously change the initial state by varying the initial coupling constant \tilde{J}_1 and temperature. Summarizing, for each of the cases, we consider two scenarios of quenching – either both the initial as well as final coupling strengths are in the same phase or they are across the critical point that connects two different phases. We demonstrate that when the system is quenched from the disordered to ordered phase, any finite entanglement in the initial state eventually vanishes at large times via the dynamical process involving successive collapse and revival phenomena. On the contrary, when the system is quenched from ordered to disordered phase, then the final state is blessed with enhanced entanglement compared to the initial state. Such

observation can be advantageous in setting up quantum protocols. Since suddenly switching from highly interacting to weakly interacting spin configuration enables us to achieve higher amounts of entanglement between two neighboring spins than that of the initial state. Also, in the entire parametric regime, the maximum amount of entanglement that can be confined between the two nearest-neighbor spins via quenching exceeds the maximum amount of entanglement that can be present between the two nearest-neighbor spins of the unperturbed system. Moreover, we found that such enhancement of entanglement is also possible via quenching within the same phase, specifically when $\tilde{J}_2 > \tilde{J}_1$ and \tilde{J}_2 is not too close to the phase transition point at zero-temperature. We established that this feature is generic by scanning \tilde{J}_2 itself over the entire range covering the disordered to ordered phases of the driving Hamiltonian and by taking $t \rightarrow \infty$, where the system supposedly reaches steady state. We found that the behavior of quantum discord is similar to entanglement. However, unlike entanglement, quantum discord survives with small values when quenched from the disordered to ordered phase.

We extended the analysis from the zero temperature initial state to the initial state with finite temperature, in order to see the effect of thermal fluctuations on the quantum correlations. We find that irrespective of the quenching scheme, the quantum correlations are more robust against thermal fluctuation if the initial state is in ordered phase compared to the disordered phase.

The new results of this chapter are based on the following papers

1. *Tuning interaction strength leads to an ergodic-nonergodic transition of quantum correlations in the anisotropic Heisenberg model*, **Utkarsh Mishra**, R. Prabhu, Aditi Sen(De), and Ujjwal Sen, Phys. Rev. A **87**, 052318 (2013).
2. *Survival of time-evolved quantum correlations depends on whether quenching is across critical point in XY spin chain*, **Utkarsh Mishra**, Debraj Rakshit, and R. Prabhu, accepted for publication in Phys. Rev. A (arXiv:1510.00685 [quant-ph]).

Constructive interference between disordered couplings

7.1 Introduction

In chapter 6, we discussed the behavior of bipartite quantum correlations under sudden quenching. In particular, we considered temporal quenching in the magnetic field in XYZ Hamiltonian and in the nearest-neighbor couplings in the XY model. In this way we have explored the characteristic difference in the behavior of quantum correlations measures belonging to two different paradigm. In this chapter, we investigate single- and two-site classical correlators, two-site and multisite quantum entanglement measures and uncover the difference in their behavior in disordered many-body systems. We, therefore, make further progress in establishing the relation between quantum information theory and many-body physics which could be helpful in the development of quantum technologies.

More precisely, we investigate the single-site magnetization and two-site classical correlators, concurrence between two nearest-neighbor sites and generalized geometric measure of entanglement in the ground state of the disordered Heisenberg spin model in one-dimension with random coupling interactions. The quenched average of the quantities, in the “disordered” Hamiltonian, is compared with their value in the corresponding “clean” Hamiltonian. We observed that the above quantities show enhancement in the disordered case with respect to the ordered one, a phenomenon termed “order from disorder” or disorder induce order”. We further observe that there are ranges of the physical parameters where simultaneous application of independent quenched disorders in the coupling constants results in enhancement in

multisite entanglement while such enhancement is absent for individual applications of the disorders. We term the phenomenon as constructive interference, a novel effect qualitatively distinct from the order from disorder phenomena. The phenomenon is absent in the other, two- and single-particle, observables considered in this chapter.

Disorder-induced order and order by disorder have been investigated in different spin glass models [220–223]. The term *order by disorder* was used by Villain *et al.* [221] while studying effect of dilution induced long range order in classical Ising model in a two-dimensional lattice. Further investigation of the phenomena in quantum systems was reported in [214]. The term “disorder-induced order” was used in [224] to report about long-range order induced by a random field that breaks the continuous symmetry of the model.

Most of the above investigations were in classical spin models. We have considered quenched disorder in a quantum spin model and look for disorder-induced enhancement in the system. In the next section, we define the enhancement score for the quenched disordered systems, that quantifies the amount by which a given quantity is enhanced by introduction of disorder as compared to the case when no disorder is present.

7.2 The ordered and disordered quantum Heisenberg models

In this section, we first discuss the quenched averaging of a physical quantity and then we introduce the Hamiltonians that we investigate.

7.2.1 Quenched averaging

In the disordered models, that we consider here, the physical parameters of the system are “quenched”, i.e., the time scales in which the dynamics of the system takes place is much shorter in comparison to the time in which the disordered system parameters equilibrate. It implies that during the time-evolution of the system, a particular realization of the random disorder parameters remains frozen. The physically relevant values of the system observables (physical quantities) are, therefore, their quenched averaged values, where we first compute the value of the physical quantity of interest for a given disorder configuration of the system and subsequently perform the averaging over probability distribution of the disorder.

7.2.2 The Heisenberg quantum spin glasses

We now introduce the four different Heisenberg Hamiltonians which will be studied in this chapter.

Case 0: The one-dimensional disordered quantum Heisenberg (or XYZ) model with nearest-neighbor interactions in an external magnetic field is described by the Hamiltonian

$$H_{\langle J, \delta \rangle} = \kappa \left[\sum_{\langle i, j \rangle} \frac{J_{ij}}{4} \left[(1 + \gamma) \sigma_i^x \sigma_j^x + (1 - \gamma) \sigma_i^y \sigma_j^y \right] + \sum_{\langle i, j \rangle} \frac{\delta_{ij}}{4} \sigma_i^z \sigma_j^z - \frac{h}{2} \sum_i^N \sigma_i^z \right]. \quad (7.1)$$

Here, $J_{ij}(1-\gamma)$ and $J_{ij}(1+\gamma)$ are proportional to the xx and yy interactions, while δ_{ij} is that to the zz one. γ measures the anisotropy between the first two interactions, and is dimensionless. J_{ij} , δ_{ij} , and h are also dimensionless. κ is a constant, and has the units of energy. J_{ij} are independently and identically distributed (i.i.d.) Gaussian random variables with mean $\langle J \rangle$ and unit standard deviation. Similarly, δ_{ij} are i.i.d. Gaussian random variables with mean $\langle \delta \rangle$ and unit standard deviation. We set $\langle \lambda \rangle = \langle J \rangle / h$ and $\langle \mu \rangle = \langle \delta \rangle / h$, which are therefore again dimensionless. σ_i^k ($k = x, y, z$) are the Pauli spin matrices at the i^{th} site and $\langle i, j \rangle$ indicates that the corresponding summation is over nearest-neighbor spins. The applied field, h , is kept ordered throughout the paper.

Case 1: Quantum Heisenberg model. In this case, the Hamiltonian, which we denote by H , has site-independent couplings, i.e., $J_{ij} = J$ and $\delta_{ij} = \delta$. Since we will be in need of multisite state characteristics, the Bethe ansatz [308] is difficult to apply in an efficient way, especially in the disordered cases considered. We denote J/h and δ/h as λ and μ respectively.

Case 2: Quantum Heisenberg “planar” spin glass. The Hamiltonian in this case is given by

$$H_{\langle J \rangle} = \kappa \left[\sum_{\langle i, j \rangle} \frac{J_{ij}}{4} \left[(1 + \gamma) \sigma_i^x \sigma_j^x + (1 - \gamma) \sigma_i^y \sigma_j^y \right] + \sum_{\langle i, j \rangle} \frac{\delta}{4} \sigma_i^z \sigma_j^z - \frac{h}{2} \sum_i^N \sigma_i^z \right], \quad (7.2)$$

where the couplings δ_{ij} are considered to be site-independent, and fixed at δ .

Case 3: Quantum Heisenberg “azimuthal” spin glass. The system in this case is governed by the Hamiltonian, $H_{\langle \delta \rangle}$, in which $J_{ij} = J$, while the couplings, δ_{ij} , are i.i.d. Gaussian random variables with mean $\langle \delta \rangle$ and unit standard deviation.

7.3 Enhancement score for the quenched disordered systems

Intuitively, disorder or defects in a system are supposed to have adverse effects on physical properties like magnetization, classical correlations, quantum correlation, etc. While this is true in many cases [215, 216], there are also a significant number of physical systems, both classical and quantum, where certain physical properties get enhanced in the presence of disorder, as compared to the corresponding clean systems [220, 221, 225, 226]. In this section, we first introduce a quantity called the “enhancement score” in order to quantify such disorder-induced advantage for a given quantity and then we study its behavior for different observables in Heisenberg spin glass systems.

7.3.1 Enhancement score and physical quantities

In a disordered system, if a quenched averaged physical quantity, \mathcal{Q}_{av} , associated with a state of the system is larger than the same quantity, \mathcal{Q} , of the corresponding ordered system in the analogous state, then the value of the physical quantity is said to exhibit a disorder-induced enhancement. To characterize such advantage, we introduce the enhancement score, $\Delta^{\mathcal{Q}}$, of a physical quantity \mathcal{Q} , which is defined as

$$\Delta_{a,b,\dots}^{\mathcal{Q}} = |\mathcal{Q}_{av}(\langle a \rangle, \langle b \rangle, \dots)| - |\mathcal{Q}(\langle a \rangle, \langle b \rangle, \dots)|. \quad (7.3)$$

Here, $\mathcal{Q}_{av}(\langle a \rangle, \langle b \rangle, \dots)$ is the quenched averaged value of a physical quantity, \mathcal{Q} , of the system where the averaging is performed over the system parameters, a, b, \dots , which follow Gaussian distributions with mean $\langle a \rangle, \langle b \rangle, \dots$ and standard deviations $\sigma_a, \sigma_b, \dots$ respectively. The definition can of course be generalized to the case of other probability distributions. $\mathcal{Q}(\langle a \rangle, \langle b \rangle, \dots)$ is the corresponding physical quantity for the ordered case of the same system, where the values of the system parameters a, b, \dots are kept constant (i.e., they are not disordered) at $\langle a \rangle, \langle b \rangle, \dots$ respectively. Both \mathcal{Q}_{av} and \mathcal{Q} will also usually depend on other systems parameters (that are not disordered) which are kept the same for both the systems (disordered and ordered) and which are kept silent in the notation. A positive enhancement score for a physical quantity, \mathcal{Q} , in a certain range of the system parameters will imply that “disorder-induced enhancement” or “order from disorder” is attained for \mathcal{Q} in that region of the parameter space. Whereas a negative value of the same will indicate that \mathcal{Q} gets degraded.

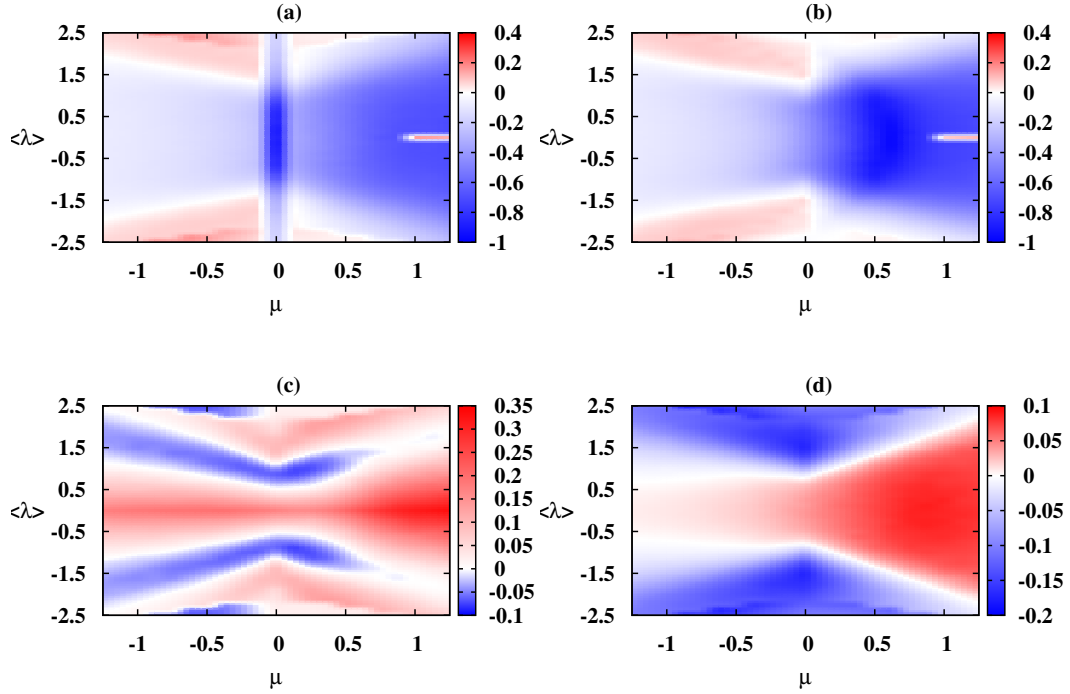


Figure 7.1: Order from disorder in the planar spin glass. The enhancement scores ($\Delta_\lambda^{\mathcal{Q}}$) for different physical quantities are plotted in the different panels. In all cases, the disordered Hamiltonian is $H_{\langle J \rangle}$, while the ordered one is H . For the plots, we consider a system of 6 spins. And, we choose $\gamma = 0.7$ and $h = 0.8$. The planar spin glass Hamiltonian consists of 6 i.i.d Gaussian random variables, J_{ij} , which are each of mean $\langle J \rangle$ and standard deviation unity. The quantities that are plotted here are the enhancement scores for (a) magnetization (Δ_λ^{Mz}), (b) the zz -classical correlator (Δ_λ^{Tzz}) (c) bipartite quantum correlation as quantified by concurrence (Δ_λ^C), and (d) genuine multipartite quantum correlation measure quantified by GGM (Δ_λ^E). In these panels, the quantities along ordinates are $\langle \lambda \rangle$, while the abscissae represent the μ . Quenched average of the observable is performed over 5×10^3 random realizations. The regions represented in red are the ones for which $\Delta^{\mathcal{Q}}$ is positive indicating that the corresponding physical quantity \mathcal{Q} attains a higher value with the introduction of disorder in these regions. The areas represented in blue are the ones for which $\Delta^{\mathcal{Q}}$ is negative and they point to parameter regions where the \mathcal{Q} is higher in the corresponding clean system. In the white regions, \mathcal{Q} remains unaltered by the introduction of disorder in the system. All the parameters plotted here are dimensionless.

In this chapter, the physical quantities that we study are single-site observables like magnetization, two-site observables like classical correlators, and bipartite as well as multipartite quantum correlation measures. We calculate two-site concurrence (Sec. 3.1.1) to quantify the entanglement. For multisite entanglement, we calculate generalized geometric measure (Sec. 3.3.1). For the Heisenberg Hamiltonian, that we consider here, in both ordered as well as disordered cases, the x and y components of the magnetization of the ground state vanish, while the z component of the magnetization, $M_z^i = \text{tr}(\sigma_i^z \rho^i)$, of the single-site reduced density matrix (ρ^i) at the i^{th} site of the ground state is in general non-vanishing. In the disordered case, one has to further perform a quenched averaging over the relevant variables to obtain the physically meaningful quenched averaged magnetization. The classical correlators between the i^{th} and j^{th} sites are defined as $T_{\alpha\beta}^{ij} = \text{tr}(\sigma_i^\alpha \otimes \sigma_j^\beta \rho_{AB}^{ij})$ with $\alpha, \beta = x, y, z$ and ρ_{AB}^{ij} being the bipartite density matrix obtained from the ground state. It can be shown that the off-diagonal correlators of the ground state vanish in both ordered and disordered cases [189].

7.3.2 Enhancement score for the Heisenberg quantum spin glasses

In this subsection, we investigate the behavior of different measurable quantities in all the three disordered models, introduced in Sec. 7.2.2. We compute the ground state in each of these models and investigate the behavior of the enhancement score, $\Delta_\xi^{\mathcal{Q}}$, corresponding to physical quantities like transverse magnetization, classical correlations, concurrence, and generalized geometric measure. Here, ξ denotes the aggregate of system parameters that are quenched disordered. There is a wide range of the anisotropy parameter, γ , and magnetic field strength, h , of these models for which order from disorder phenomena of several quantities of the ground state are observed. For the purpose of depiction of the effects, throughout this paper, we choose $\gamma = 0.7$ and $h = 0.8$. However, it is worth mentioning that the qualitative behavior of all the observables in the disordered as well as in the ordered cases remain unchanged with the variation of γ and h . Quantitatively, the values of enhancement score of the quantities increase or decrease with the change of the system parameters, like anisotropy, coupling strengths, and magnetic field. Interestingly, we find that in all these models, there are large surfaces in the parameter space in which the magnetization and classical correlators behave in a complementary way to bipartite and multipartite entanglement, i.e., when $\Delta_\xi^{M_z}$, $\Delta_\xi^{T_{zz}}$ are positive, Δ_ξ^C , $\Delta_\xi^{\mathcal{E}}$ are negative,

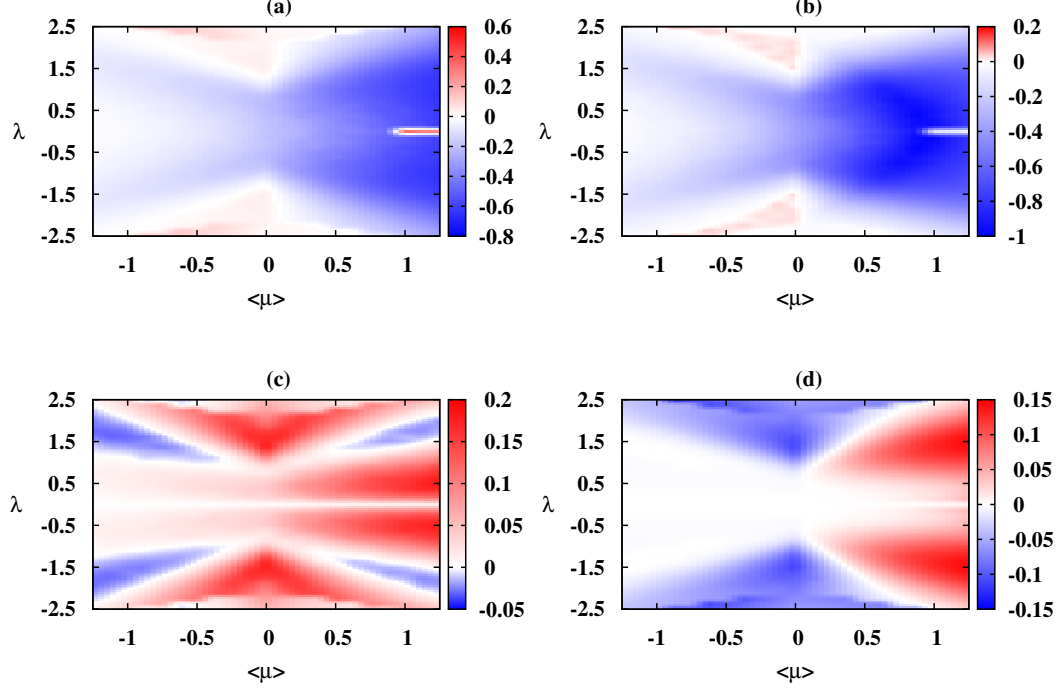


Figure 7.2: Order from disorder in azimuthal spin glass. The plots in the different panels are for (a) Δ_μ^{Mz} , (b) Δ_μ^{Tzz} , (c) Δ_μ^C , and (d) $\Delta_\mu^\mathcal{E}$. The disordered Hamiltonian for the enhancement scores is $H_{\langle\delta\rangle}$, whose 6 i.i.d. Gaussian random variables, δ_{ij} , have mean $\langle\delta\rangle$ and unit standard deviation. In each of these panels, the ordinate is λ and the abscissa is $\langle\mu\rangle$. All other considerations are the same as in Fig. 7.1.

and vice versa.

In the following cases of the disordered systems, quenched averaging is performed over 5×10^3 realizations. For fixed values of $\langle\lambda\rangle$, $\langle\delta\rangle$, and h , we have performed the numerical simulations for higher number of realizations and have found that the corresponding quenched physical quantities have already converged for 5×10^3 realizations or before.

7.3.2.1 Order from disorder in planar spin glass

We investigate here the behavior of enhancement scores of different physical quantities for the case when the disorder is introduced in the planar coupling, i.e., in the xx - and yy -couplings. The Hamiltonian for such a system is given in Eq. (7.2). In Fig. 7.1, we show the behavior of the enhancement scores of magnetization, zz -correlator, concurrence, and GGM, with the variation of $\langle\lambda\rangle$ and μ . In all the cases considered, we have observed disorder-induced enhancement also for T_{xx} and T_{yy} . We do not exhibit them in the figures given.

The investigation shows that for all observables, there exist regions in which the enhancement score is vanishing. These appear as white regions in the panels in Figs. 7.1, 7.2, and 7.3. Also, for large mean values of the disordered interactions, where the simultaneous presence of ferro- and anti-ferromagnetic couplings due to the disorder is absent, the enhancement scores vanish. These features are true for all types of disorder considered here.

In all the observables considered, viz. magnetization, classical correlators, and bipartite as well as multipartite entanglement, for a given μ , there typically appears oscillations in the surface of the enhancement score as we scan the $\langle\lambda\rangle$ axis and occasionally such oscillations have a positive enhancement score in their crests and negative one in their troughs. The parameter regions, which have a positive enhancement for a certain physical quantity, indicates an order from disorder phenomenon for that quantity. See Fig. 7.1 for a depiction.

7.3.2.2 Order from disorder in azimuthal spin glass

We now move on to study the behavior of the enhancement scores of physical quantities, when the disorder is introduced in the “azimuthal” coupling, for which the Hamiltonian is introduced as Case 3 in Sec. 7.2.2. In Fig. 7.2, we plot the physical quantities, M_z, T_{zz}, C , and \mathcal{E} , with respect to the planar coupling constant, λ , and the mean azimuthal coupling constant, $\langle\mu\rangle$. We have chosen the anisotropy constant as 0.7 and the external applied magnetic field as 0.8, as before.

As seen in the panels of Fig. 7.2, there are again order from disorder phenomena for all the observables considered. The behavior of the enhancement scores for magnetization and classical correlators are quite similar to those in the proceeding case. For concurrence and GGM, there are some differences. In particular, the $\lambda = 0$ line has $\Delta_\mu^C \approx 0$ in this case, while in the preceding case, the $\langle\lambda\rangle = 0$ line had $\Delta_\lambda^C > 0$.

7.3.2.3 The case of disorder in both planar and azimuthal couplings

When both planar and azimuthal couplings are disordered (see Eq. (7.1)), one may expect that the effects of disorder may suppress the physical quantities in a stronger way, and result in a complete absence of phenomena akin to “order from disorder”. However, we find that this is not the case. All the observables that we consider again exhibit regions in which disorder-induced order can be seen (as shown in Fig. 7.3).

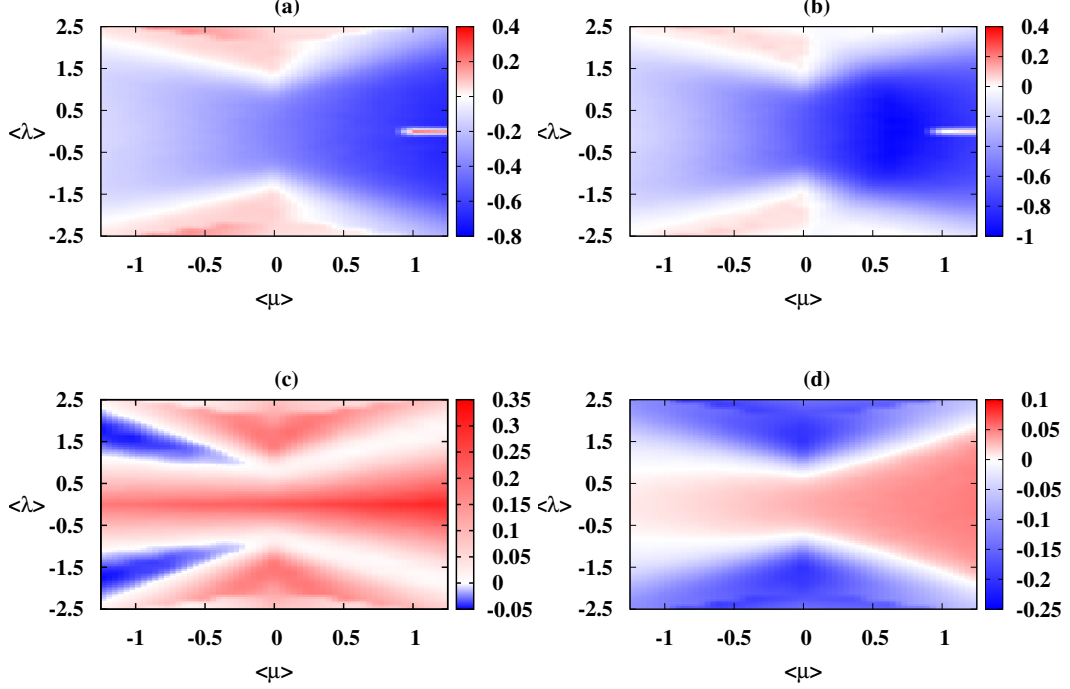


Figure 7.3: Order from disorder when both planar and azimuthal couplings are quenched disordered. The plots in the different panels are for (a) $\Delta_{\lambda,\mu}^{M_z}$, (b) $\Delta_{\lambda,\mu}^{T_{zz}}$, (c) $\Delta_{\lambda,\mu}^C$, and (d) $\Delta_{\lambda,\mu}^\mathcal{E}$. The disordered Hamiltonian in this case is $H_{\langle J, \delta \rangle}$. The J_{ij} (δ_{ij}) are i.i.d. Gaussian random variables with mean $\langle J \rangle$ ($\langle \delta \rangle$) and unit standard deviation. In the panels, the ordinates represent $\langle \lambda \rangle$ while the abscissae represent $\langle \mu \rangle$. All other considerations are as in Fig. 7.1.

7.4 Constructive interference between planar and azimuthal couplings in GGM

The Hamiltonian that we study involve planar and azimuthal interaction strengths, which may both be Gaussian distributed quenched disordered variables. We have already seen that irrespective of whether they are individually or jointly present, a spectrum of measurable quantities show order from disorder, instead of getting diminished in the presence of defects. At this juncture, we ask a more radical question: *Does there exist any observable which gets enhanced in the joint presence of the disorders while it deteriorates when the randomness is applied individually in either of the couplings, in the Heisenberg spin glass models?* Mathematically, we are looking

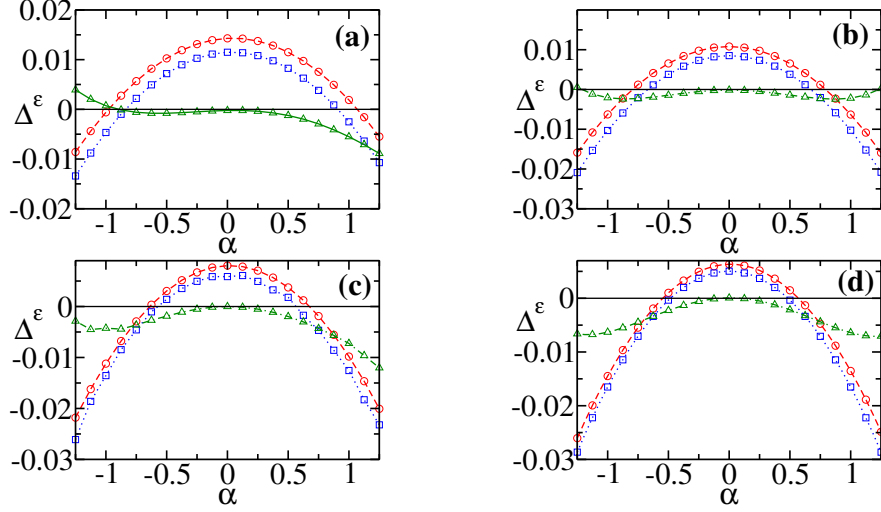


Figure 7.4: Constructive interference. The panels exhibit plots with the enhancement score of GGM, denoted as Δ^ε , as the ordinate, and the system parameter, α , as the abscissa for Heisenberg spin glasses with (a) $N = 5$, (b) $N = 6$, (c) $N = 7$, and (d) $N = 8$, where N is the number of quantum spin-1/2 particles in the system. In all these plots, red circles connected with dashed lines represent the cases when disorder is present in both the couplings (planar as well as azimuthal), and for these cases, α represents $\langle \lambda \rangle$ and Δ^ε represents $\Delta_{\lambda, \mu}^\varepsilon$. We choose $\langle \delta \rangle = -0.9$. The blue squares connected with dotted lines are for the cases when disorder is present only in the planar coupling. In these cases, α represents $\langle \lambda \rangle$, Δ^ε represents $\Delta_\lambda^\varepsilon$, and δ is fixed at -0.9 . The green triangles connected with dash-dotted lines represent the cases when disorder is present only in the azimuthal coupling. In these cases, α represents λ , Δ^ε represents Δ_μ^ε , and $\langle \delta \rangle = -0.9$. The black solid lines, parallel to the horizontal axes are drawn to separate the positive and negative regions of the enhancement score of GGM. For all the plots, we have chosen $\gamma = 0.7$ and $h = 0.8$. All quantities plotted here are dimensionless.

for the following conditions to be satisfied simultaneously by an observable \mathcal{Q} :

$$\Delta_{\lambda,\mu}^{\mathcal{Q}} = |\mathcal{Q}_{av}(\langle\lambda\rangle, \langle\mu\rangle)| - |\mathcal{Q}(\langle\lambda\rangle, \langle\mu\rangle)| > 0, \quad (7.4a)$$

$$\Delta_{\lambda}^{\mathcal{Q}} = |\mathcal{Q}_{av}(\langle\lambda\rangle)| - |\mathcal{Q}(\langle\lambda\rangle)| < 0, \quad (7.4b)$$

$$\Delta_{\mu}^{\mathcal{Q}} = |\mathcal{Q}_{av}(\langle\mu\rangle)| - |\mathcal{Q}(\langle\mu\rangle)| < 0. \quad (7.4c)$$

Here, $\mu = \langle\mu\rangle$ in Eq. (7.4b) and $\mathcal{Q}_{av}(\langle\lambda\rangle)$ corresponds to the planar spin glass. Similarly, $\lambda = \langle\lambda\rangle$ in Eq. (7.4c) and $\mathcal{Q}_{av}(\langle\mu\rangle)$ corresponds to the azimuthal spin glass. Any observable satisfying the above set of equations would imply that the competing random interactions can interfere constructively for the quantity \mathcal{Q} . We refer to this phenomenon as the “constructive interference of \mathcal{Q} ”.

We have extensively investigated the above equations for various finite number of spins in the Heisenberg Hamiltonian ranging from $N = 5$ to $N = 20$, and scanned over significant ranges of the system parameters. While smaller system sizes are handled by exact diagonalization, the relatively larger ones are investigated by employing the density matrix renormalization group techniques. The investigations help us to identify certain parameter ranges, where the system exhibits the phenomenon of the constructive interference in the genuine multipartite quantum correlation measure, GGM. Interestingly, no other observable, considered here, shows such a behavior.

7.4.1 Constructive interference in systems realizable with current technology

Let us first discuss the results corresponding to the Heisenberg spin glass models, consisting of a comparatively small number of spins. The behavior of quantum correlations, in this case can be examined in experimentally realizable systems like ion traps, photons, etc [16, 112, 311, 323–327], and hence the results obtained in this subsection can be verified and observed in the laboratories. All the results presented in this subsection are obtained by performing exact diagonalization of the Hamiltonians. Fig. 7.4 shows the enhancement scores for the GGM for different system sizes, and for different blending of disordered couplings. The anisotropy and external magnetic field strength are again chosen as 0.7 and 0.8 respectively. The coupling strength, δ , in the azimuthal direction, is -0.9 for the case when it is ordered, while in the cases when the azimuthal couplings, δ_{ij} , are disordered, they are chosen with mean -0.9 and unit standard deviation.

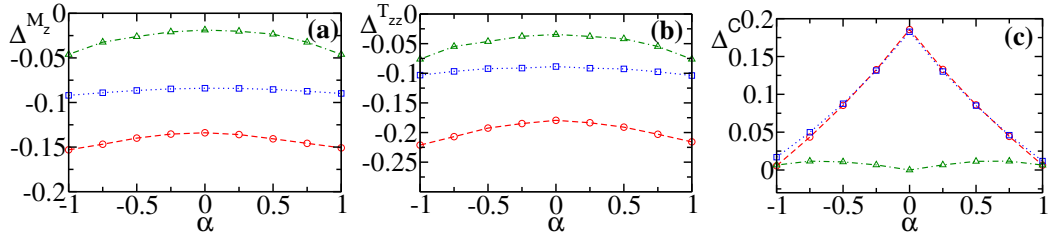


Figure 7.5: The enhancement scores for (a) magnetization, M_z , (b) T_{zz} -correlator, and (c) concurrence, C , against α for systems with $N = 6$. All other descriptions are the same as given in Fig. 7.4.

Whenever any of the curves, in the panels of Fig. 7.4, is positive, the corresponding disordered system has higher value of GGM as compared to that of the ordered system. It is clear from Fig. 7.4 that Δ_λ^ξ , Δ_μ^ξ , as well as $\Delta_{\lambda,\mu}^\xi$ show order from disorder, although in different parameter ranges. There are several other parameter ranges than those exhibited in the panels of Fig. 7.4 where such phenomenon occurs. The choice of the parameters and parameter ranges in Fig. 7.4 are for the following specific purpose. Near the two values of α ($= \langle \lambda \rangle$, here), where the curves of $\Delta_{\lambda,\mu}^\xi$ crosses the horizontal axes, one obtains regions where order from disorder for GGM is exhibited with the introduction of both planar and azimuthal disorders, while the same is absent with the inclusion of just any one of these disorders. We call these as “Venus regions”. For example, for $N = 6$ (see Fig. 7.4(b)), the two distinct ranges of α (which represents either $\langle \lambda \rangle$ or λ), in which the constructive interference can be observed are $[-0.78, -0.67]$ and $[0.68, 0.78]$. In these regions, the enhancement score, $\Delta_{\lambda,\mu}^\xi$ (red circles connected by dashed line), is positive while the other two enhancement scores, viz., the Δ_λ^ξ (blue squares connected by dotted line) and Δ_μ^ξ (green triangles connected by dot-dashed line), remain negative. Note that with increasing number of particles, the Venus regions, i.e., the windows of α demonstrating constructive interference moves towards $\alpha = 0$. Interestingly, no such phenomenon is found in other quantities considered in this chapter, viz., magnetization, two-point correlators, and bipartite entanglement (see Fig. 7.5). It is worth mentioning here that the Venus regions do not surface without an external magnetic field. In fact, depending on N , there exists a critical magnetic field strength, h_c , only beyond which the constructive interference can be observed. Below h_c , the Δ_λ^ξ lies above the $\Delta_{\lambda,\mu}^\xi$ and the Δ_μ^ξ . As the external magnetic field is increased beyond h_c , the curve corresponding to the $\Delta_{\lambda,\mu}^\xi$ goes above that of Δ_λ^ξ and Δ_μ^ξ , resulting in the emerging of the Venus regions. We find that the h_c is approximately 0.6 for $N = 6$.

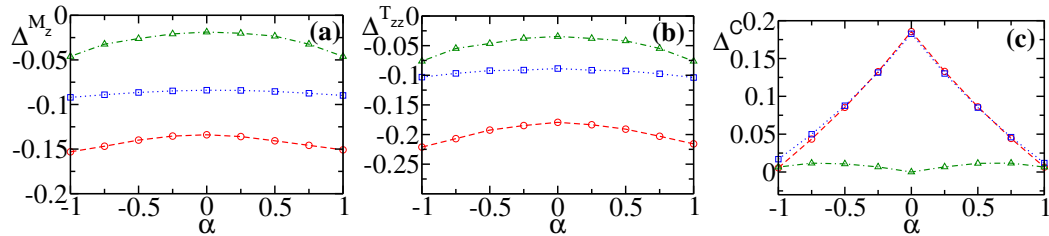


Figure 7.6: DMRG data of the enhancement score $\Delta^{\mathcal{E}^{(2)}}$ as a function of α for (a) $N = 8$, (b) $N = 12$, (c) $N = 16$, and (d) $N = 20$. All other descriptions are the same as in Fig. 7.4. The insets show blow-ups of the regions with constructive interference.

7.4.2 Approximate GGM and sustenance of Venus regions in larger systems

It is natural to ask if the results presented in the previous subsection also holds for the disordered Heisenberg systems with larger number of spins. However, exact computation of the quenched averaged GGM, in systems with large number of parties, is hindered, due to the following three key reasons: (i) An exponential growth of the Hilbert space with increasing number of parties essentially prohibits one from performing exact diagonalization of the Hamiltonian. (ii) For obtaining the desired accuracy, as one tries to obtain convergence in the quenched averaging of physical quantities, it typically requires a large number (approximately 5×10^3 to 8×10^3) of random realizations, unless the quantities are self-averaging, which is not the case for all genuine multipartite observables. (iii) Determination of multipartite entanglement, as quantified by the GGM, requires all possible bipartite splits, and the number of bipartitions in an N -party system is $\sum_{r=1}^{N/2} \binom{N}{r}$, which increases substantially with increasing N . For example, the number of bipartitions required to evaluate the GGM for the $N = 8$ system is 162, whereas it grows to over half a million for the system involving just 20 parties.

The difficulty in computing GGM can partly be curbed by choosing selective bipartitions instead of considering all possible bipartitions. We therefore introduce $\mathcal{E}^{(2)}$ as a measure of multipartite entanglement, defined as

$$\mathcal{E}^{(2)} = 1 - \max \left\{ \{ \eta_i^2 \}, \{ \eta_{i,i+1}^2 \} \Big|_{i=1, \dots, N} \right\}, \quad (7.5)$$

where η_i and $\eta_{i,i+1}$ are the maximum Schmidt coefficients of the single- and nearest-neighbor two-body reduced density matrices respectively. We call it the ‘‘approximate GGM’’. Although $\mathcal{E}^{(2)}$ may not be a *genuine* multipartite entanglement measure,

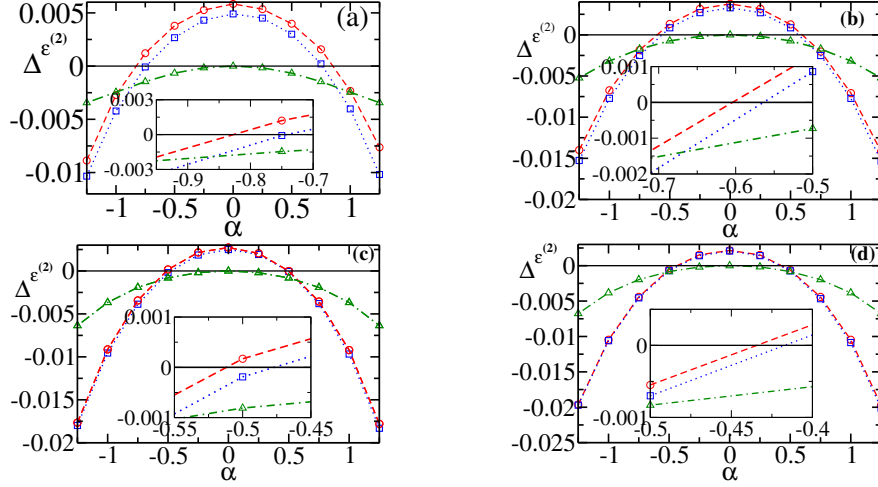


Figure 7.7: The DMRG data of the enhancement scores for (a) magnetization, M_z (b) classical correlator, T_{zz} , and (c) concurrence for systems with $N = 20$. All other considerations are the same as given in Fig. 7.4. The magnetizations used here in panel (a) are for the site $N/2$.

it does quantify multiparty entanglement and it is certainly an entanglement monotone.

In order to perform numerical simulations with larger number of spins, we adopt the finite size density matrix renormalization group method [328–330] with the open boundary condition in the system, which is an iterative numerical approach for obtaining highly accurate low energy physics of quantum many-body systems. In the DMRG approach, starting from a portion of the system, known as system block, the system size is enlarged step by step until the desired system size is reached. The value of physical quantities for the disordered spin chain can be achieved by performing several sweeps of the finite system DMRG [328–330]. We choose to work with open boundary conditions as it is well known that the accuracy drops significantly for closed boundary conditions. For N -site systems, the bipartite classical and quantum correlations are calculated for the $(N/2, N/2 + 1)$ pairs, so that boundary effect are minimized.

For the Heisenberg spin models with and without disorder, we evaluate the approximate GGM and plot the enhancement scores in Fig. 7.6. Here we consider the spin systems with sizes $N = 8$ (Fig. 7.6(a)), $N = 12$ (Fig. 7.6(b)), $N = 16$ (Fig. 7.6(c)), and $N = 20$ (Fig. 7.6(d)). The symbols are kept consistent with Fig. 7.4. It can clearly be noticed that the $\Delta^{\mathcal{E}^{(2)}}$ again identify two distinct ranges of the parameter α (on the negative and positive sides of α), where the Venus regions materialize. We also find that the conclusions drawn from the $\mathcal{E}^{(2)}$ are consistent

with the physics discussed by studying the system with smaller sizes. For example, the windows of α exhibiting constructive interference shifts towards $\alpha = 0$ with increasing number of spins. We find that even for $N = 20$, there is a non-zero region where constructive interference occurs. It is to be noted the shrinking observed, of the Venus regions, could be due to the modification of the multiparty party entanglement measure, since we have already observed that no two-party or single-site observables exhibit the constructive interference. It is plausible that in the presence of both the disorders, multipartite entanglement will exhibit a Venus region even in the thermodynamical limit. We additionally investigate the magnetization, two-point correlations in the zz direction and the concurrence in this regime. Fig. 7.7 shows their behavior for $N = 20$. We find no constructive interference phenomena in any of these quantities.

7.5 Chapter summary

In summary, we have studied the quantum Heisenberg spin system in one-dimension with random coupling interactions. We have examined the behavior of the magnetization, classical as well as the two-party quantum correlations, and multipartite entanglement for the ground states. The relevant results are presented for various system sizes ranging from five to twenty quantum spin-1/2 particles. While the small systems were dealt by exact numerical diagonalization, we adopt the density matrix renormalization technique to investigate comparatively larger spin systems. In the presence of impurities in the couplings, there exists different parameter regions for the different observables which show enhancement due to disorder – also known as the order from disorder phenomenon. The physical quantities like magnetization, classical correlators, bipartite and multipartite entanglement always find a range of parameters in which they increase with the introduction of disorder. Our studies uncover the phenomenon of constructive interference, where we observe that the parameters of the system can be tuned in such a way that disorder-induced order appears due to simultaneous presence of randomness in two different couplings, while it is absent when disorder is present individually in either of the couplings.

The constructive interference, which is caused due to the interplay between competing random coupling strengths in different directions, appears only in the multipartite entanglement, and is absent in bipartite as well as single-site physical quantities considered.

The new results of this chapter are on the preprint server arXiv.org as

1. *Constructive interference between disordered couplings enhances multiparty entanglement in quantum Heisenberg spin glass models*,
Utkarsh Mishra, Debraj Rakshit, R. Prabhu, Aditi Sen De, Ujjwal Sen,
arXiv:1408.0179 (2014).

Summary and conclusion

Quantum correlations form an intrinsic aspect of quantum theory that enables the manifestation of several interesting phenomena that are not possible within the realms of the classical world. In order to develop a coherent understanding of the use of quantum correlations as well as to attain ability to efficiently manipulate the same in real situations, it is of importance to study the behavior of quantum correlations in many-particle states.

In this thesis, we have investigated the dynamics of entanglement and other quantum correlations in states of systems of many-particles. This investigation is carried out in macroscopic quantum superposition states composed of many particles and in the ground and thermal states of many-body statistical mechanical models. The main points of the thesis and possible future directions inspired by the analysis of the work carried out in this thesis are highlighted as follows:

- We have investigated effects of local decoherence on the quantum correlation properties of states composed of a large number of parties. In particular, we have identified a family of macroscopic quantum superposition states, called them H-cat and $H_{C_N}^m$ states, and investigated their robustness against particle loss and particle-conserving decoherence models. The robustness is measured by calculating quantum correlation, in a natural division of the whole system into microscopic and macroscopic parts, of the states as a functions of the decoherence parameters. We find that the state the H-cat and the $H_{C_N}^m$ states are more robust against lossy and non-lossy quantum channels as compared to the other existing macroscopic superposition (cat) states. These investigations, reported in chapter 5 of the thesis, contribute to the existing notions of what is termed in the literature as “macroscopic quantum superpositions”.

There are several proposals in the literature to characterize macroscopic quantum superposition. However, most of such characterizations are limited to situations with a fixed number of particles, so that lossy quantum channels are disallowed. It will be very interesting to find a way that unifies the existing measures of characterization of macroscopic quantum superpositions.

- In the next part of the thesis, we have investigated the long-time behavior of quantum correlations in the Heisenberg spin model in presence of a time-dependent magnetic field and asked the following question: Are quantum correlations ergodic in this model? Such investigations are important from both technological and fundamental perspectives of nonequilibrium dynamics of quantum many-body systems. In particular, this is important for understanding the role of entanglement and other quantum correlations in thermalization and prethermalization. In our study, we focused on quantum correlation measures belonging to the entanglement-separability as well as the information-theoretic paradigm. We found that while quantum correlation measures belonging to the entanglement-separability paradigm remain non-ergodic irrespective of the Hamiltonian parameters, information-theoretic measures shows a richer behavior. While for some parameter ranges, the information theoretic measures remain ergodic, they become non-ergodic in others. The investigations, reported in chapter 6 of the thesis, once again underline the rich connections between quantum information and quantum many-body physics. The results reported here could be simulated with the help of current experimental advances e.g., in cold atoms, optical lattices, nuclear magnetic resonance (NMR), solid state setups.

A further analysis was performed to check for shifting of the nonergodic-ergodic transition point with change in the dimension of the lattice. It will be interesting to study the effects of interaction beyond nearest neighbor on the above conclusions about ergodicity.

- In chapter 6 of the thesis, we also report the observation that the survival of quantum correlations in the model depends on whether quenching is across different phases or within the same phase of the considered model. We have analysed the finite-time and long-time phase diagram of quantum correlations in the XY model with respect to quenching parameters. In this way, one can identify the parameter regions where quantum correlations enhance as compared to the initial state.

- In chapter 7 of the thesis, we have investigated the behavior of different observables in the ground states of one-dimensional quenched disordered quantum Heisenberg (XYZ) models, also known as the quantum Heisenberg spin glass models, and look for the region of parameter space where entanglement in the quenched disordered state is more as compared to the ordered case. More importantly, we find that quenched disordered couplings in a quantum Heisenberg spin glass model can constructively interfere to enhance genuine multipartite entanglement in the ground state, while the phenomenon is absent for the single- and two-party classical and quantum correlations.

In our analysis, we have fixed the variance of the probability distribution from which the coupling strengths of the Hamiltonian are drawn. This quantity measures the strength of the disorder. It will be interesting to investigate the scaling of quantum correlations with the strength of the disorder, i.e., with the variation of the variance.

APPENDIX A

LOCC

LOCC or “local operations and classical communication” are a special class of operations that were introduced to understand the resource perspective of the entanglement and other quantum correlations as a resource in quantum information tasks [23, 24]. A general LOCC protocol consists of both local quantum operations and classical communications. Let Alice and Bob share a bipartite quantum state. Let Alice perform quantum operations on her side of the state of the two-component system. Suppose that after performing the local operations, Alice communicates the outcome of a possible measurement that she has performed, to Bob by some classical channel. Depending on the the outcome at Alice’s side, Bob performs his operations, and obtains an outcome. Bob then communicates the outcome of any measurement performed by him to Alice through a classical channel. This process may be repeated as many times as a s desire.

The above protocol may be generalized to the case of more than two observers.

APPENDIX B

Entropy of entanglement

For a pure bipartite state, $|\Psi\rangle_{AB}$, entropy of entanglement is a useful measure of entanglement. It is defined as

$$E(|\Psi\rangle_{AB}) = S(\rho_A) = S(\rho_B), \quad (\text{B.1})$$

where, $S(\rho_A)$ (or $S(\rho_B)$) is the von Neumann entropy of the state ρ_A (or ρ_B). If the state, $|\Psi\rangle_{AB}$, is written in the Schmidt form,

$$|\Psi\rangle_{AB} = \sum_{i=1}^{\min(d_A, d_B)} \sqrt{\lambda_i} |i\rangle_A \otimes |\tilde{i}\rangle_B, \quad (\text{B.2})$$

then the entropy of entanglement is obtained in term of the Schmidt coefficients, λ_i 's, and is given as

$$E(|\Psi\rangle_{AB}) = - \sum_{i=1}^{\min(d_A, d_B)} \lambda_i \log_2 \lambda_i. \quad (\text{B.3})$$

APPENDIX C

The Jordan-Wigner transformation for the infinite quantum XY spin chain

Following the approach discussed in Refs. [189, 190], it is possible to obtain exact analytical expressions for the single- and two-body density matrices. Below we briefly discuss the method and present the final expressions.

We define the raising and the lowering spin operators, b_i^\dagger and b_i , in terms of the spin operators by $S_i^x = (b_i^\dagger + b_i)/2$, $S_i^y = (b_i^\dagger - b_i)/2i$ and $S_i^z = b_i^\dagger b_i - 1/2$. The raising and the lowering operators are further expressed in terms of Fermi operators c_j , where $b_j = \exp\left(-\pi i \sum_{i=1}^{j-1} c_i^\dagger c_i\right) c_j$, and its complex conjugate, c_j^\dagger . It is the last transformation that is called the Jordan-Wigner transformation. By performing a Fourier transformation, we obtain a new set of operators a_p and a_p^\dagger , where $c_j^\dagger = \frac{1}{\sqrt{N}} \sum_{p=-N/2}^{N/2} \exp(ij\phi_p) a_p^\dagger$. Here $\phi_p = 2\pi p/N$.

Expressing the Hamiltonian, H , in Eq. (6.12) in terms of the newly introduced operators, a_p and a_p^\dagger , we can write $H = \sum_{p=1}^{N/2} \bar{H}_p$, where

$$\bar{H}_p = \frac{1}{2} \left[\alpha_p(t) (a_p^\dagger a_p + a_{-p}^\dagger a_{-p}) + i\delta_p(t) (a_p^\dagger a_p^\dagger + a_p a_p) + 2h \right], \quad (\text{C.1})$$

where $\alpha_p(t) = 2(J(t) \cos \phi_p - h)$ and $\delta_p(t) = -2\gamma J(t) \sin \phi_p$. Recognizing that $[\bar{H}_p, \bar{H}_{p'}] = 0$ for $p, p' = 1, 2, \dots, N/2$, the Hilbert space corresponding the Hamiltonian H can be broken down in $N/2$ non-interacting subspaces each of which are in four-dimensional Hilbert spaces. Choosing $\{|0\rangle, a_p^\dagger a_{-p}^\dagger |0\rangle, a_p^\dagger |0\rangle, a_{-p}^\dagger |0\rangle\}$ as the

basis for the p th subspace, \bar{H}_p can be represented in matrix form as

$$\bar{H}_p = \begin{pmatrix} h & \frac{i\delta_p(t)}{2} & 0 & 0 \\ -\frac{i\delta_p(t)}{2} & 2J(t) \cos \phi_p - h & 0 & 0 \\ 0 & 0 & J(t) \cos \phi_p & 0 \\ 0 & 0 & 0 & J(t) \cos \phi_p \end{pmatrix}. \quad (\text{C.2})$$

At time $t = 0$, if we assume the system to be in thermal equilibrium state, the corresponding density matrix for the p th subspace, $\rho_p(0)$ is given by

$$\rho_p(0) = \frac{\exp(-\beta \bar{H}_p)}{\text{Tr}(\exp(-\beta \bar{H}_p))}, \quad (\text{C.3})$$

where $\beta = 1/(\kappa T)$, κ is the Boltzmann constant and T being the absolute temperature of the system.

Using Eq. (C.2), the matrix form of $\rho_p(0)$ can be obtained as

$$\rho_p(0) = \frac{1}{E(0)} \begin{pmatrix} k_{11} & k_{12} & 0 & 0 \\ k_{21} & k_{22} & 0 & 0 \\ 0 & 0 & k_{33} & 0 \\ 0 & 0 & 0 & k_{44} \end{pmatrix}, \quad (\text{C.4})$$

where

$$\begin{aligned} E(0) &= k_{11} + k_{22} + 2 \exp(-J_1 \beta \cos \phi_p), \\ k_{11} &= \frac{1}{2\Lambda(J_1)} \exp[-\beta(-J_1 \cos \phi_p + \Lambda(J_1))] \\ &\quad (\Lambda(J_1) - J_1 \cos \phi_p + h) + \exp[-\beta(-J_1 \cos \phi_p - \Lambda(J_1))] (\Lambda(J_1) + J_1 \cos \phi_p - h), \\ k_{22} &= \frac{1}{2\Lambda(J_1)} \exp[-\beta(-J_1 \cos \phi_p + \Lambda(J_1))] \\ &\quad (\Lambda(J_1) + J_1 \cos \phi_p - h) + \exp[-\beta(-J_1 \cos \phi_p - \Lambda(J_1))] (\Lambda(J_1) - J_1 \cos \phi_p + h), \\ k_{44} &= \exp(-\beta J_1 \cos \phi_p) = k_{33}, \\ k_{12} &= i \frac{J_1 \gamma \sin \phi_p}{\Lambda(J_1)} \exp(-\beta J_1 \cos \phi_p) \sinh(\beta \Lambda(J_1)) = k_{21}^*, \text{ and} \\ \Lambda(J) &= \sqrt{J^2 \gamma^2 \sin^2 \phi_p + (\cos \phi_p - h)^2}. \end{aligned} \quad (\text{C.5})$$

In Eq. (C.5), we have replaced $J(t=0)$ by J_1 as assumed in Eq. (6.13).

Solving the Liouville equation of the system [189], it can be shown that the

evolution of the density matrix, $\rho_p(t)$, corresponding to the p th subspace satisfies

$$i\frac{d}{dt}\rho_p(t) = [H_p(t), \rho_p(t)], \quad (\text{C.6})$$

where $p = 1, 2, \dots, N/2$. Considering $U_p(t)$ as the time evolution matrix satisfying

$$U_p(t) = \exp(-it\bar{H}_p(t)), \quad (\text{C.7})$$

the solution of the Eq. (C.6) is given by

$$\rho_p(t) = U_p(t)\rho_p(0)U_p(t)^\dagger. \quad (\text{C.8})$$

Using Eqs. (C.2) and (C.7), we obtain

$$U_p(t) = \exp(-itJ_2 \cos \phi_p) \begin{pmatrix} v_{11} & v_{12} & 0 & 0 \\ -v_{12}^* & v_{11}^* & 0 & 0 \\ 0 & 0 & 1 & 0 \\ 0 & 0 & 0 & 1 \end{pmatrix}, \quad (\text{C.9})$$

where we put $J(t) = J_2$. v_{11} and v_{12} are given by

$$\begin{aligned} v_{11} &= \frac{i(J_2 \cos \phi_p - \hbar)}{\Lambda(J_2)} \sin\left(\frac{\Lambda(J_2)t}{\hbar}\right) + \cos\left(\frac{\Lambda(J_2)t}{\hbar}\right), \\ v_{12} &= -\frac{J_2 \sin \phi_p}{\Lambda(J_2)} \sin\left(\frac{\Lambda(J_2)t}{\hbar}\right). \end{aligned} \quad (\text{C.10})$$

Plugging Eqs. (C.9) and (C.4) in Eq. (C.8), we have

$$\rho_p(t) = \begin{pmatrix} l_{11} & l_{12} & 0 & 0 \\ l_{21} & l_{22}^* & 0 & 0 \\ 0 & 0 & 1 & 0 \\ 0 & 0 & 0 & 1 \end{pmatrix}, \quad (\text{C.11})$$

where

$$\begin{aligned} l_{11} &= k_{11}|v_{11}|^2 + k_{12}v_{11}v_{12}^* + k_{12}^*v_{11}^*v_{12} + k_{22}|v_{12}|^2, \\ l_{12} &= -k_{11}v_{11}v_{12} + k_{12}|v_{11}|^2 - k_{12}v_{12}^2 + k_{22}v_{11}v_{12}, \\ l_{21} &= -k_{11}v_{12}^*v_{11}^* - k_{12}(v_{12}^*)^2 + k_{12}^*(v_{11}^*)^2 + k_{22}v_{11}^*v_{12}^*, \\ l_{22} &= k_{11}|v_{12}|^2 - k_{12}v_{11}v_{12}^* - k_{12}^*v_{11}^*v_{12} + k_{22}|v_{11}|^2. \end{aligned} \quad (\text{C.12})$$

APPENDIX D

Magnetization in the quantum XY model

The magnetization operator per spin in z -direction is given by $m_z = (1/N) \sum_j \langle \sigma_j^z \rangle$, which can again be written in terms of the a_p and a_p^\dagger operators as

$$m_z(t) = (2/N) \sum_{p=1}^{N/2} \langle a_p^\dagger a_p + a_{-p}^\dagger a_{-p} - 1 \rangle. \quad (\text{D.1})$$

We therefore have

$$m_z = \frac{2}{N} \sum_{p=1}^{N/2} \frac{-(A_p(0)B_p(t) + 4 \operatorname{Re} [C_p(0)D_p(t)])}{E_p(0)}, \quad (\text{D.2})$$

where $A_p(0) = (k_{11} - k_{22})$, $B_p(t) = |v_{11}|^2 - |v_{22}|^2$, $A_p(0) = k_{12}$, $D_p(t) = v_{11}v_{12}^*$ and $E_p(0) = (k_{11} + k_{22} + 2 \exp(-J_1\beta \cos \phi_p))$. Using set of Eqs. (C.5) and (C.10) into Eq. (D.2), and simplifying further, the final expression for the magnetization is obtained as

$$m_z = \frac{2}{N} \sum_{p=1}^{N/2} \frac{\tanh(\beta\Lambda(J_1)/2)}{\Lambda(J_1)\Lambda(J_2)^2} \left[(J_2 \cos \phi_p - h)Q \right. \\ \left. + J_2(J_1 - J_2)\gamma^2 h \sin^2 \phi_p \cos\left(\frac{2\Lambda(J_2)t}{\hbar}\right) \right], \quad (\text{D.3})$$

where $Q = (J_1 \cos \phi_p - h)(J_2 \cos \phi_p - h) + J_1 J_2 \gamma^2 \sin^2 \phi_p$.

APPENDIX E

Nearest-neighbour correlators in the quantum XY model

The nearest-neighbour spin-spin correlators are given by $t^{\alpha\beta} = (1/N) \sum_j \langle s_j^\alpha s_{j+1}^\beta \rangle$, where α, β stands for x, y , and z . The correlators, t^{xx} and t^{yy} , are given by $G(R)$, where $R = -1$ and 1 for the xx and the yy correlator, respectively. Expressing $G(R)$ in terms of the a_p and a_p^\dagger operators, we find $G(R) = \langle T_1 \rangle + \langle T_2 \rangle$, where

$$\langle T_1 \rangle = \frac{1}{N} \sum_1^{N/2} \left[2 \cos\left(\frac{2\pi p}{N} R\right) \langle a_p^\dagger a_p + a_{-p}^\dagger a_{-p} - 1 \rangle \right], \quad (\text{E.1})$$

and

$$\langle T_2 \rangle = \frac{1}{N} \sum_1^{N/2} \left[2i \sin\left(\frac{2\pi p}{N} R\right) \langle a_p^\dagger a_{-p}^\dagger + a_p a_{-p} \rangle \right]. \quad (\text{E.2})$$

Now, the term $\langle a_p^\dagger a_p + a_{-p}^\dagger a_{-p} - 1 \rangle$ which appears in $\langle T_1 \rangle$, has already been calculated while deriving the magnetization, $m_z(t)$. It can be shown that

$$\langle T_2 \rangle = \frac{-1}{N} \sum_{p=1}^{N/2} 4 \sin\left(\frac{2\pi p}{N} R\right) \left[\frac{A_p(0)P_p(t) + iC_p(0)Q_p(t)}{E_p(0)} \right], \quad (\text{E.3})$$

where $P_p(t) = \text{Re}[iv_{11}^*v_{12}^*]$ and $Q_p(t) = \text{Re}[(v_{11}^*)^2 + (v_{12}^*)^2]$. Using Eqs. (C.5), (C.10) and (E.3), the final expression for $\langle T_2 \rangle$ is given by

$$\begin{aligned} \langle T_2 \rangle &= \frac{1}{N} \sum_{p=1}^{N/2} \frac{2 \sin(\phi_p R) \tanh(\beta \Lambda(J_1)/2)}{\Lambda(J_1) \Lambda(J_2)^2} (\gamma \sin \phi_p) \left[J_2 (J_2 \cos \phi_p - h) Q \right. \\ &\quad \left. - h (J_1 - J_2) (J_2 \cos \phi_p - h) \cos \left(\frac{2\Lambda(J_2)t}{\hbar} \right) \right]. \end{aligned} \quad (\text{E.4})$$

In an analogous way, we find the expression of the the xy -correlator, t_{xy} , as

$$t_{xy} = \frac{1}{N} \sum_{p=1}^{N/2} \frac{\tanh(\beta \Lambda(J_1)/2)}{\Lambda(J_1) \Lambda(J_2)} h (J_1 - J_2) \gamma \sin^2 \phi_p \sin \left(\frac{2\Lambda(J_2)t}{\hbar} \right). \quad (\text{E.5})$$

It can readily be seen that t_{xy} vanishes for the equilibrium case, i.e., if $J_1 = J_2$. By using Wick's theorem the zz -correlator, t_{zz} , can be now be expressed as $t_{zz} = m_z^2 - G(-1)G(1) + t_{xy}^2$.

Bibliography

- [1] A. Einstein, B. Podolsky, and N. Rosen, *Phys. Rev.* **47**, 777 (1935).
- [2] M. A. Nielsen and I. L. Chuang, *Quantum Computation and Quantum Information* (Cambridge University Press, Cambridge, 2000); D. Bouwmeester, A. K. Ekert, A. Zeilinger, *The Physics of Quantum Information*, (Springer, Berlin Heidelberg, 2000); M. M. Wilde, *Quantum Information Theory* (Cambridge University Press, 2013).
- [3] C. H. Bennett and S. J. Wiesner, *Phys. Rev. Lett.* **69**, 2881 (1992).
- [4] C. H. Bennett, G. Brassard, C. Crépeau, R. Jozsa, A. Peres, and W. K. Wootters, *Phys. Rev. Lett.* **70**, 1895 (1993).
- [5] A. R. Calderbank and P. W. Shor, *Phys. Rev. A* **54**, 1098 (1996); A. M. Steane, *Phys. Rev. Lett.* **77**, 793 (1996); *Phys. Rev. A* **54**, 4741 (1996); A. R. Calderbank, E. M. Rains, P. W. Shor, and N. J. A. Sloane, *Phys. Rev. Lett.* **78**, 405 (1997).
- [6] C. H. Bennett and G. Brassard, in *Proceedings of the International Conference on Computers, Systems and Signal Processing, Bangalore, India* (IEEE, NY, 1984); N. Gisin, G. Ribordy, W. Tittel, and H. Zbinden, *Rev. Mod. Phys.* **74**, 145 (2002).
- [7] D. Deutsch, *Proc. R. Soc. A* **425**, 73 (1989).
- [8] P. W. Shor, in *Proceedings of the 35th Annual Symposium on Foundations of Computer Science, edited by S. Goldwasser*, (IEEE Computer Society, Los Alamitos, CA, 1994), p. 124.

- [9] L. K. Grover, *Proceedings, 28th Annual ACM Symposium on the Theory of Computing*, (May 1996) p. 212.
- [10] R. Raussendorf, and H. J. A. Briegel, *Phys. Rev. Lett.* **86**, 5188 (2001); H. J. Briegel, D. E. Browne, W. Dür, R. Raussendorf, and M. V. den Nest, *Nat. Phys.* **5**, 19 (2009).
- [11] D. Bouwmeester, J.-W. Pan, K. Mattle, M. Eibl, H. Weinfurter, and A. Zeilinger, *Nature* **390**, 575 (1997); J.-W. Pan, M. Daniell, S. Gasparoni, G. Weihs, and A. Zeilinger *Phys. Rev. Lett.* **86**, 4435 (2001).
- [12] T. S. -Manderbach, H. Weier, M. Fürst, R. Ursin, F. Tiefenbacher, T. Scheidl, J. Perdigues, Z. Sodnik, C. Kurtsiefer, J. G. Rarity, A. Zeilinger, and H. Weinfurter, *Phys. Rev. Lett.* **98**, 010504 (2007).
- [13] S. Gaertner, C. Kurtsiefer, M. Bourennane, and H. Weinfurter, *Phys. Rev. Lett.* **98**, 020503 (2007).
- [14] L. M. K. Vandersypen, M. Steffen, G. Breyta, C. S. Yannoni, M. H. Sherwood, and Isaac L. Chuang, *Nature* **414**, 883 (2001).
- [15] J.-W. Pan, Z.-B. Chen, C.-Y. Lu, H. Weinfurter, A. Zeilinger, M. Żukowski, *Rev. Mod. Phys.* **84**, 777 (2012).
- [16] H. Häffner, C. F. Roos, and R. Blatt, *Phys. Rep.* **469**, 155 (2008); L.-M. Duan and C. Monroe, *Rev. Mod. Phys.* **82**, 1209 (2010); K. Singer, U. Poschinger, M. Murphy, P. Ivanov, F. Ziesel, T. Calarco, and F. Schmidt-Kaler, *Rev. Mod. Phys.* **82**, 2609 (2010).
- [17] D. Jaksch, *Contemp. Phys.* **45** 367 (2004); D. Jaksch and P. Zoller, *Ann. Phys.* **315** 52 (2005).
- [18] L. M. K. Vandersypen and I. L. Chuang, *Rev. Mod. Phys.* **76**, 1037 (2005).
- [19] D. O. Soares-Pinto, L. C. Celeri, R. Auccaise, F. F. Fanchini, E. R. deAzevedo, J. Maziero, T. J. Bonagamba, and R. M. Serra, *Phys. Rev. A* **81**, 062118 (2010); I. A. Silva, B. Çakmak, G. Karpat, E. L. G. Vidoto, D. O. Soares-Pinto, E. R. deAzevedo, F. F. Fanchini, and Z. Gedik, *Sci. Rep.* **5**, 14671 (2015).
- [20] R. Horodecki, P. Horodecki, M. Horodecki, and K. Horodecki, *Rev. Mod. Phys.* **81**, 865 (2009).

- [21] K. Modi, A. Brodutch, H. Cable, T. Paterek, and V. Vedral, *Rev. Mod. Phys.* **84**, 1655 (2012).
- [22] E. Schrödinger, *Naturwissenschaften* **23**, 807 (1935).
- [23] C. H. Bennett, G. Brassard, S. Popescu, B. Schumacher, J. Smolin, and W. K. Wootters, *Phys. Rev. Lett.* **76**, 722 (1996).
- [24] C. H. Bennett, D. P. DiVincenzo, J. Smolin, and W. K. Wootters, *Phys. Rev. A* **54**, 3824 (1996).
- [25] For a review on quantum communication, see, e.g., A. Sen(De) and U. Sen, *Phys. News* **40**, 17 (2010).
- [26] E. Knill and R. Laflamme, *Phys. Rev. Lett.* **81**, 5672 (1998).
- [27] C. H. Bennett, D. P. DiVincenzo, C. A. Fuchs, T. Mor, E. Rains, P. W. Shor, J. A. Smolin, and W. K. Wootters, *Phys. Rev. A* **59**, 1070 (1999).
- [28] C. H. Bennett, D. P. DiVincenzo, T. Mor, P. W. Shor, J. A. Smolin, and B. M. Terhal, *Phys. Rev. Lett.* **82**, 5385 (1999).
- [29] S. L. Braunstein, C. M. Caves, R. Jozsa, N. Linden, S. Popescu, and R. Schack, *Phys. Rev. Lett.* **83**, 1054 (1999).
- [30] J. Walgate, A. J. Short, L. Hardy, and V. Vedral, *Phys. Rev. Lett.* **85**, 4972 (2000).
- [31] D. A. Meyer, *Phys. Rev. Lett.* **85**, 2014 (2000).
- [32] S. Virmani, M. F. Sacchi, M. B. Plenio, and D. Markham, *Phys. Lett. A* **288**, 62 (2001).
- [33] S. L. Braunstein and A. K. Pati, *Quant. Inf. Comp.* **2**, 399 (2002).
- [34] Y.-X. Chen and D. Yang, *Phys. Rev. A* **64**, 064303 (2001); *Phys. Rev. A* **65**, 022320 (2002).
- [35] D. P. DiVincenzo, T. Mor, P. W. Shor, J. A. Smolin, and B. M. Terhal, *Comm. Math. Phys.* **238**, 379 (2003).
- [36] M. Horodecki, A. Sen(De), U. Sen, K. Horodecki, *Phys. Rev. Lett.* **90**, 047902 (2003).

- [37] A. Datta, S. T. Flammia, and C. M. Caves, Phys. Rev. A **72**, 042316 (2005).
- [38] M. Lucamarini and S. Mancini, Phys. Rev. Lett. **94**, 140501 (2005).
- [39] A. Cerè, M. Lucamarini, G. Di Giuseppe, and P. Tombesi, Phys. Rev. Lett. **96**, 200501 (2006).
- [40] A. Datta and G. Vidal, Phys. Rev. A **75**, 042310 (2007).
- [41] S. Boixo, A. Datta, S. T. Flammia, A. Shaji, E. Bagan, C. M. Caves, Phys. Rev. A **77**, 012317 (2007).
- [42] A. Datta, A. Shaji, and C. M. Caves. Phys. Rev. Lett. **100**, 050502 (2008); A. Datta, arXiv:0807.4490 [quant-ph]; M. D. Lang, C. M. Caves, A. Shaji, Int. J. Quantum Inf. **9**, 1553 (2011); A. Datta, A. Shaji, Int. J. Quantum Inf. **9**, 1787 (2011).
- [43] M. F. Cornelio, M. C. de Oliveira, and F. F. Fanchini, Phys. Rev. Lett. **107** 020502 (2011).
- [44] B. P. Lanyon, M. Barbieri, M. P. Almeida, and A. G. White, Phys. Rev. Lett. **101**, 200501 (2008).
- [45] Z. Ma, Z. Chen, F. F. Fanchini, and S.-M. Fei, Sci. Rep. **5**, 10262 (2015).
- [46] H. Ollivier and W. H. Zurek, Phys. Rev. Lett. **88**, (2001).
- [47] L. Henderson and V. Vedral, J. Phys. A: Math. Gen. **34**, 6899 (2001).
- [48] J. Oppenheim, M. Horodecki, P. Horodecki, and R. Horodecki, Phys. Rev. Lett. **89**, 180402 (2002).
- [49] M. Horodecki, K. Horodecki, P. Horodecki, R. Horodecki, J. Oppenheim, A. Sen(De), and U. Sen, Phys. Rev. Lett. **90**, 100402 (2003).
- [50] I. Devetak, Phys. Rev. A **71**, 062303 (2005).
- [51] M. Horodecki, P. Horodecki, R. Horodecki, J. Oppenheim, A. Sen(De), U. Sen, and B. Synak-Radtke, Phys. Rev. A **71**, 062307 (2005).
- [52] A. Osterloh, L. Amico, C. Falci, and R. Fazio, Nature (London) **416**, 608 (2002).
- [53] T. J. Osborne and M. A. Nielsen, Phys. Rev. A **66**, 032110 (2002).

- [54] L. Amico, R. Fazio, A. Osterloh, and V. Vedral, *Rev. Mod. Phys.* **80**, 517 (2008).
- [55] R. Dillenschneider, *Phys. Rev. B* **78**, 224413 (2008).
- [56] M. S. Sarandy, *Phys. Rev. A* **80**, 022108 (2009).
- [57] T. Werlang, C. Trippe, G. A. P. Ribeiro, and G. Rigolin, *Phys. Rev. Lett.* **105**, 095702 (2010).
- [58] Y. X. Chen and S. W. Li, *Phys. Rev. A* **81**, 032120 (2010).
- [59] J. Maziero, H. C. Guzman, L. C. Céleri, M. S. Sarandy and R. M. Serra, *Phys. Rev. A* **82**, 012106 (2010).
- [60] B. Q. Liu, B. Shao, and J. Zou, *Phys. Rev. A* **82**, 062119 (2010).
- [61] H. S. Dhar, R. Ghosh, A. Sen(De), and U. Sen, *Europhys. Lett.* **98**, 30013 (2012); *Phys. Lett. A* **378**, 1258 (2014).
- [62] Y. C. Li and H.Q. Lin, *Phys. Rev. A* **83**, 052323 (2011).
- [63] A. K. Pal and I. Bose, *J. Phys. B: At. Mol. Opt. Phys.* **44**, 045101 (2011).
- [64] G. F. Zhang, H. Fan, A. L. Ji, Z. T. Jiang, A. Abliz, and W. M. Liu, *Ann. Phys.* **326**, 2694 (2011) and references therein.
- [65] G. Karpat, B. Çakmak, F. F. Fanchini, *Phys. Rev. B* **90**, 104431 (2014); B. Çakmak, G. Karpat, and F. F. Fanchini, *Entropy* **172**,790 (2015); A. L. Malvezzi, G. Karpat, B. Çakmak, F. F. Fanchini, T. Debarba, R. O. Vianna, arXiv:1602.03731 [quant-ph].
- [66] S. Ghosh, T. F. Rosenbaum, G. Aeppli, S. N. Coppersmith, *Nature* **425**, 48 (2003).
- [67] A. M. Souza, M. S. Reis, D. O. Soares-Pinto, I. S. Oliveira, and R. S. Sarthour, *Phys. Rev. B* **77**, 104402(2008); D. Das, T. Chakraborty, H. Singh, and C. Mitra, arXiv:1109.1640v2 [quant-ph].
- [68] H. Singh, T. Chakraborty, D. Das, H. S. Jeevan, Y. Tokiwa, P. Gegenwart, and C. Mitra, *New J. Phys.* **15** 113001 (2013); T. Chakraborty, H. Singh, D. Das, T. K. Sen, S. K. Mandal, and C. Mitra, *Phys. Lett. A* **376**, 2967 (2012).
- [69] J. Adolphs and T. Renger, *Biophys. J.* **91**, 2778 (2006).

- [70] M. Mohseni, P. Rebentrost, S. Lloyd, and A. A. Guzik, *J. Chem. Phys.* **129**, 174106 (2008); M. B. Plenio, S. F. Huelga, *New J. Phys.* **10**, 113019 (2008); P. Rebentrost, M. Mohseni, I. Kassal, S. Lloyd, and A. A. Guzik, *New J. Phys.* **11**, 033003 (2009).
- [71] F. Caruso, A. W. Chin, A. Datta, S. F. Huelga, and M. B. Plenio, *J. Chem. Phys.* **131**, 105106 (2009).
- [72] G. Panitchayangkoon, D. Hayes, K. A. Fransted, J. R. Carama, E. Harela, J. Wenb, R. E. Blankenship, and G. S. Engela, *Proc. Natl. Acad. Sci.* **107**, 12766 (2010).
- [73] M. Sarovar, A. Ishizaki, G. R. Fleming, and K. B. Whaley, *Nat. Phys.* **6**, 462 (2010).
- [74] N. Lambert, Y.-N. Chen, Y.-C. Cheng, C.-M. Li, G.-Y. Chen, and F. Nori, *Nat. Phys.* **9**, 10 (2013).
- [75] E. C. G. Sudarshan, P. M. Mathews, and J. Rau, *Phys. Rev.* **121**, 920 (1961); T. F. Jordan and E. C. G. Sudarshan, *J. Math. Phys.* **2**, 772 (1961); T. F. Jordan, M. A. Pinsky, and E. C. G. Sudarshan, *J. Math. Phys.* **3**, 848 (1962).
- [76] A. Jamiolkowski, *Rep. Math. Phys.* **3**, 275 (1972).
- [77] M. D. Choi, *Can. J. Math.* **24**, 520 (1972); M. D. Choi, *Ill. J. Math.* **18**, 565 (1974); M. D. Choi, *Linear Algebra and its applications* **10**, 285 (1975).
- [78] K. Krauss, *States, Effects, and Operations Fundamental Notions of Quantum Theory*, Springer Lecture Notes in Physics **190**, 1983.
- [79] E. B. Davies, *Quantum Theory of Open Systems* (Academic Press, New York, 1976); H. P. Breuer and F. Petruccione, *The Theory of Open Quantum Systems* (Oxford University Press, New York, 2002).
- [80] J. Preskill, *Lecture Notes*, available at theory.caltech.edu/~preskill/ph229/.
- [81] T. F. Jordan, A. Shaji, E. C. G. Sudarshan, *Phys. Rev. A* **70**, 052110 (2004).
- [82] S. Hill and W. K. Wootters, *Phys. Rev. Lett.* **78**, 5022 (1997); W. K. Wootters, *Phys. Rev. Lett.* **80**, 2245 (1998).
- [83] P. M. Hayden, M. Horodecki, and B. M. Terhal, *J. Phys. A: Math. Gen.* **34**, 6891 (2001).

- [84] J. Lee, M. S. Kim, Y. J. Park, and S. Lee, *J. Mod. Opt.* **47**, 2151 (2000).
- [85] G. Vidal and R. F. Werner, *Phys. Rev. A* **65**, 032314 (2002).
- [86] A. Peres, *Phys. Rev. Lett.* **77**, 1413 (1996).
- [87] M. Horodecki, P. Horodecki, and R. Horodecki, *Phys. Lett. A* **223**, 1 (1996).
- [88] K. Zyczkowski, P. Horodecki, A. Sanpera, and M. Lewenstein, *Phys. Rev. A* **58**, 883 (1998).
- [89] K. Audenaert, M. B. Plenio, and J. Eisert, *Phys. Rev. Lett.* **90**, 027901 (2003);
M. B. Plenio, *Phys. Rev. Lett.* **95**, 090503 (2005).
- [90] W. Zurek, *Rev. Mod. Phys.* **75**, 715 (2003).
- [91] H. Jeong, M. Kang, and H. Kwon, *Opt. Commun.* **337**, 12 (2015).
- [92] A. J. Leggett, *Progress of Theoretical Physics Supplement* **69**, 80 (1980).
- [93] N. D. Mermin, *Phys. Rev. Lett.* **65**, 1838 (1990).
- [94] T. Monz, P. Schindler, J. T. Barreiro, M. Chwalla, D. Nigg, W. A. Coish, M. Harlander, W. Hänsel, M. Hennrich, and R. Blatt, *Phys. Rev. Lett.* **106**, 130506 (2011) and references therein.
- [95] D. M. Greenberger, M. A. Horne, and A. Zeilinger, in *Bell's Theorem, Quantum Theory, and Conceptions of the Universe*, ed. M. Kafatos (Kluwer Academic, Dordrecht, The Netherlands, 1989).
- [96] D. Mermin, *Am. J. Phys.* **58**, 731 (1990).
- [97] J. -W. Pan, D. Bouwmeester, M. Daniell, H. Weinfurter, and A. Zeilinger, *Nature* **403**, 515 (2000).
- [98] D. Leibfried, E. Knill, S. Seidelin, J. Britton, R. B. Blakestad, J. Chiaverini, D. B. Hume, W. M. Itano, J. D. Jost, C. Langer, R. Ozeri, R. Reichle, and D. J. Wineland, *Nature* **438**, 639 (2005).
- [99] W. -B. Gao, C. -Y. Lu, X. -C. Yao, P. Xu, O. Gühne, A. Goebel, Y. -A. Chen, C. -Z. Peng, Z. -B. Chen, and J.-W. Pan, *Nat. Phys.* **6**, 331 (2010).
- [100] R. Rouse, S. Han, and J. E. Luckens, *Phys. Rev. Lett.* **75**, 1614 (1995).

- [101] R. Rouse, S. Han, and J. E. Luckens, *Phenomenology of unification from present to future*, eds. G. D. Palazi, C. Cosmelli, and L. Zanello, (World Scientific, Singapore, 1998).
- [102] J. Clarke, A. N. Cleland, M. H. Devoret, D. Esteve, and J. M. Martinis, *Science* **239**, 992 (1988).
- [103] P. Silvestrini, V. G. Palmieri, B. Ruggiero, and M. Russao, *Phys. Rev. Lett.* **79**, 3046 (1997).
- [104] Y. Nakamura, Y. A. Pashkin, and J. S. Tsai, *Nature* **398**, 786 (1999).
- [105] J. R. Friedman, M. P. Sarachik, J. Tejada, and R. Ziolo, *Phys. Rev. Lett.* **76**, 3830 (1996).
- [106] E. del Barco, N. Vernier, J. M. Hernandez, J. Tejada, E. M. Chudnovsky, E. Molins, and G. Bellessa, *Europhys. Lett.* **47**, 722 (1999).
- [107] W. Wernsdorfer, E. B. Orozco, K. Hasselbach, A. Benoit, D. Mailly, O. Kubo, H. Nakano, and B. Barbara, *Phys. Rev. Lett.* **79**, 4014 (1997).
- [108] C. Monroe, D. M. Meekhof, B. E. King, and D. J. A. Wineland, *Science* **272**, 1131 (1996).
- [109] M. Brune, E. Hagley, J. Dreyer, X. Maître, A. Maali, C. Wunderlich, J. M. Raimond, and S. Haroche, *Phys. Rev. Lett.* **77**, 4887 (1996).
- [110] M. Arndt, O. Nairz, J. Vos-Andriase, C. Keller, G. van der Zouw, and A. Zeilinger, *Nature* **401**, 680 (1999).
- [111] J. R. Friedman, V. Patel, W. Chen, S. K. Tolpygo, and J. E. Lukens, *Nature* **406**, 43 (2000).
- [112] Y. Makhlin, G. Schön, and A. Shnirman, *Rev. Mod. Phys.* **73**, 357 (2001).
- [113] Y. Yu, S. Han, X. Chu, S.-I. Chu, and Z. Wang, *Science* **296**, 889 (2002).
- [114] W. Marshal, C. Simon, R. Penrose, and D. Bouwmeester, *Phys. Rev. Lett.* **91**, 130401 (2003).
- [115] W. Dür, C. Simon, and J. I. Cirac, *Phys. Rev. Lett.* **89**, 210402 (2002).
- [116] A. Shimizu and T. Miyadera, *Phys. Rev. Lett.* **89**, 270403 (2002).

- [117] G. Björk and P. G. L. Mana, *J. Opt. B* **6**, 429 (2004).
- [118] A. Shimizu and T. Morimae, *Phys. Rev. Lett.* **95**, 090401 (2005).
- [119] A. N. Salgueiro, *Phys. Rev. A* **72**, 032104 (2005).
- [120] T. Morimae and A. Shimizu, *Phys. Rev. A* **74**, 052111 (2006).
- [121] J. I. Korsbakken, K. B. Whaley, J. Dubois, and J. I. Cirac, *Phys. Rev. A* **75**, 042106 (2007).
- [122] F. Marquardt, B. Abel, and J. von Delft, *Phys. Rev. A* **78**, 012109 (2008).
- [123] T. Morimae, *Phys. Rev. A* **81**, 010101(R) (2010).
- [124] C.-W. Lee and H. Jeong, *Phys. Rev. Lett.* **106**, 220401 (2011).
- [125] F. Fröwis and W. Dür, *Phys. Rev. Lett.* **109**, 170401 (2012); F. Fröwis and W. Dür, *New J. of Phys.* **14**, 093039 (2012).
- [126] G. Vidal and R. Tarrach, *Phys. Rev. A* **59**, 141 (1999).
- [127] C. Simon and J. Kempe, *Phys. Rev. A* **65**, 052327 (2002).
- [128] H.-J. Briegel and R. Raussendorf, *Phys. Rev. Lett.* **86**, 910 (2001).
- [129] W. Dür and H.-J. Briegel, *Phys. Rev. Lett.* **92**, 180403 (2004).
- [130] G. Tóth and O. Gühne, *Phys. Rev. Lett.* **94**, 060501 (2005).
- [131] M. Hein, W. Dür, and H.-J. Briegel, *Phys. Rev. Lett.* **94**, 032350 (2005).
- [132] L. Aolita, R. Chaves, D. Cavalcanti, A. Acín, and L. Davidovich, *Phys. Rev. Lett.* **100**, 080501 (2008); D. Cavalcanti, R. Chaves, L. Aolita, L. Davidovich, and A. Acín, *Phys. Rev. Lett.* **103**, 030502 (2009); L. Aolita, D. Cavalcanti, A. Acín, A. Salles, M. Tiersch, A. Buchleitner, and F. de Melo, *Phys. Rev. A* **79**, 032322 (2009); L. Aolita, D. Cavalcanti, C. Dhara, L. Davidovich, and A. Acín, *Phys. Rev. A* **82**, 032317 (2010); D. Cavalcanti, L. Aolita, A. Ferraro, A. Garc a-Saez, A. Acín, *New J. Phys.* **12**, 025011 (2010); R. Chaves and F. de Melo, *Phys. Rev. A* **84**, 022324 (2011); R. Chaves, D. Cavalcanti, L. Aolita, and A. Acín, *Phys. Rev. A* **86**, 012108 (2012).
- [133] O. Gühne, F. Bodoky, M. Blaauuboer, *Phys. Rev. A* **78**, 060301 (2008).

- [134] T. Vértesi and K. F. Pál, Phys. Rev. A **84**, 042122 (2011).
- [135] S. Bandyopadhyay and D. A. Lidar, Phys. Rev. Lett. **72**, 042339 (2005).
- [136] Z.-X. Man, Y.-J. Xia, and N. Ba An, Phys. Rev. A **78**, 064301 (2008).
- [137] A. Borrás, A. P. Majtey, A. R. Plastino, M. Casas, and A. Plastino, Phys. Rev. A **79**, 022108 (2009).
- [138] F. Fröwis and W. Dür, Phys. Rev. Lett. **106**, 110402 (2011).
- [139] R. Chaves, L. Aolita, and A. Acín, Phys. Rev. A **86**, 020301(R) (2012).
- [140] F. Fröwis and W. Dür, Phys. Rev. A **85**, 052329 (2012).
- [141] U. Mishra, A. Sen(De), and U. Sen, Phys. Rev. A **87**, 052117 (2013); U. Mishra, A. Sen(De), and U. Sen, Phys. Lett. A **379**, 261 (2015).
- [142] A. Zeilinger, M. A. Horne, and D. M. Greenberger, in *NASA Proceedings of the International Conference on Squeezed States and Quantum Uncertainty*, edited by D. Han et al., NASA Conf. Publ. No. 3135 (NASA, Washington, DC, 1992).
- [143] W. Dür, G. Vidal, and J. I. Cirac, Phys. Rev. **62**, 062314 (2000).
- [144] A. Sen(De), U. Sen, M. Wieśniak, D. Kaszlikowski, and M. Żukowski, Phys. Rev. A **68**, 062306 (2003).
- [145] A. Sen(De), U. Sen, and M. Żukowski, Phys. Rev. A **68**, 032309 (2003).
- [146] R. H. Dicke, Phys. Rev. **93**, 99 (1954).
- [147] M. Lewenstein, A. Sanpera, V. Ahufinger, B. Damski, A. Sen De, U. Sen, Adv. Phys. **56**, 243 (2007).
- [148] S. Sachdev, *Quantum Phase Transitions* (Cambridge University Press, Cambridge, 1999).
- [149] A. Dutta, G. Aeppli, B. K. Chakrabarti, U. Divakaran, T. F. Rosenbaum, and D. Sen, *Quantum Phase Transitions in Transverse Field Spin Models From Statistical Physics to Quantum Information* (Cambridge University Press, Cambridge, 2015).
- [150] F. Verstraete, J. I. Cirac, and V. Murg, Adv. Phys. **57**, 143 (2008).

- [151] G. Vidal, Phys. Rev. Lett. **101**, 110501 (2008).
- [152] A. J. Ferris and G. Vidal, Phys. Rev. B **85**, 165147 (2012) and references therein.
- [153] A. Polkovnikov, K. Sengupta, A. Silva, and M. Vengalattore, Rev. Mod. Phys. **83**, 863 (2011); A. Sen and K. Sengupta, arXiv:1511.03668 [cond-mat.str-el].
- [154] G. Vidal, Phys. Rev. Lett. **93**, 040502 (2004).
- [155] S. R. Clark and D. Jaksch, Phys. Rev. A **70**, 043612 (2004).
- [156] L. Amico, A. Osterloh, F. Plastina, R. Fazio, and G. M. Palma, Phys. Rev. A **69**, 022304 (2004).
- [157] W. Dür, L. Hartmann, M. Hein, M. Lewenstein, and H.-J. Briegel, Phys. Rev. Lett. **94**, 097203 (2005).
- [158] N. T. Jacobson, L. C. Venuti, and P. Zanardi, Phys. Rev. A **84**, 022115 (2011).
- [159] J. Cardy, Phys. Rev. Lett. **106**, 150404 (2011).
- [160] A. Gambassi and A. Silva, Phys. Rev. Lett. **109**, 250602 (2012).
- [161] J. Häppölä, Gabor B. Halász, and A. Hamma, Phys. Rev. A **85**, 032114 (2012).
- [162] S. Mondal, D. Sen, K. Sengupta, *Quantum Quenching, Annealing and Quantum Computation*, Lect. Notes in Phys., Springer, Heidelberg (2010).
- [163] J. Eisert, M. Friesdorf, and C. Gogolin, Nat. Phys. **11**, 124 (2015).
- [164] A. del Campo and K. Sengupta, Eur. Phys. J. Special Topics **224**, 189 (2015).
- [165] A. Dutta, A. Das, and K. Sengupta, Phys. Rev. E **92**, 012104 (2015).
- [166] F. Iglói and H. Rieger, Phys. Rev. Lett. **85**, 3233 (2000).
- [167] K. Sengupta, S. Powell, and S. Sachdev, Phys. Rev. A **69**, 053616 (2004).
- [168] S. R. Manmana, S. Wessel, R. M. Noack, and A. Muramatsu, Phys. Rev. Lett. **98**, 210405 (2007).
- [169] K. Sengupta and Diptiman Sen, Phys. Rev. A **80**, 032304 (2009).
- [170] G. Mazza and M. Fabrizio, Phys. Rev. B **86**, 184303 (2012).

- [171] K. R. A. Hazzard, M. van den Worm, M. Foss-Feig, S. R. Manmana, E. G. Dalla Torre, T. Pfau, M. Kastner, and A. M. Rey, *Phys. Rev. A* **90**, 063622 (2014).
- [172] L. Bonnes, F. H. L. Essler, and A. M. Läuchli, *Phys. Rev. Lett.* **113**, 187203 (2014).
- [173] M. Greiner, O. Mandel, T. Esslinger, T. W. Hänsch, and I. Bloch, *Nature* **415**, 39 (2002).
- [174] C. Regal, and D. S. Jin, arXiv:cond-mat/0601054 [cond-mat.other].
- [175] L. E. Sadler, J. M. Higbie, S. R. Leslie, M. Vengalattore, and D. M. Stamper-Kurn, *Nature (London)* **443**, 312 (2006).
- [176] A. K. Tuchman, C. Orzel, A. Polkovnikov, and M. Kasevich, *Phys. Rev. A* **74**, 051601 (2006).
- [177] I. Bloch, J. Dalibard, and W. Zwerger, *Rev. Mod. Phys.* **80**, 885 (2008).
- [178] A. Flesch, M. Cramer, I. McCulloch, U. Schollwoeck, and J. Eisert, *Phys. Rev. A* **78**, 033608 (2008).
- [179] P. Reimann, *Phys. Rev. Lett.* **101**, 190403 (2008).
- [180] M. Rigol, V. Dunjko, and M. Olshanii, *Nature (London)* **452**, 854 (2008).
- [181] N. Linden, S. Popescu, A. Short, and A. Winter, *Phys. Rev. E* **79**, 061103 (2009).
- [182] M. Cramer, and J. Eisert, *New J. Phys.* **12**, 055020 (2010).
- [183] C. Gogolin, M. P. Müller, and J. Eisert, *Phys. Rev. Lett.* **106**, 040401 (2011).
- [184] A. Sen(De), U. Sen, and M. Lewenstein, *Phys. Rev. A* **72**, 052319 (2005).
- [185] T. Kinoshita, T. Wenger, and D. S. Weiss, *Nature* **440**, 900 (2006).
- [186] H. Wichterich and S. Bose, *Phys. Rev. A* **79**, 060302(R) (2009); Z. Chang and N. Wu, *Phys. Rev. A* **81**, 022312 (2010).
- [187] L. Cincio, J. Dziarmaga, M. M. Rams, and W. H. Zurek, *Phys. Rev. A* **75**, 052321 (2007).

- [188] A. Sen(De), U. Sen, and M. Lewenstein, Phys. Rev. A **70**, 060304(R) (2004).
- [189] E. Barouch, B. M. McCoy, and M. Dresden, Phys. Rev. A **2**, 1075 (1970); E. Barouch and B. M. McCoy, Phys. Rev. A **3**, 786 (1971).
- [190] E. Barouch and B. M. McCoy, Phys. Rev. A **3**, 2137 (1971); B. M. McCoy, E. Barouch, and D. B. Abraham, Phys. Rev. A **4**, 2331 (1971).
- [191] P. Mazur, Physica **43**, 533 (1969).
- [192] J. H. H. Perk, H. W. Capel, and Th. J. Siskens, Physica **89A**, 304 (1977).
- [193] J. H. H. Perk and H. Au-Yang, J. Stat. Phys. **135**, 599 (2009).
- [194] T. Prosen, Phys. Rev. E **60**, 3949 (1999).
- [195] E. Plekhanov, A. Avella, and F. Mancini, Phys. Rev. B **74**, 115120 (2006).
- [196] S. Deng, G. Ortiz, and L. Viola, Europhys. Lett. **84**, 67008 (2008).
- [197] M. Znidaric, T. Prosen, G. Benenti, G. Casati, and D. Rossini, Phys. Rev. E **81**, 051135 (2010).
- [198] Z. Huang and S. Kais, Phys. Rev. A **73**, 022339 (2006); B. Alkurtass, G. Sadiq, and S. Kais, Phys. Rev. A **84**, 022314 (2011).
- [199] G. Sadiq, Q. Xu, and S. Kais, Phys. Rev. A **85**, 042313 (2012).
- [200] A. D. Luca and A. Scardicchio, Europhys. Lett. **101**, 37003 (2013).
- [201] R. Prabhu, A. Sen(De), and U. Sen, Europhys. Lett. **102**, 30001 (2013).
- [202] R. Prabhu, A. Sen(De), and U. Sen, Phys. Rev. A **86**, 012336 (2012).
- [203] U. Mishra, R. Prabhu, A. Sen(De), and U. Sen, Phys. Rev. A **87**, 052318 (2013).
- [204] U. Mishra, D. Rakshit, and R. Prabhu, accepted for publication in Phys. Rev. A (arXiv:1510.00685 [quant-ph]).
- [205] G. Refael and J. E. Moore, J. Phys. A: Math. Theor. **42**, 504010 (2009).
- [206] F. C. Nix and W. Shockley, Rev. Mod. Phys. **10**, 1 (1938).
- [207] P. Dean, Rev. Mod. Phys. **44**, 127 (1972).

- [208] R. J. Elliott, J. A. Krumhansl, and P. L. Leath, *Rev. Mod. Phys.* **46**, 465 (1974).
- [209] A. S. Barker, Jr. and A. J. Sievers, *Rev. Mod. Phys.* **47**, S1 (1975).
- [210] P. A. Lee and T. V. Ramakrishnan, *Rev. Mod. Phys.* **57**, 287 (1985).
- [211] A. G. Aronov and Yu.V. Sharvin, *Rev. Mod. Phys.* **59**, 755 (1987).
- [212] J. C. Dyre and T. B. Schrøder, *Rev. Mod. Phys.* **72**, 873 (2000).
- [213] F. Iglói and C. Monthus, *Phys. Rep.* **412**, 277 (2005).
- [214] G. Misguich and C. Lhuillier, *Two-dimensional quantum antiferromagnets, Frustrated Spin Systems*, edited by H. T. Diep (World-Scientific, Singapore, 2005); arxiv:cond-mat/0310405
- [215] J. T. Karvonen, L. J. Taskinen, and I. J. Maasilta, *Phys. Rev. B* **72**, 012302 (2005).
- [216] J. Salafranca and L. Brey, *Phys. Rev. B* **73**, 214404 (2006).
- [217] H. C. Hsu, W. L. Lee, J.-Y. Lin, H. L. Liu, and F. C. Chou, *Phys. Rev. B* **81**, 212407 (2010).
- [218] T. Berlijn, D. Volja, and W. Ku, *Phys. Rev. Lett.* **106**, 077005 (2011).
- [219] B. Jaworowski, P. Potasz, and A. Wojs, *Superlattices and Microstructures*, **64**, 44 (2013).
- [220] A. Aharony, *Phys. Rev. B* **18**, 3328 (1978).
- [221] J. Villain, R. Bidaux, J.-P. Carton, and R. Conte, *J. Physique* **41**, 1263 (1980).
- [222] A. Niederberger, T. Schulte, J. Wehr, M. Lewenstein, L. Sanchez-Palencia, and K. Sacha, *Phys. Rev. Lett.* **100**, 030403 (2008).
- [223] P. V. Martín, J. A. Bonachela, and M. A. Muñoz, *Phys. Rev. E* **89**, 012145 (2014).
- [224] J. Wehr, A. Niederberger, L. Sanchez-Palencia, and M. Lewenstein, *Phys. Rev. B* **74**, 224448 (2006).
- [225] L. F. Santos, G. Rigolin, and C. O. Escobar, *Phys. Rev. A* **69**, 042304 (2004).

- [226] R. Prabhu, S. Pradhan, A. Sen(De), and U. Sen, *Phys. Rev. A* **84**, 042334 (2011).
- [227] K. Binder and A. P. Young, *Rev. Mod. Phys.* **58**, 801 (1986).
- [228] D. Belitz, T. R. Kirkpatrick, and T. Vojta, *Rev. Mod. Phys.* **77**, 579 (2005).
- [229] A. Das and B. K. Chakrabarti, *Rev. Mod. Phys.* **80**, 1061 (2008).
- [230] H. Alloul, J. Bobroff, M. Gabay, and P. J. Hirschfeld, *Rev. Mod. Phys.* **81**, 45 (2009).
- [231] J. P. Á. Zúñiga and N. Laflorencie, *Phys. Rev. Lett.* **111**, 160403 (2013).
- [232] Z. Yao, K. P. C. da Costa, M. Kiselev, and N. Prokofiev, *Phys. Rev. Lett.* **112**, 225301 (2014).
- [233] P. W. Anderson, *Phys. Rev.* **109**, 1492 (1958).
- [234] E. Dagotto, *Rev. Mod. Phys.* **66**, 763 (1994).
- [235] P. A. Lee, N. Nagaosa, and X.-G. Wen, *Rev. Mod. Phys.* **78**, 17 (2006).
- [236] X.-L. Qi and S.-C. Zhang, *Rev. Mod. Phys.* **83**, 1057 (2011).
- [237] L. Fallani, J. E. Lye, V. Guarrera, C. Fort, and M. Inguscio, *Phys. Rev. Lett.* **98**, 130404 (2007).
- [238] G. Roati, C. D’Errico, L. Fallani, M. Fattori, C. Fort, M. Zaccanti, G. Modugno, M. Modugno, and M. Inguscio, *Nature* **453**, 895 (2008).
- [239] J. Billy, V. Josse, Z. Zuo, A. Bernard, B. Hambrecht, P. Lugan, D. Clément, L. Sanchez-Palencia, P. Bouyer, and A. Aspect, *Nature* **453**, 891 (2008).
- [240] R. Yu, L. Yin, N. S. Sullivan, J. S. Xia, C. Huan, A. Paduan-Filho, N. F. Oliveira Jr., S. Haas, A. Steppke, C. F. Miclea, F. Weickert, R. Movshovich, E.-D. Mun, V. S. Zapf, and T. Roscilde, *Nature* **489**, 379 (2012).
- [241] D. Hönig, S. Zhao, M. Månsson, T. Yankova, E. Ressouche, C. Niedermayer, M. Laver, S. N. Gvasaliya, and A. Zheludev, *Phys. Rev. B* **85**, 100410(R) (2012).
- [242] S. Krinner, D. Stadler, J. Meineke, J.-P. Brantut, and T. Esslinger, arXiv: 1311.5174 [quant-ph].

- [243] K. R. A. Hazzard, B. Gadway, M. Foss-Feig, B. Yan, S. A. Moses, J. P. Covey, N. Y. Yao, M. D. Lukin, J. Ye, D. S. Jin, and A. M. Rey, arXiv: 1402.2354 [quant-ph] and references therein.
- [244] U. Mishra, D. Rakshit, R. Prabhu, A. Sen(De), and U. Sen, arXiv:1408.0179 [quant-ph].
- [245] P. Walther, K. J. Resch, T. Rudolph, E. Schenck, H. Weinfurter, V. Vedral, M. Aspelmeyer, and A. Zeilinger, *Nature* **434**, 169 (2005).
- [246] W. Dür, *Phys. Rev. Lett.* **87**, 230402 (2001).
- [247] D. Kaszlikowski, L. C. Kwek, J. Chen, and C. h. Oh, *Phys. Rev. A* **66**, 052309 (2002).
- [248] A. Sen(De), U. Sen, and M. Żukowski, *Phys. Rev. A* **66**, 062318 (2002).
- [249] R. Augusiak and P. Horodecki, *Phys. Rev. A* **74**, 010305 (2006).
- [250] T. Vértesi and N. Brunner, *Phys. Rev. Lett.* **108**, 030403 (2012).
- [251] T. Vértesi and N. Brunner, *Nat. Comm.* **5**, 5297 (2014).
- [252] T. Moroder, O. Gittsovich, M. Huber, and O. Gühne, *Phys. Rev. Lett.* **113**, 050404 (2014).
- [253] M. Horodecki and M. Piani, *J. Phys. A: Math. Theor.* **45**, 105306 (2012).
- [254] R. F. Werner, *Phys. Rev. A* **40**, 4277 (1989).
- [255] J. Eckhoff, *Helly, Radon, and Carathéodory type theorems*, *Handbook of Convex Geometry* **A, B**, Amsterdam: North-Holland (1993).
- [256] P. Horodecki, *Phys. Lett. A* **232**, 333 (1997).
- [257] M. Horodecki, P. Horodecki, and R. Horodecki, *Phys. Rev. Lett.* **80**, 5239 (1998).
- [258] B. Dakić, V. Vedral, and Č. Brukner, *Phys. Rev. Lett.* **105**, 190502 (2010).
- [259] C. N. Lunkes, Č. Brukner, and V. Vedral, *Phys. Rev. Lett.* **95**, 030503 (2005).
- [260] T. Vértesi, *Phys. Rev. A* **75**, 042330 (2007).
- [261] D. Patané, R. Fazio, and L. Amico, *New J. Phys.* **9**, 322 (2007).

- [262] C. H. Bennett, H. J. Bernstein, S. Popescu, and B. Schumacher, *Phys. Rev. A* **53**, 2046 (1996).
- [263] V. Coffman, J. Kundu, and W. K. Wootters, *Phys. Rev. A* **61**, 052306 (2000); M. Koashi and A. Winter, *Phys. Rev. A* **69**, 022309 (2004); T. J. Osborne and F. Verstraete, *Phys. Rev. Lett.* **96**, 220503 (2006); G. Adesso, A. Serafini, and F. Illuminati, *Phys. Rev. A* **73**, 032345 (2006); T. Hiroshima, G. Adesso, and F. Illuminati, *Phys. Rev. Lett.* **98**, 050503 (2007); Y.-C. Ou and H. Fan, *Phys. Rev. A* **75**, 062308 (2007); M. Seevinck, *Phys. Rev. A* **76**, 012106 (2007); S. Lee and J. Park, *Phys. Rev. A* **79**, 054309 (2009); A. Kay, D. Kaszlikowski and R. Ramanathan, *Phys. Rev. Lett.* **103**, 050501 (2009); M. Hayashi and L. Chen, *Phys. Rev. A* **84**, 012325 (2011).
- [264] F. F. Fanchini, M. C. de Oliveira, L. K. Castelano, and M. F. Cornelio, *Phys. Rev. A* **87**, 032317 (2013); F. F. Fanchini, M. F. Cornelio, M. C. de Oliveira, A. O. Caldeira, *Phys. Rev. A* **84**, 012313 (2011) and references therein.
- [265] A. Shimony, *Ann. N.Y. Acad. Sci.* **755**, 675 (1995).
- [266] H. Barnum and N. Linden, *J. Phys. A* **34**, 6787 (2001).
- [267] T.-C. Wei and P. M. Goldbart, *Phys. Rev. A* **68**, 042307 (2003).
- [268] M. Balsone, F. Dell'Anno, S. De Siena, and F. Illuminati, *Phys. Rev. A* **77**, 062304 (2008).
- [269] A. Sen(De) and U. Sen, *Phys. Rev. A* **81**, 012308 (2010); M. N. Bera, R. Prabhu, A. Sen(De), and U. Sen, arXiv:1209.1523; A. Biswas, A. Sen(De), and U. Sen, *Phys. Rev. A* **89**, 032331 (2014); H. S. Dhar, A. Sen(De), and U. Sen, *New J. Phys.* **15**, 013043 (2013); H. S. Dhar, A. Sen(De), and U. Sen, *Phys. Rev. Lett.* **111**, 070501 (2013); S. S. Roy, H. S. Dhar, D. Rakshit, A. Sen(De), and U. Sen, *New J. Phys.* **18**, 023025 (2016).
- [270] D. A. Meyer and N. R. Wallach, *J. Math. Phys.* **43**, 4273 (2002).
- [271] A. Osterloh and J. Siewert, *Phys. Rev. A* **72**, 012337 (2005); *Int. J. Quant. Inf.* **4**, 531 (2006).
- [272] D. Ž. Doković and A. Osterloh, *J. Math. Phys.* **50**, 033509 (2009).
- [273] O. Gühne, G. Tóth, and H. J. Briegel, *New J. Phys.* **7**, 229 (2005).

- [274] T.-C. Wei, D. Das, S. Mukhopadhyay, S. Vishveshwara, and P. M. Goldbart, *Phys. Rev. A* **71**, 060305(R) (2005).
- [275] A. Anfossi, P. Giorda, A. Montorsi, and F. Traversa, *Phys. Rev. Lett.* **95**, 056402 (2005).
- [276] T. R. de Oliveira, G. Rigolin, M. C. de Oliveira, and E. Miranda, *Phys. Rev. Lett.* **97**, 170401 (2006).
- [277] T. Roscilde, P. Verrucchi, A. Fubini, S. Haas, and V. Tognetti, *Phys. Rev. Lett.* **93**, 167203 (2007).
- [278] R. Orús, *Phys. Rev. Lett.* **100**, 130502 (2008).
- [279] R. Orús, S. Dusuel, and J. Vidal, *Phys. Rev. Lett.* **101**, 025701 (2008).
- [280] R. Orús, *Phys. Rev. A* **78**, 062332 (2008).
- [281] Q.-Q. Shi, R. Orús, J. O. Fjærestad, and H.-Q. Zhou, *New J. Phys.* **12**, 025008 (2010).
- [282] D. Buhr, M. E. Carrington, T. Fugleberg, R. Kobes, G. Kunstatter, D. McGillis, C. Pugh, and D. Ryckman, *J. Phys. A: Math. Theor.* **44**, 365305 (2011).
- [283] A. J. Leggett, *J. Phys. Condens. Matter* **14**, 414 (2002).
- [284] D. M. Greenberger, *Rev. Mod. Phys.* **55**, 875 (1983).
- [285] M. Schlosshauer, *Rev. Mod. Phys.* **76**, 1267 (2005); J. Kofler and Č. Brukner, *Phys. Rev. Lett.* **99**, 180403 (2007); S. Raeisi, P. Sekatski, and C. Simon, *Phys. Rev. Lett.* **107**, 250401 (2011); P. Sekatski, N. Gisin, and N. Sangouard, *Phys. Rev. Lett.* **113**, 090403 (2014).
- [286] R. P. Feynman, *Found. Phys.* **16**, 507 (1986).
- [287] A. Steane, *Rep. Prog. Phys.* **61**, 117 (1998).
- [288] J. M. Raimond, M. Brune, and S. Haroche, *Rev. Mod. Phys.* **73**, 565 (2001).
- [289] K. Hammerer, A. S. Sørensen, and E. S. Polzik, *Rev. Mod. Phys.* **82**, 1041 (2010).

- [290] J. S. Bell, *Speakable and Unsayable in Quantum Mechanics* (Cambridge University Press, Cambridge, 1987).
- [291] J. F. Clauser, M. A. Horne, A. Shimony, and R. A. Holt, Phys. Rev. Lett. **23**, 880 (1969).
- [292] R. Horodecki, P. Horodecki, and M. Horodecki, Phys. Lett. A **200**, 340 (1995).
- [293] S. Popescu and D. Rohrlich, Phys. Lett. A **166**, 293 (1992).
- [294] M. Popp, F. Verstraete, M. A. Martín-Delgado, and J. I. Cirac, Phys. Rev. A **71**, 042306 (2005).
- [295] A. J. Leggett and A. Garg, Phys. Rev. Lett. **54**, 857 (1985).
- [296] K. Park and H. Jeong, Phys. Rev. A **82**, 062325 (2010).
- [297] R. Chaves and L. Davidovich, Phys. Rev. A **82**, 052308 (2010).
- [298] The negativity of the GHZ state for general N and k , under local bit flip channels is given by $\frac{(1-2p)}{2}(\min\{0, p^{N+k-1} - (1-p)^{N+k-1}\} + \sum_{i=1}^{(N+k-1)/2} \frac{(N+k-1)!}{i!(N+k-i)!} \min\{0, p^{N+k-i-1}(1-p)^i - (1-p)^{N+k-i-1}p^i\})$.
- [299] S. Bose, Phys. Rev. Lett. **91**, 207901 (2003).
- [300] D. Burgarth, S. Bose, and V. Giovannetti, Int. J. Quantum Inform. **04**, 405 (2006).
- [301] Z.-M. Wang, M. S. Byrd, B. Shao, and J. Zou, Phys. Lett. A **373**, 636 (2009).
- [302] P. J. Pemberton-Ross and A. Kay, Phys. Rev. Lett. **106**, 020503 (2011).
- [303] N. Y. Yao, L. Jiang, A. V. Gorshkov, Z.-X. Gong, A. Zhai, L.-M. Duan, and M. D. Lukin, Phys. Rev. Lett. **106**, 040505 (2011).
- [304] H. Yadsan-Applby and T. J. Osborne, Phys. Rev. A **85**, 012310 (2012).
- [305] T. J. G. Apollaro, S. Lorenzo, and F. Plastina, Int. J. Mod. Phys. B **27**, 1345035 (2013).
- [306] P. Lemmens, G. Güntherodt, and C. Gros, Phys. Rep. **375**, 1 (2003).
- [307] E. Manousakis, Rev. Mod. Phys. **63**, 1 (1991).
- [308] H. Bethe, Z. Phys. **71**, 205 (1931).

- [309] C. Lhuillier, arXiv:cond-mat/0502464.
- [310] F. Alet, A. M. Walczak, and M. P. A. Fisher, *Physica A* **369** 122 (2006).
- [311] T. E. Northup and R. Blatt, *Nat. Photonics* **8**, 356 (2014); X.-S. Ma, B. Dakic, W. Naylor, A. Zeilinger, and P. Walther, *Nat. Phys.* **7**, 399 (2011); K. Chen, C.-M. Li, Q. Zhang, Y.-A. Chen, A. Goebel, S. Chen, A. Mair, and J.-W. Pan, *Phys. Rev. Lett.* **99**, 120503 (2007); Yu-Li Dong, Shi-Qun Zhu, and W.-L. You, *Phys. Rev. A* **85**, 023833 (2012).
- [312] A. Friedenauer, H. Schmitz, J. T. Glueckert, D. Porras, and T. Schaetz, *Nat. Phys.* **4**, 757 (2008).
- [313] A. Imamoglu, D. D. Awschalom, G. Burkard, D. P. DiVincenzo, D. Loss, M. Sherwin, and A. Small, *Phys. Rev. Lett.* **83**, 4204 (1999); S.B. Zheng and G.C. Guo, *Phys. Rev. Lett.* **85**, 2392 (2000).
- [314] K. Yosida, *Theory of Magnetism* (Springer, Berlin, 2010).
- [315] E. Lieb, T. Schultz, and D. Mattis, *Ann. Phys. (N.Y.)* **16**, 407 (1961).
- [316] M. C. Arnesen, S. Bose, and V. Vedral, *Phys. Rev. Lett.* **87**, 017901 (2001); K. M. O'Connor and W. K. Wootters, *Phys. Rev. A* **63**, 0523202 (2001); L. Zhou, H. S. Song, Y. Q. Guo, and C. Li, *Phys. Rev. A* **68**, 024301 (2003).
- [317] E. Dagotto and T. M. Rice, *Science*, **271**, 618 (1996).
- [318] P. Calabrese and A. Lefevre, *Phys. Rev. A* **78**, 032329 (2008).
- [319] D. Poilblanc, *Phys. Rev. Lett.* **105**, 077202 (2010).
- [320] L. O. Manuel, M. I. Micheletti, A. E. Trumper, and H. A. Ceccatto, *Phys. Rev. B* **58**, 8490 (1998); S. Miyahara and K. Ueda, *J. Phys.: Condens. Matter* **15**, R327 (2003).
- [321] S. Korenblit, D. Kafri, W. C. Campbell, R. Islam, E. E. Edwards, Z.-X. Gong, G.-D. Lin, L.-M. Duan, J. Kim, and K. Kim, *New J. Phys.* **14** 095024 (2012).
- [322] M. Lubasch, V. Murg, U. Schneider, J. I. Cirac, and M.-C. Bañuls, *Phys. Rev. Lett.* **107**, 165301 (2011).
- [323] D. Leibfried, R. Blatt, C. Monroe, and D. Wineland, *Rev. Mod. Phys.* **75**, 281 (2003).

- [324] I. Bloch, Nat. Phys. **1**, 23 (2005); P. Treutlein, T. Steinmetz, Y. Colombe, B. Lev, P. Hommelhoff, J. Reichel, M. Greiner, O. Mandel, A. Widera, T. Rom, I. Bloch, and T. W. Hänsch, Fortschr. Phys. **54**, 702 (2006); Xiang-bin Wang, J. Q. You, and Franco Nori, arXiv:quant-ph/0608205; A. Wallraff, D. I. Schuster, A. Blais, L. Frunzio, R.-S. Huang, J. Majer, S. Kumar, S. M. Girvin, and R. J. Schoelkopf, Nature **431**, 162 (2004).
- [325] D. Vion, A. Aassime, A. Cottet, P. Joyez, H. Pothier, C. Urbina, D. Esteve, and M. H. Devoret, Science **296**, 866 (2002); M. H. Devoret, A. Wallraff, and J. M. Martinis, arXiv:cond-mat/0411174 (2004).
- [326] J. Q. You and F. Nori, Phys. Today **58**, 42 (2005); G. Wendin and V. Shumeiko, *Handbook of Theoretical and Computational Nanotechnology* (American Scientific Publishers, 2006), chap. Superconducting Quantum Circuits, Qubits and Computing.
- [327] J. Clarke and F. Wilhelm, Nature (London) **453**, 1031 (2008).
- [328] S. R. White, Phys. Rev. Lett. **69**, 2863 (1992); Phys. Rev. B **48**, 10345 (1993).
- [329] U. Schollwöck, Rev. Mod. Phys. **77**, 259 (2005).
- [330] G. De Chiara, M. Rizzi, D. Rossini, and S. Montangero, J. Comput. Theor. Nanosci. **5**, 1277 (2008).